Development of a Multi-Regime Tribometer and Investigation of Zinc Dialkyldithiophosphate Tribofilm Development in the Presence of Overbased Calcium Sulfonate

by

H. Arthur Kariya

B.S., Mechanical Engineering, 2005
University of California, Berkeley

Submitted to the Department of Mechanical Engineering
in partial fulfillment of the requirements for the degree of

Master of Science in Mechanical Engineering

at the

MASSACHUSETTS INSTITUTE OF TECHNOLOGY

February 2009

Signature of Author .....
Department of Mechanical Engineering
February 4, 2009

Certified by .....
Victor W. Wong
Principal Research Scientist and Lecturer in Mechanical Engineering

Accepted by .....
David E. Hardt
Chairman, Department Committee on Graduate Students

Development of a Multi-Regime Tribometer and Investigation of Zinc Dialkyldithiophosphate Tribofilm Development in the Presence of Overbased Calcium Sulfonate

by

H. Arthur Kariya

Submitted to the Department of Mechanical Engineering in partial fulfillment of the requirements for the degree of Master of Science in Mechanical Engineering

ABSTRACT

A custom tribometer was developed to investigate the production of nano-scale films from the anti-wear additive zinc dialkyldithiophosphate (ZDDP). The tribometer was designed to operate in various conditions of lubrication severity, from boundary to hydrodynamic lubrication regimes. A cylinder-on-plate layout, in which a cylinder rotates and rubs against a plate in a line contact, was employed for this purpose.

ZDDP, a wear preventative additive universally used in engine and gear oil formulations, was studied in detail with respect to tribofilm production. As typical oil formulations contain an assortment of additives, the development of these films in the presence of other additives was studied. Of these, overbased detergents have recently been under scrutiny with mixed findings of synergetic and antagonistic effects. This project investigates the effects of overbased calcium sulfonate, a basic detergent used to neutralize acids and solubilize contaminants in oil, using electrical contact resistance (ECR), Auger electron spectroscopy (AES) and 31-phosphorous nuclear magnetic resonance (P_{31}NMR). Oil blends of 2.4% (mass) ZDDP with varying concentrations of calcium sulfonate were mixed for rubbing and heating tests. ECR was used to monitor the development of the tribofilm in-situ of the tribometer and AES was used in post-mortem analysis to measure the film thickness. Analysis with P_{31} NMR was employed for a series of heating experiments to characterize the chemical interactions between the two additives. Tests in light boundary lubrication show a trend of suppression of ZDDP tribofilm formation with the introduction of the detergent.

Thesis Supervisor: Victor W. Wong
Title: Principal Research Scientist and Lecturer in Mechanical Engineering

Acknowledgements

I would like to thank the following people for their invaluable help in the completion of this project.

Foremost, I would like express my utmost gratitude to Dr. Victor Wong for the opportunities and support he has given me. Through his guidance, I was able to learn the fundamentals of experimental research and hands on problem-solving. I am always inspired by his passion to unravel the mysteries that cover lubrication chemistry and impressed at his depth in knowledge. His guidance and trust in my work opened all doors to fully exert myself in this project, and grow as a graduate student and as a researcher. For this, I am truly grateful.

I would also like to thank the Consortium to Optimize Lubricant and Diesel Engines for Robust Emission Aftertreatment Systems for supporting this project. Without their advice and contributions in providing the test oils, this project would not have been possible.

Much appreciation goes to the members of the Sloan Automotive Laboratory. The smooth progress of my project was greatly due to Thane's experienced advice and help in procuring supplies for my project. The miracles Raymond works with his hands is probably beyond science, and I thank him for the revival of the tribometer. I am thankful to Simon and Alex for all the advice and teaching me the ropes to the lab as well as research. To Kai, who put up with my random talk through all those days and months and kept office-life fun. Many thanks go to Amir for his help in troubleshooting the tribometer.

Also, I would like to express my gratitude to the following, for their immeasurable help during the experimentation process: Libby Shaw at CMSE for her guidance in AES analysis, M&S Grinding for their incredible polishing work and turnaround times, and Gary Juneau for his quick and no-hassle NMR analysis.

Most of all, I would like thank my family and friends. My mother and father, for their understanding and unwavering support and belief in me, and my brother, who still is the base figure of my ideals. My friends in Bellflower, for always keeping a spot open for me, and my friends in Japan for cheering me up with interesting stories.

H. Arthur Kariya
January, 2009

Table of Contents

List of Figures

Figures in Appendices

List of Tables

Tables in Appendices

1. Introduction

Automotive lubricants are a complex blend of base oil and additives. Depending on the specification, base oils compose 70 to 90 percent of the formulation [1]. Additives are added to the oil to increase the performance of the base oil for the severe lubrication conditions found in automotive engines. Examples include dispersants, viscosity index improvers, extreme pressure additives, detergents, and anti-wear additives. Additives have been in use since the 1930's and although their general effects on engine protection are known, the mechanisms of their operation as well as the specific interactions between are yet to be completely documented [2].

As a result of the stringent emissions regulations being enacted worldwide, emission standards have closed the window on permissible exhaust gases to 1/10 of what was allowed 15 years ago. These changes are forcing a renewed effort on modifying or even overhauling modern oil formulations, as engine oil additives are sources of certain exhaust emissions. In a conventional piston engine, a small amount of oil left on the cylinder walls is unavoidably burned as it comes into contact with combustion. Problems come into play when the burned oil either forms noxious particulates, or the metals in the additives become ash. The ash effectively deactivates the catalytic converters used in the post-engine emissions reduction and drastically reduces their efficiency over the life of the engine. Among other additives, zinc and phosphorous-based anti-wear additives and detergents that contain calcium and magnesium are the primary sources of the metals and are currently under revaluation for optimization and reduction. Many researchers are now revisiting the operating mechanisms of the additives in hopes of finding alternatives or complementary blends that result in lower total ash. The result is a shift towards engine oil formulations for meeting emissions regulations rather than simply for engine performance goals.

This project serves to provide useful information to assist the efforts directed at lubricant optimization for the future. This project is divided into two parts. First, a lubrication test-rig is developed. Second, the performance of zinc dialkyldithiophosphate (ZDDP), a

universally used anti-wear additive is investigated in the presence of overbased calcium sulfonate detergent (OBCaSu).

ZDDP is the principal anti-wear additive used in modern engine and gear oil formulations, and is also a source of sulfated ash from zinc and phosphorous. There are many benefits to using ZDDP. To name a few, it is relatively cheap to produce, works as an antioxidant as well as an anti-wear agent, and is extremely effective. Presently, there is no competitive substitute for ZDDP, but the pressure to reduce ash levels in oils continues to escalate.

Stated in simplistic terms, ZDDP is known to prevent wear by the chemical formation of nano-scale films on the lubricated surface. To this day, the step-wise reaction mechanisms for film formation is not fully understood and moreso the effects of other additives on them. However, much experimental work is currently being done by researchers to empirically characterize the behavior of ZDDP.

This study will investigate the effects of OBCaSu on ZDDP. OBCaSu is an alkaline, or basic, derivative of a calcium sulfonate detergent, and is known to have characteristics that both resemble and differ from calcium sulfonate. It possesses a wear-preventative ability of its own, yet some studies have found wear to increase when OBCaSu is added to oils containing only ZDDP [3, 4]. To better understand the magnitude of each known effect of OBCaSu on ZDDP, this study will involve a series of experiments to assess the magnitude of each on the overall anti-wear performance. It should be noted, however, that this study will not address the detailed chemistry of tribofilm formation and additive interaction. This study will be conducted in hopes that a better understanding of the relationship between the two commonly used additives will help future efforts in oil formulation.

2. Background

2.1. Lubrication Fundamentals and Definitions

Lubrication is a process in which an intermediary medium is placed between two contacting surfaces to reduce direct contact and thus wear. Therefore, it must be related to wear, which is when the profiles of the contacting surfaces are changed. This change may be due to plastic deformation, say of the folding over of asperity peaks, or to the shearing of surface features. To describe the level of severity of the lubrication conditions, three regimes are determined. In the order of increasing severity, they are: hydrodynamic, mixed, or boundary lubrication. In hydrodynamic lubrication, negligible wear occurs as there is complete separation of the rubbing surfaces by the lubricant. Hydrodynamic lubrication occurs when conditions allow the hydrodynamic pressure of the liquid lubricant to separate the surfaces, and is facilitated by high rubbing speed, high lubricant viscosity, low load, or smooth surfaces. On the opposite extreme is boundary lubrication, which occurs when the lubricated surfaces are not separated but are in physical contact. The coefficient of friction is high for boundary lubrication and extreme cases of hydrodynamic lubrication, due to the rubbing of the surfaces and the viscous shear of the lubricant, respectively. Mixed lubrication is regime between boundary and hydrodynamic, in which incomplete separation occurs and the surfaces undergo a moderate level of wear. Although the criterion defining the onset of boundary lubrication depends on the literature, for the purpose of experimental analysis, boundary lubrication will be considered to occur when the coefficient of friction exceeds 0.1[5].

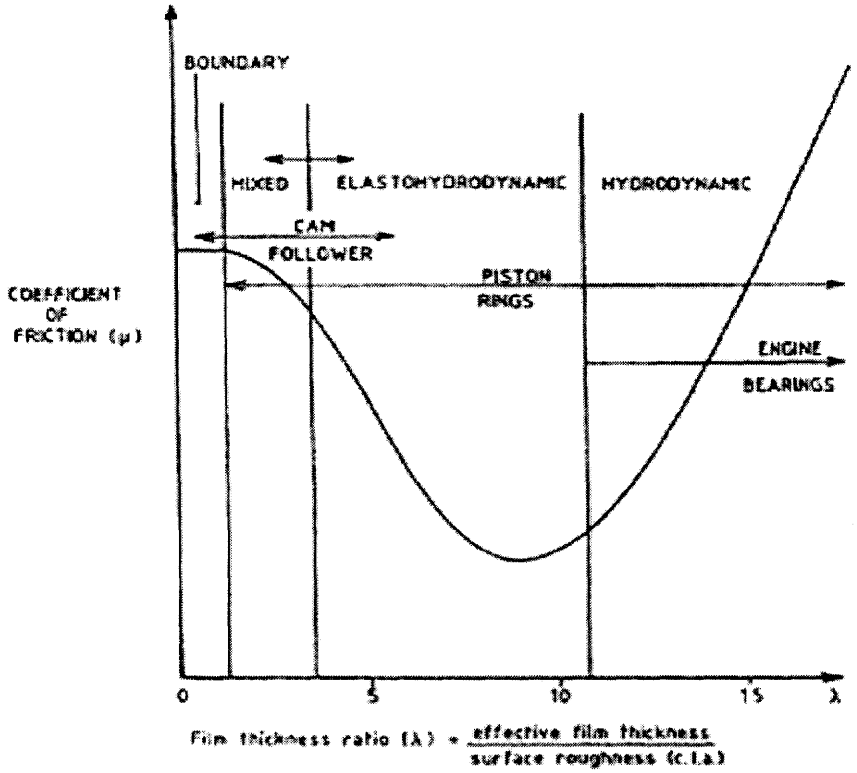

Figure 2-1 Lubrication regimes and their effect on the coefficient of friction [9]

2.2. Oil Additives

2.2.1. ZDDP

Zinc dialkyldithiophosphate (ZDDP) is arguably the most influential lubricant additive up to date. It was introduced mainly as an antioxidant additive in the early 1940's. As the 1950's saw engines with higher compression ratios and increased component stresses, it became noticed that engines operating on higher levels of ZDDP generally had less wear problems than engines without it. Since then, ZDDP has been in such widespread use in lubrication that as of 2004, the United States is estimated to use 30,000,000 pounds of ZDDP on a yearly basis [2].

ZDDP is an effective anti-wear additive through its formation of nano-scale films on metal surfaces. These films can be formed through high temperature or pressure. Though there is not a specific threshold temperature that must be exceeded in order for

the thermal film formation, it is generally understood that temperatures exceeding 80°C will induce slow film development and temperatures beyond 150°C will drastically accelerate the rate of formation [6, 1]. Under rubbing conditions seen in actual lubrication, films have been found to form at room temperature, although higher temperatures greatly increase the rate of formation [7].

Although many chemical pathways have been suggested by researchers on the development of films by ZDDP, the most dominant pathway is the following. Under conditions noted above, ZDDP is decomposed. The decomposition products, which is said by some to further catalyze the ZDDP decomposition process, is adsorbed onto the metal surface, where it undergoes oxidative reactions that make the film precursors [6, 2, 8]. The widely accepted observation is that temperature increases the rates of these reactions, such that they can be estimated with an Arrhenius relationship. Though a consensus is yet to be reached about the effect of pressure on the film formation rate, it is suggested by some that flash temperatures generated by the micro / nano-scale asperities of the lubricated surfaces help produce the film [9].

Other parameters that affect the rate of film formation are: ZDDP concentration, sliding speed, type of base oil, presence of other additives, type of lubricated surface and type of ZDDP. Greater concentration of ZDDP increases the formation rate. Sliding speed, type of base oil and the presence of other additives have mixed effects. As can be seen in figure 2.2 below, sliding speed can increase or decrease the rate, depending on the lubrication conditions [10]. It has also been found that interactions between the base oil and ZDDP have noticeable effects on film formation. In general, Group 2 base stock oils allow for faster formation than group 1 stock oils [11]. Other additives, such as detergents and dispersants, have been found to both positively and negatively influence the film formation rate. Currently, experimental results are contradictory: some find these additives to have a synergistic effect, while others state that the decomposition of ZDDP is hampered by the presence of detergents [12, 13, 14]. Most studies on tribometers have been done using AISI 52100 steel or grey cast iron as test specimens,

and a study has shown that anti-wear films are more easily formed on 52100 steel than on cast iron [15].

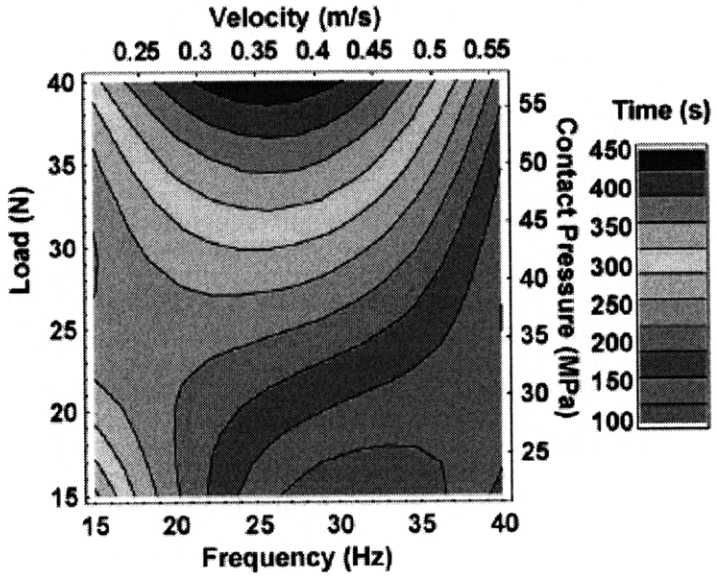

Figure 2-2 Contour plot of the induction time, or the time taken until film formation occurs, for a variety of contact pressures and sliding speeds [10]

The functional group on the ZDDP molecule has a large effect on its thermal stability, affecting the decomposition rate for a given lubrication condition. The most common types of ZDDP, defined by their functional groups, are: secondary alkyl ZDDP, primary alkyl ZDDP and aryl ZDDP. Aryl ZDDP is most thermally stable, followed by primary akyl and then secondary alkyl ZDDP. In terms of anti-wear film formation, high instability is desired due to better reactivity. For the range of temperatures generally seen in an engine, experimental evidence show that alkyl ZDDP forms anti-wear film faster, with secondary alkyl being fastest [15, 2]. Typical engine oil formulations contain approximately 85% secondary alkyl and 15% primary alkyl ZDDP.

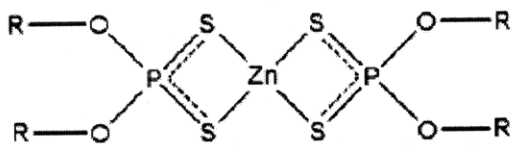

Figure 2-3 Typical structure of ZDDP [8]

In addition, ZDDP is known to exist in different forms. While figure 2-3 shows ZDDP in its simplest (monomeric) form, it exits in an equilibrium between monomer and dimer

state in solution (figure 2-4). Furthermore, ZDDP may also be in an agglomerate state, called "basic ZDDP," in contrast to the "neutral," simpler, forms described above. Past studies have found that basic ZDDP can convert to its neutral form and ZnO at high temperatures [2, 16]. In general, ZDDP in its neutral form is more reactive and therefore more effective as an anti-wear agent. Of the neutral form, the monomer is most reactive.

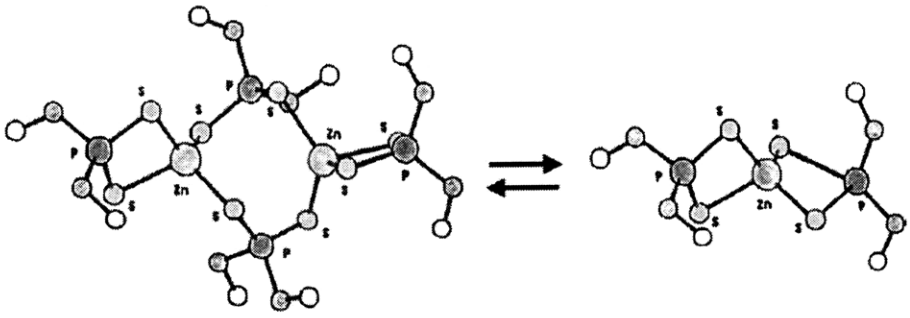

$Zn[PS_2(OR)_2]_2$ $Zn_2[PS_2(OR)_2]_4$

Figure 2-4 Forms of ZDDP: dimer (left) and monomer (right)

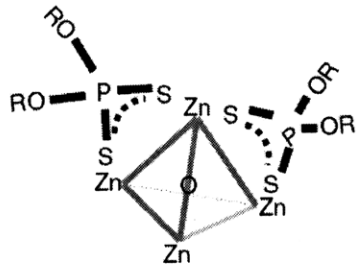

basic-ZnDTP. $(DTP)_6Zn_4O$

(two of four DDP ligands shown)

Figure 2-5 Basic ZDDP, Zn4 [PS2(OR) 2]6O

Anti-wear films from ZDDP are structured in layers, as shown in the figure below. The outermost layer consists of organic sulphides and undecomposed ZDDP. In general, higher concentrations of ZDDP result in more undecomposed ZDDP on the surface [6]. Certain studies have found the surface to contain undecomposed ZDDP in the form of a viscous layer, increasing friction [17]. The next layer is comprised of metallic polyphosphates. The polyphophate chain length is longer near the surface and more iron is found near the iron substrate. Below the phosphate layer is an iron-rich bonding layer. Film thickness depends on the conditions, and can range from 1 to 150 nm [11].

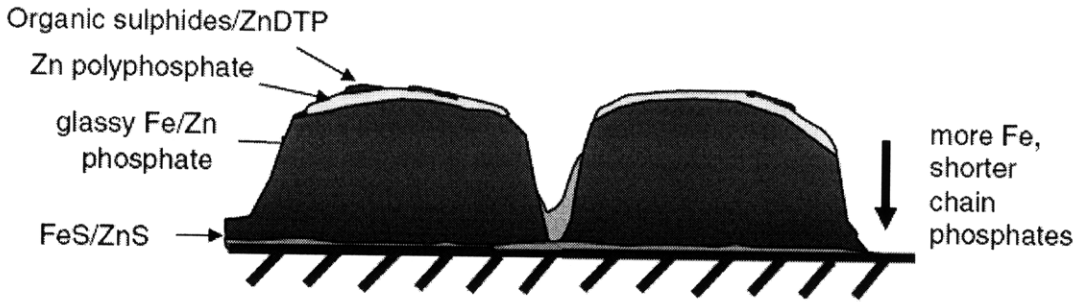

Figure 2-6 Typical layer diagram of an anti-wear film produced from ZDDP [2]

Most studies have found that the anti-wear performance is better when polyphosphate chain length is longer [18, 10]. Longer rubbing time, higher concentration of ZDDP, moderate temperature, higher load, and smooth surfaces facilitate the formation of long chain phosphates [18]. Researchers have also found that the addition of overbased calcium sulfonate detergent resulted in shorter chain phosphates due to the cations from the detergent cleaving the chains [4].

2.2.2. Overbased Calcium Sulfonate

Detergents and dispersants are surfactant species included in oil packages to keep oil-insoluble contaminants such as soot in suspension. They also prevent oil thickening, sludge and varnish deposition on metal surfaces and corrosive wear. Detergents contain alkaline metals, typically calcium or magnesium, while dispersants are typically ashless, or without metal. Both are structured with a hydrophilic "head" and an oleophilic hydrocarbon "tail" that enable them to dissolve in oil. Contaminants are suspended in oil by being surrounded by the additives in a manner such that the heads face the contaminant while the tails face the oil. Detergents and dispersants are considered interchangeable in role, but if a distinction is to be made, detergents are normally considered for high temperature deposit control while dispersants for low-temperature sludge[19].

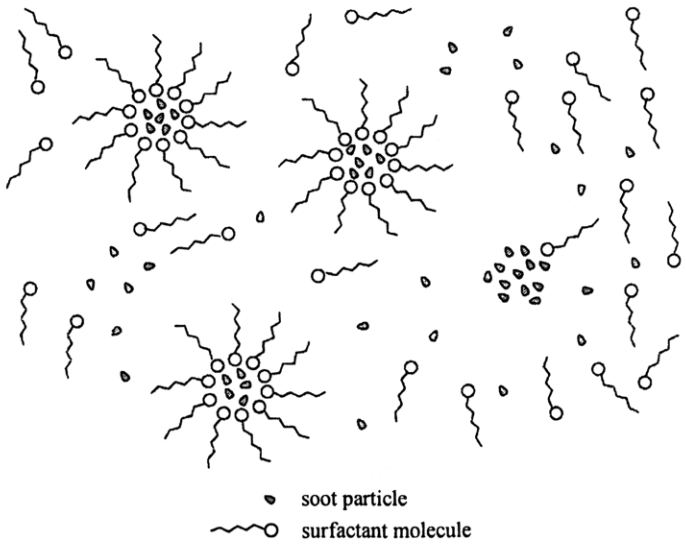

Figure 2-7 Solubilization of a soot contaminant by surfactant molecules in oil [6]

Various types of detergent are used for engine oil, the most common being calcium or magnesium based sulfonates, phenates, salicylates and phosphonates with long-chain alkyl tails. For example, a typical calcium sulfonate detergent consists of calcium sulfonate alkylbenzene molecules [6]. Of these detergents, the most widely used are calcium sulfonates [20].

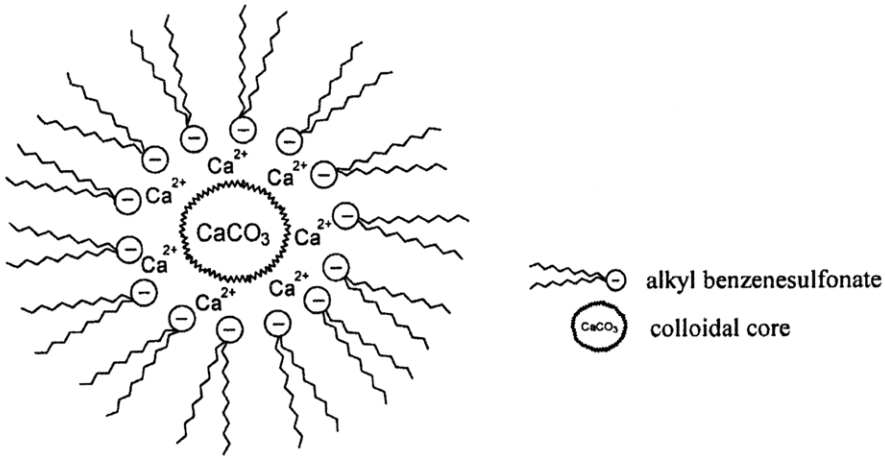

Figure 2-8 Overbased calcium sulfonate structure [6]

Overbased detergents are structured as if the detergent molecules are encapsulating, or solubilizing, a strong base core. The core is a metal carbonate, usually calcium, and ranges in size from 10 to over 20nm in diameter [21]. Overbased detergents play a dual

role of surfactant as well as neutralizer of acids. They are widely used, as oil change intervals are usually limited by the anti-wear and acid-neutralizing capacity. This capacity to neutralize acids is typically measured in units of total base number (TBN), which range from 5 to 10 for modern formulations.

Various instances of detergent interaction with ZDDP have been documented in the past. Detergents have been found to solubilize ZDDP in oil, slowing its decomposition and limiting its ability to contact the metal surface [6]. Others studies report a synergistic effect in the total anti-wear action [3]. In addition, detergents have also been found to shift ZDDP equilibrium towards the basic state, increasing wear due to the decrease in anti-wear activity [6]. In this case, overbased detergents had a greater effect on shifting ZDDP equilibrium than normal detergents. Other effects on tribofilm composition have been noted as well. The calcium cations from the basic core of overbased detergents were seen to cut the polyphosphate chains in ZDDP tribofilms and incorporate themselves in the form of calcium phosphates. The shorter chains reduced the effectiveness of the anti-wear film [4].

Overbased calcium sulfonate detergents are known to have an independent anti-wear capability. The calcium carbonate cores, under rubbing conditions, form a protective layer on the metal surfaces. Some have found a viscous film while others a robust solid film [22]. Furthermore, some report the film to be composed of calcium oxide and others calcium carbonate in the form of calcite [23, 24, 25].

2.3. Diagnostic Techniques

A variety of diagnostic techniques was used in this study, and they will be briefly introduced here. Anti-wear film development was monitored in-situ during rubbing by Electrical Contact Resistance (ECR) and the film composition and thickness was measured with Auger Electron Spectroscopy (AES). Other microscopic features are examined using Scanning Electron Microscopy (SEM). The decomposition of oil is analyzed by 31-Phosphorous Nuclear Magnetic Resonance (P_{31}NMR).

ECR is essentially an electrical circuit used to measure the resistance between two surfaces. Simple setups used in the past consist of the measured resistance connected in parallel or series to a known resistance, closing a circuit connected to a battery [15, 26]

AES is an ultra-high vacuum surface analysis technique that closely parallels SEM. An electron gun is used in SEM to send a ray of electrons to the surface atoms of the analyzed sample to induce an energy exchange. This can result in the elastic scattering of the electrons, inelastic scattering of different electrons, or the emission of electromagnetic radiation. This is picked up by a detector, from which signal is used to produce an image. AES operates by the same principle, but different only in that Auger electrons are excited from the sample, and these are detected instead. Due to the similarity in operation, AES machines commonly have SEM imaging settings as well. AES is often used in conjunction with ion sputtering for depth analysis; this entails an ion gun to erode away nanometer-thick layers while the AES examines the surface [27, 28, 29, 30].

P_{31}NMR is a type of nuclear magnetic resonance (NMR) technique that analyzes the 31-phosphorous isotope. The basic operation of NMR is based on the phenomenon that an isotope resonates at a characteristic frequency when subject to a magnetic field. Typical isotopes used are P_{31}, H_{13} and C_{13}. Depending on the chemical state of the isotope, a frequency shift from resonance can occur, and this shift, together with the resonant frequency, is used to calculate a non-dimensional value known as the chemical shift. The chemical shift is expressed in ppm, and is used in plotting the NMR spectrum [31, 32]. The chemical shift of an isotope is defined by its peak in the spectrum.

3. Development of a Custom Tribometer

3.1. Design Goals

In the development of the tribometer, possible designs were considered by weighing the desired uses. It was determined that the tribometer will have future use in hydrodynamic as well as boundary lubrication testing.

1. Boundary lubrication testing
    - effect of lubricant chemistry on tribofilm development
2. Hydrodynamic lubrication testing
    - effects of oil contaminants
    - effects of material / surface property

For hydrodynamic testing, measurement of the oil film thickness was a high priority. For boundary lubrication testing, oil film measurement was unnecessary but in-situ monitoring of anti-wear film development was to be an integral part of the design. In both cases, the friction force acting at the interface was to be measured.

3.2. Typical Tribometer Designs

In consideration of various tribometer designs, the designs were categorized by two classifications: point vs. line contact and reciprocating vs. continuous motion. Common examples of point contact layouts include the four-ball wear tester and the ball-on-disc tribometers. Line contact designs are generally in the form of a cylinder-on-flat.

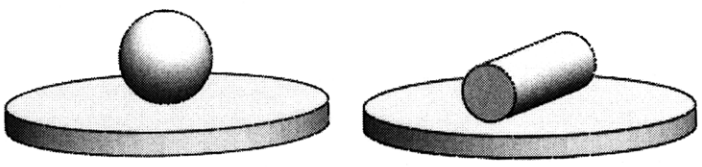

a. b.

Figure 3-1 Example of point contact a) and line contact b) tribometer designs

Continuous rubbing motion was chosen over reciprocating motion as reciprocation involves a series of different speeds, from zero velocity to a maximum at the middle of the stroke. Focusing analysis on one speed would allow for a greater control over the lubrication regime and reduce the number of parameters varied per test. A line-contact layout was employed over point contact for reasons later explained in this section.

3.3. Experimental Apparatus – Line Contact Tribometer

3.3.1. Overview

The tribometer design was largely determined by the methods of measurement. The design was chosen through the following steps: first, the required measurements were determined and second, the modes of measurement were selected. And finally, various tribometer designs that would allow for the implementation of these methods and sensors were considered.

The following parameters were chosen for measurement:

1) Oil film thickness
2) Friction force
3) Tribofilm development

However, as oil film thickness will only be measured during hydrodynamic testing and tribofilm development will be monitored during boundary tests, only two of the three parameters were needed to be measured at once.

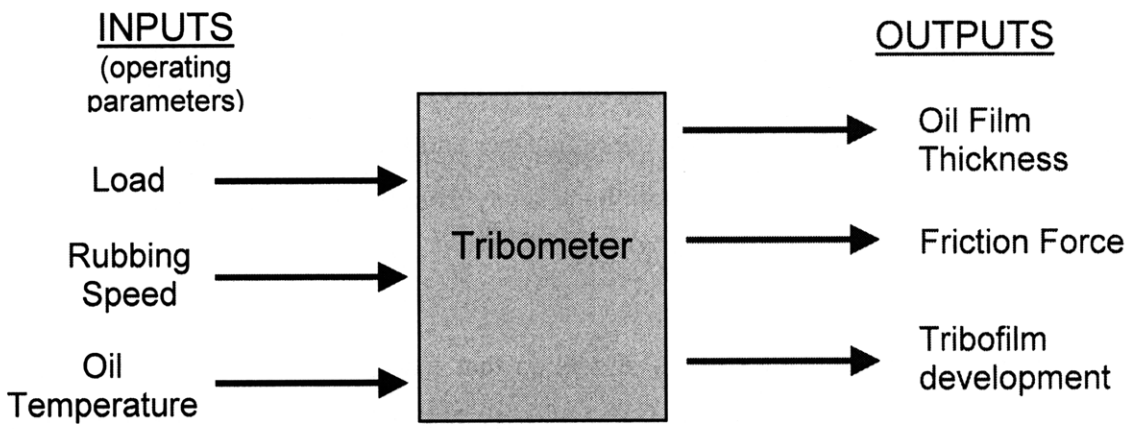

Figure 3-2 Inputs and outputs of tribometer

3.3.2. Cylinder-on-Flat Design for Hydrodynamic Testing

The technique of Laser-Induced Fluorescence (LIF) was chosen for oil film thickness measurements, due to the availability of hardware and knowledge of implementation. LIF has been used for in-engine film measurement at MIT for over 20 years [33, 34, 35]. Furthermore, as LIF has been in use since the early 1970's, there is a wealth of literature regarding its application.

Being a laser-based technique, LIF requires optical access to the location of measurement. For oil film measurement without a large disturbance of the rubbing interface, the line-contact design was employed. Point-contact with a ball and plate may have been likewise used, with the optical window for laser access mounted onto the plate. With this design, however, the oil film can only be measured when the ball rides over the window and the measurements will be momentary. A cylinder-on-flat design was adopted, in which a plate is held stationary while a cylinder spins against it. Continuous measurements will be possible if the optical window is located on the plate. If the window is kept small in respect to the length of the contact, measurements can be taken at minimum disturbance of the rubbing surfaces. Further detail regarding the LIF setup can be found in Appendix-A.

As a result of having the optical access on the plate, it was necessary to keep the plate from being completely immersed in the oil. Especially in high temperature conditions, the heated oil may deform or degrade the optic fiber and seep into the lens of the focusing probe. Thus the flat was to be held stationary, away from the oil sump, while the cylinder transported the oil to the lubricated interface.

The plate was mounted onto a set of sliders so that it was free to move along a plane tangent to the cylinder (figure 3-3). A compressive load cell was mounted in the path of the sliders so that frictional forces acting on the flat during rubbing will be transmitted onto the load cell. Low friction sliders were chosen to prevent introduction additional forces to the load cell readings. This subassembly was then attached to another set of sliders, which allowed the plate to move towards or away from the cylinder. By connecting these sliders to a set of weights with a cable, the plate was able to be pressed against the cylinder with a known force. Additional accommodation was made to allow the plate to pivot on an axis perpendicular to that of the cylinder rotation (see figure 3-4). Given that the cylinder is truly concentric and the plate flat, this allowance was designed to provide a small amount of auto-alignment to compensate for the tolerances stacked from the number of components that align the plate.

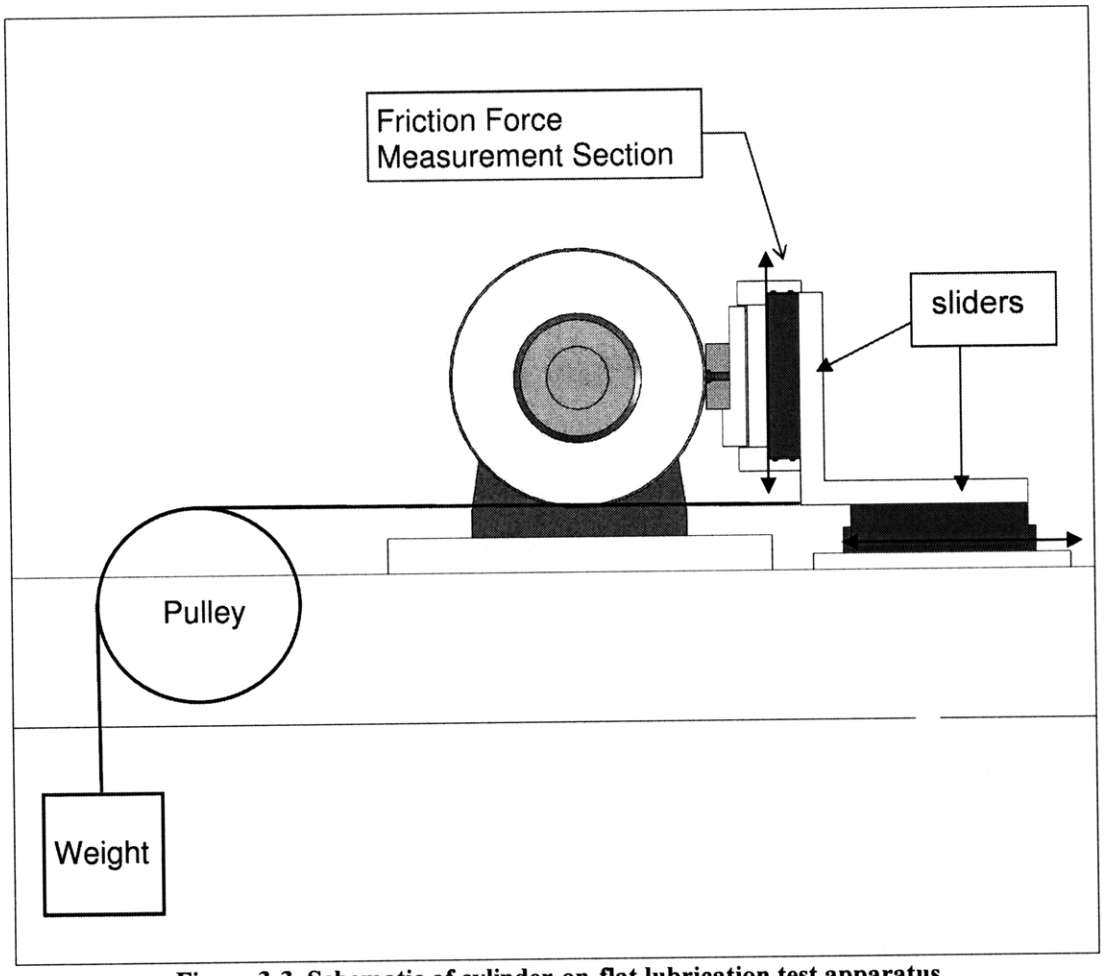

Figure 3-3 Schematic of cylinder-on-flat lubrication test apparatus

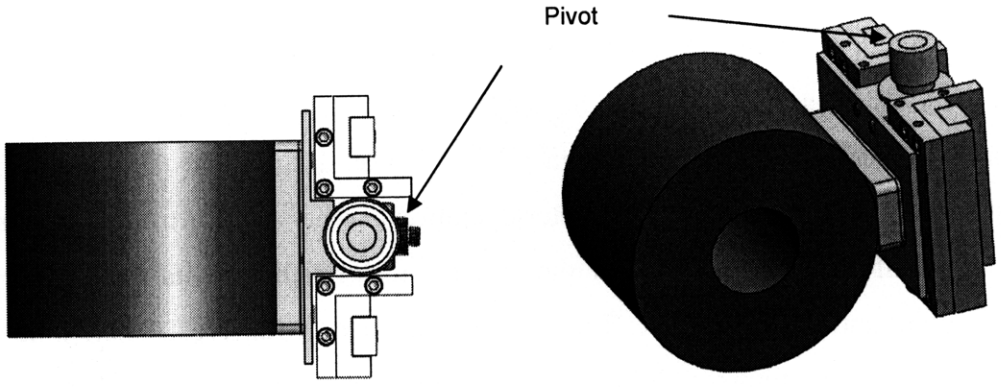

Figure 3-4 Design of pivot made to allow for plate rotation for auto-alignment to cylinder

The cylinders were made of grey cast iron and AISI 52100 chrome steel with the dimensions of 3.5" OD, 1.25" ID and 2.5" length. The plate was made of grey cast iron with dimensions: 2.5" length, 1" width and 0.3125" height. These metals were selected to closely resemble the materials found in the cylinder liner and piston rings of reciprocating combustion engines.

The cylinder was rotated using a 1hp, 90V DC motor with a controller. To prevent rotation runout, tapered roller bearings were used to hold the cylinder spindle. The rotation speed was monitored using an encoder with a tachometer readout mounted onto the spindle. The cylinder was fitted onto the spindle with a close sliding fit, and held in place using a screw-type clamp. Since the spindle was made of stainless steel and the cylinder of hard chrome steel, occasional problems occurred during removal in which the internal surface of the cylinder was gouged by the spindle shaft. Mainly due to the small imperfections in the interfacing surfaces and misalignment, this could have been avoided by designing a tapered spindle and/or a brass bushing to fit between the cylinder and spindle.

The oil was contained in a housing that allowed volumes from 100mL to 250mL. The housing was made circular to promote in-sump circulation of the oil to retain uniform composition. Having corners in the sump may result in stagnation at the corners, with only a certain volume of oil constantly picked up by the cylinder. In addition, a removable window was made on the housing to allow access to the cylinder for installation and removal. During the design process it was desired that the window be transparent so that the oil level and tribometer operation can be seen for troubleshooting purposes. Polysulfonate was chosen for the window material due to its transparency, high melting point and machinability. The housing was made with five 1/8" NPT holes at the bottom for possible future additions of oil treatment features. In the setup used for this project, these holes were used to insert two 200W, 1/8" diameter, 3" length cartridge heaters and a type-K thermocouple for sump heating and temperature control. A PID controller was used to control the heating. The other holes were plugged during operation and used for draining the oil.

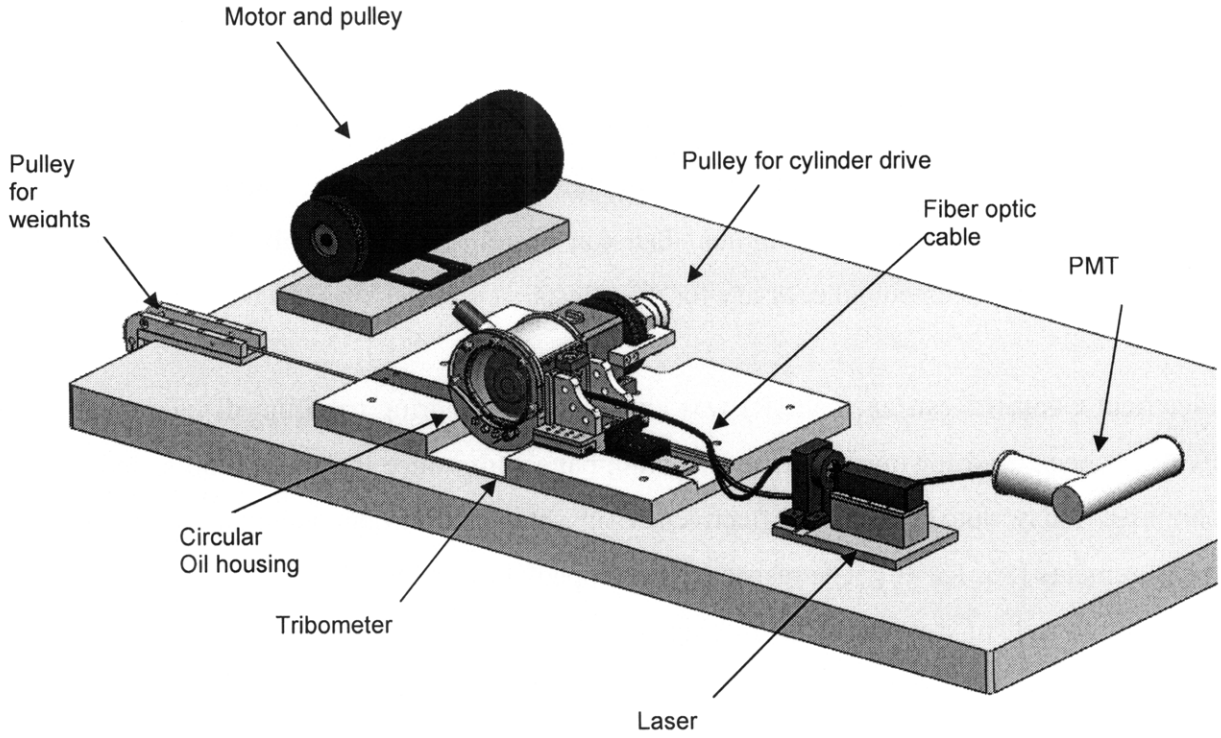

Figure 3-5 CAD drawing of entire test setup

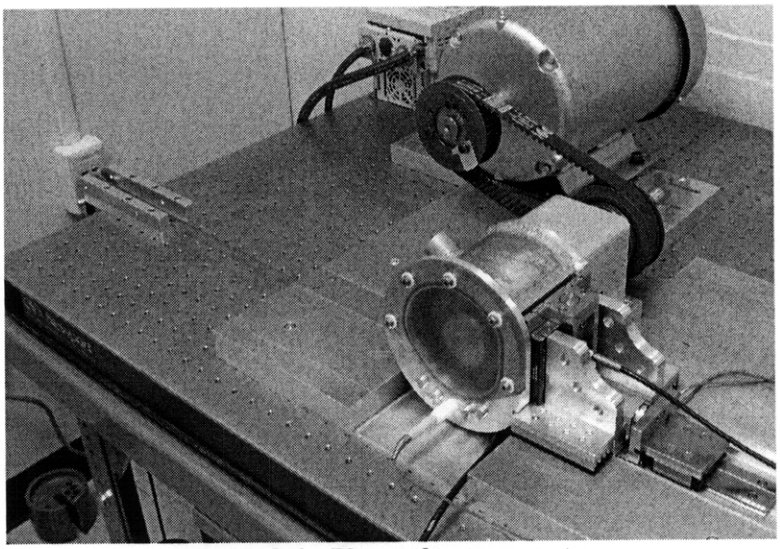

Figure 3-6 Photo of test apparatus

3.3.3. Cylinder-on-Flat Design for Boundary Lubrication

Boundary lubrication testing was performed with the same setup as for hydrodynamic lubrication but with a few modifications. The plate length was shortened to allow higher local pressures at the rubbing interface, and the LIF was removed. Since boundary lubrication resulted in oil films thinner than can be reliably detected by LIF, oil film measurement was deemed unnecessary for these tests.

Electrical Contact Resistance (ECR) was chosen for monitoring tribofilm development. ECR has been used for investigating insulating nano-films since the early 1960's, and is still used today due to its cost effectiveness in setup and strong potential for in-situ measurements [36, 15, 10]. The resistance developed at the rubbing interface is measured, with the onset of resistance signifying the initiation of a tribofilm. The main requirements for applying ECR are boundary lubrication of highly conductive metals and electrical isolation of subassembly components, which were able to be included into the design with little effort. It must be noted, however, that ECR can only be used to monitor anti-wear film development and cannot directly measure the film thickness.

Boundary lubrication for tribofilm development required much higher normal pressures at the rubbing contacts. With preliminary testing low pressures were found to result in very slow, or negligible, production of these films. The plate was redesigned accordingly for boundary lubrication testing. It was downsized to the dimensions of 1" width, 1.4" length and 3/32" thickness in 52100 steel. The rubbing contact was therefore reduced to 1.4". As controlled temperature modulation of the rubbing surface was important for repeatable production of the tribofilms, a ceramic heater was fitted behind the plate to heat the rubbing interface. The plate was designed to be small enough for post-mortem analysis in ultra-high-vacuum microscopes while still being large enough to allow the use of the smallest commercially available high-output heater (100W ceramic heater with 3/4" x 3/4" heating area). The surfaces were professionally polished to a surface roughness of 0.05 μm Ra and a flatness of 0.5 HLB. The cylinder was also polished to a smoothness of 0.05 μm Ra.

A simple voltage divider circuit was used for ECR measurements [15]. A 105 kohm resistor was placed in series with the interface resistance to a 1.5V battery. The voltage drop across the resistor was read by the data acquisition system and registered as the raw data for the ECR plot. An ECR voltage of 1.5V represented zero interface (tribofilm) resistance, and 0V represented infinite resistance at the rubbing interface, or an open circuit. Use of a 105 kohm resistor allowed for a range of detectable resistance measurements from 5 kohm to 1Mohm (figure 3-8). Contacts to connect the circuit to the tribometer were made at the cylinder spindle and the plate.

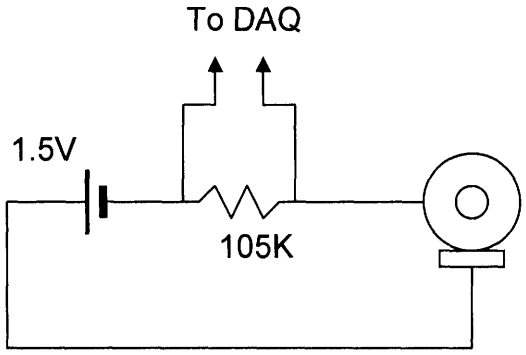

Figure 3-7 ECR circuit

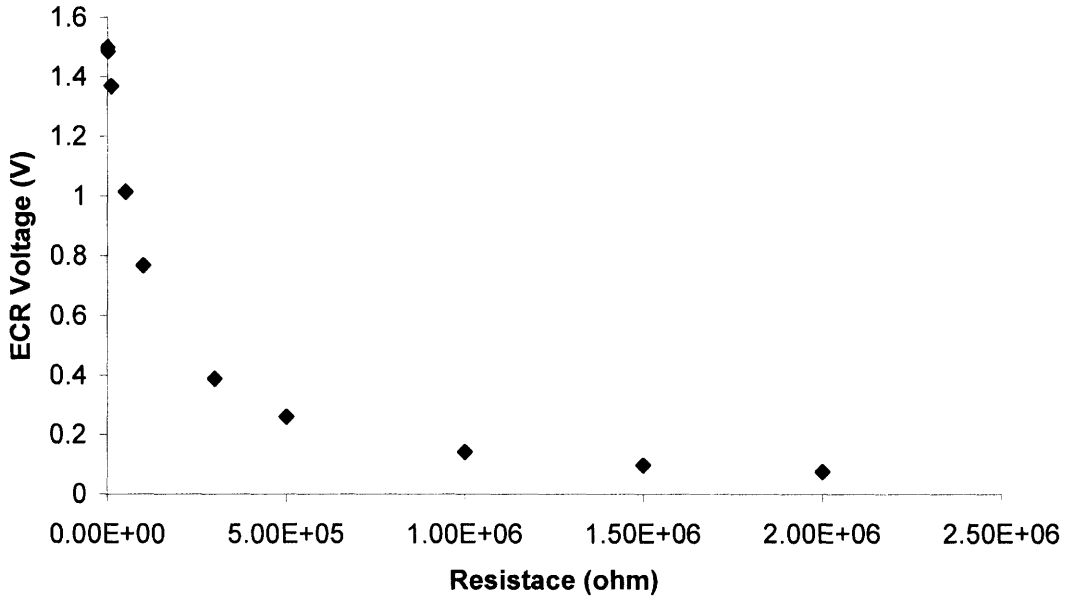

Figure 3-8 Relationship between ECR voltage and tribofilm

3.3.4. Data Acquisition

Measurements were recorded using a data acquisition (DAQ) console from National Instruments (SC-2345). Signal conditioning was performed with plug-and-play modules designed for use with the console. The DAQ console was connected to a computer through a National Instruments PCI board (PCI-6259) and interfaced with LabVIEW to further condition and save the data.

4. Experimental Methodology

This chapter discusses the methodology for the second half of this project, consisting of the experiments run on the completed tribometer. Light boundary lubrication tests were performed in investigation of zinc dialkyldithophosphate (ZDDP) performance in forming anti-wear films in the presence of overbased calcium sulfonate (OBCaSu). Non-lubrication tests were also undertaken, in which oil samples were heated to observe the in-solution interactions of two additives.

4.1. Approach

Although general effects of OBCaSu on lubrication with ZDDP were studied as well, the primary focus of this investigation was set on OBCaSu effects on the ZDDP film development and structure. For simplification for experimental purposes, the multitude of steps required for ZDDP to form an anti-wear film was classified into 2 steps:

1) decomposition / isomerization of ZDDP in oil (chemical state changes)
2) adsorption of ZDDP and ZDDP-derived products onto metal surfaces and the subsequent chemical reactions for film formation (ZDDP – metal interactions and film formation)

These steps could take place in both tribo-stressed and non-tribo-stressed areas. Anti-wear films have been found to form in both rubbing conditions and heated conditions, meaning that these 2 steps are successfully executed in both cases. For the sake of clarity, anti-wear films formed under rubbing conditions will heron be called "tribofilms" and films formed under heated conditions will be called "thermal films." There is strong agreement among past studies that composition and chemistry of the two types of films are slightly dissimilar. Zinc, phosphorous, and sulfur content have been found to differ, as well as the phosphate chain length [2, 6, 17, 37]. However, this can be thought of as an extension of the fact that different rubbing conditions, say in temperature and loading,

result in differences in film structure. Hence in this study, thermal films are considered to be tribofilms with loads asymptotically approaching zero. Considering the steps stated above, the severity of rubbing will affect step 2 far more than step 1, which takes place regardless of the presence of metal. As an example of this, some researchers consider step 1 to be a largely thermal process, affected by rubbing only through the generation of flash temperatures [9]. Therefore, the effect of OBCaSu on step 1 in a purely heated environment will be considered to be representative of (though not necessarily equal to) its effect during rubbing.

The experimental approach here is to investigate the effect of OBCaSu on step 1 in a variety of heated environments and step 2 in both tribo-stressed and non-stressed (heated) tests. An overview of the experimental schematic for heating tests are shown below. 3 scenarios of heating tests, labeled A through C, were conducted (figure 4-1). Test A was intended to analyze step 1, or the tendency of ZDDP to undergo chemical state changes in the presence of OBCaSu. Tests B and C examined the effect of OBCaSu on step 2 of the film formation process. The difference between B and C was whether ZDDP was fresh or thermally aged at the start of the heating process.

Tribofilm development was studied through rubbing tests conducted on the tribometer. 3 hour rubbing tests were performed, and the deposited films were subject to post-test analysis with AES and SEM.

Test A – decomposition effects

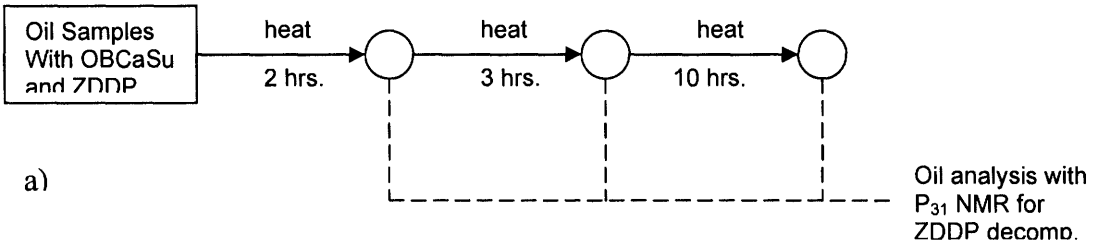

Test B – thermal film formation with fresh ZDDP

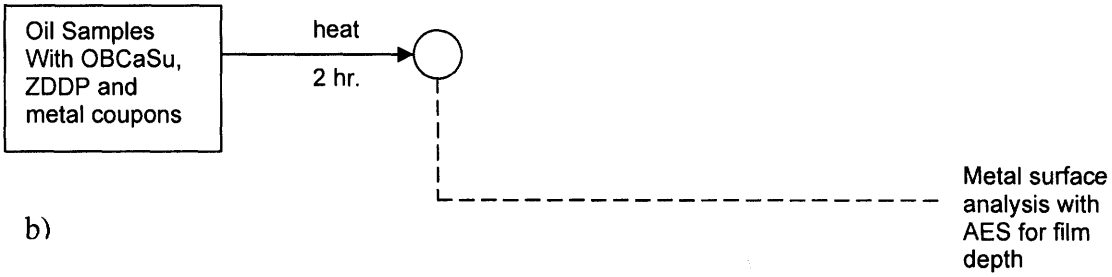

Test C – thermal film formation with aged ZDDP

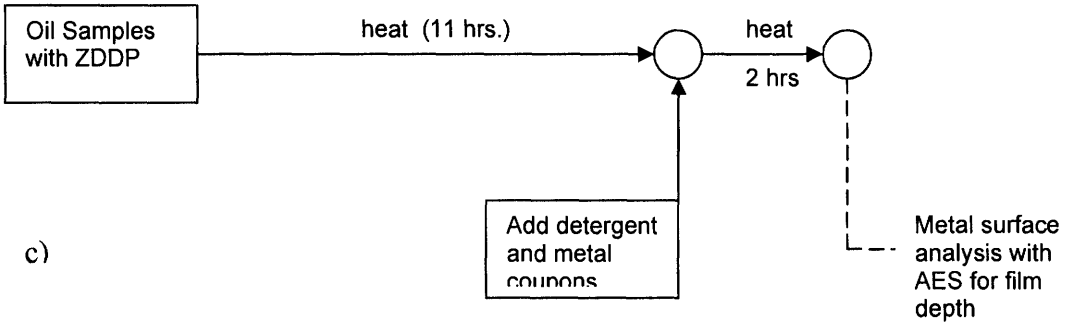

Figure 4-1 Schematic of 3 types of heating tests conducted to study the effects of OBCaSu on ZDDP activity

4.2. Experimental Procedure and Test Settings

4.2.1. Blending Oil

Test oils were blended with varying levels of additives. To closely model current engine oil formulations, a Group 2 base stock oil was used. The base oil was tested to have a viscosity of 28.8 cst. at 40° C and 5.2 cst at 100° C (tested with ASTM-D445) and a sulfur content of 23 ppm. For blending purposes, the metal content in the ZDDP was measured using ICP-AES (ASTM D-5185).

Table 4-1 Specification for 100% ZDDP solution

Secondary Alkyl ZDDP	
Phosphorous (% wt.)	8.3
Zinc (% wt.)	9.8
Sulfur (% wt.)	19

Table 4-2 Specification for OBCaSu solution

Overbased Calcium Sulfonate	
TBN (mg KOH/g)	300
Sulfated Ash (% wt.)	40

The additives were blended into the base oil by weight. ZDDP was blended on a percent-phosphorous basis and OBCaSu was blended to TBN levels comparable to those of typical oil formulations. Percent phosphorous was used as the measurement of ZDDP concentration as it is the primary means of measurement used by oil companies. The additives were first added to the base oil on a scale at room temperature. The oils were then heated to 60° C and mixed thoroughly for 30 minutes. The blends were mixed to have 2.4% of the ZDDP solution (0.2% wt. phos.) and varying levels of detergent: 0, 0.5, 1, 3, 6 and 15% OBCaSu by weight. The 15% blend was added to the analysis to observe the effect of high concentration OBCaSu. A special blend with no ZDDP and 3% OBCaSu was also made for a rubbing test. Table 4-3 shows the phosphorous and TBN content of each blend. Typical modern oil formulations are mixed with 0.08~0.12 % phosphorous to a TBN of 6~12. Although comparable ratios of ZDDP (% phos.) to TBN were used for this project, higher concentrations were employed for easier observation of changes.

Table 4-3 Specification of blended test oils

Blend	Phosphorus (% wt.)	TBN (mg KOH/g)
0	0.2	0
0.5	0.2	1.5
1	0.2	3
3	0.2	9
6	0.2	18
15	0.2	45
No ZDDP	0	9

4.2.2. Thermal Decomposition Test

Tests were also conducted to investigate the effect of OBCaSu on the thermal decomposition of ZDDP. Oil samples were heated at a controlled temperature using a PID temperature controller with a hotplate. Uniform temperature among the test oils was maintained by heating an intermediary heating oil instead of direct heating. The test oils were heated to 120° C for 2, 5 and 15 hours and 150° C for 11 hours. The oil samples were then analyzed using P_{31}NMR. The oil samples were diluted with deuterated chloroform and measured for decomposition of ZDDP in a Tecmag Apollo NMR machine at 400 Mhz. 52100 steel sheets were included in the oil samples heated for 2 hours to observe film formation by AES.

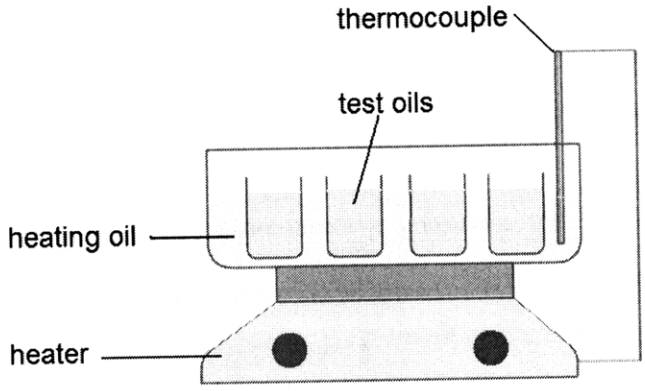

Figure 4-2 Schematic diagram of the setup used to thermally decompose ZDDP

Additional heating tests were preformed to analyze the effect of OBCaSu on the adsorption of ZDDP and its decomposition products onto metal surfaces. Oils with 2.4% ZDDP were heated for 11 hours at 150° C to ensure a sufficient level of ZDDP decomposition products to facilitate thermal film formation. Different levels (1, 3, 6, 15%) of OBCaSu and 52100 steel coupons were then introduced into the oils, and they were heated for an additional 2 hours at 120° C.

4.2.3. Rubbing test with tribometer

The tribometer was brought to thermally steady-state conditions before testing was begun. A 100 mL sample of the test oil was heated to 100° C and the cylinder and oil housing were heated with a hot-air blower to ~70° C before the oil was introduced into the tribometer. The oil preheating process was usually less than 15 minutes. The oil was continued to be heated in the housing until the testing temperature was reached. Typical heating times in the housing were ~35 minutes, making total heating time about 50 minutes, most of which was below 100° C. This kept thermal decomposition of ZDDP before testing to a minimum.

Once the operating oil temperature was reached, the heater for the plate test piece was turned on and the cylinder rotated at the testing speed. The data acquisition system (DAQ) was then initialized and the weights loaded. Temperature, friction and ECR signals were sampled with the DAQ at a rate of 1KHz, and data processing was performed by a rolling average, since quasi-steady-state operation kept transients to a minimum. Table 4-4 lists the testing parameters.

Table 4-4 Testing Conditions

Oil temperature	105° C
Cylinder speed	23 cm/s (50 RPM)
Load	150 N (16 kg)
Test time	180 minutes

4.2.4 Post mortem analysis with AES

Post-mortem analysis with Auger electron spectroscopy (AES) was performed for surface analysis of anti-wear films. Since AES operates in ultra-high vacuum, the samples need to be subjected to intensive cleaning for two reasons. One is that high levels of hydrocarbon contamination in high vacuum will disturb the vacuum by out-gassing. The second reason lies in the accuracy of the results. If a noticeable level of viscous hydrocarbon (from oil or the solvent used to clean it) is left on the sample, profiling by sputtering will not be as effective in characterizing the film. The contamination is repelled away as sputtering shaves away the surface layers, but quickly flows back into the depressed sputtered region.

As anti-wear films are known to be sensitive to chemical cleaning, a tradeoff exists between measurement accuracy and film removal through intensive cleaning. For example, certain chelating acids such as ethylenediaminetetraacetic acid (EDTA) have been found to rapidly remove films made by ZDDP and OBCaSu [25]. Researchers in the past have cleaned using hexanes and ethanol by rinsing, wiping or ultrasonic cleaning, but due to the different methods of cleaning a number of instances have been documented which reported differences in measured film thickness [10, 37, 38].

In light of this information, various methods of cleaning were attempted. Initial trials involved ultrasonic cleaning for 20 minutes with hexane. This resulted in "overcleaning," where the anti-wear film was dissolved from ~30nm to ~6nm. As hexane was adequate in cleaning the oil, following trials corrected for the film removal by reducing the cleaning time to 30 seconds. The result, as shown in figure 4-3, is a noticeable amount of (hydro)carbon contamination. The cause of the contamination may have been oil or hexane itself, as a visible hexane residue was found to remain on the samples after cleaning. To remedy this, a step-wise cleaning method was adopted. The sample was first lightly wiped with hexane to remove most of the oil and then ultrasonically cleaned in hexane for 2.5 minutes. It was then rinsed lightly in acetone to remove the hexane. The acetone was then rinsed off with water. Seemingly satisfactory

results were obtained with this method, but further literature review led to the realization that water rapidly removes the calcium-based tribofilms made from OBCaSu [25]. Another iteration followed in which the water rinsing was omitted, and this modified cleaning procedure was found to leave relatively little contamination while having minimal film disturbance.

However, it is important to note that if the longevity of the AES machine is not of concern, residual hydrocarbon contamination is not completely unfavorable and does not negate the entire analysis. At worst, there will be a misleadingly high signal for carbon, so calculations regarding elemental percentages in the film will be skewed. Besides this, the lack of cleaning means the crucial elements for analysis are left untouched, allowing for "truer" detection.

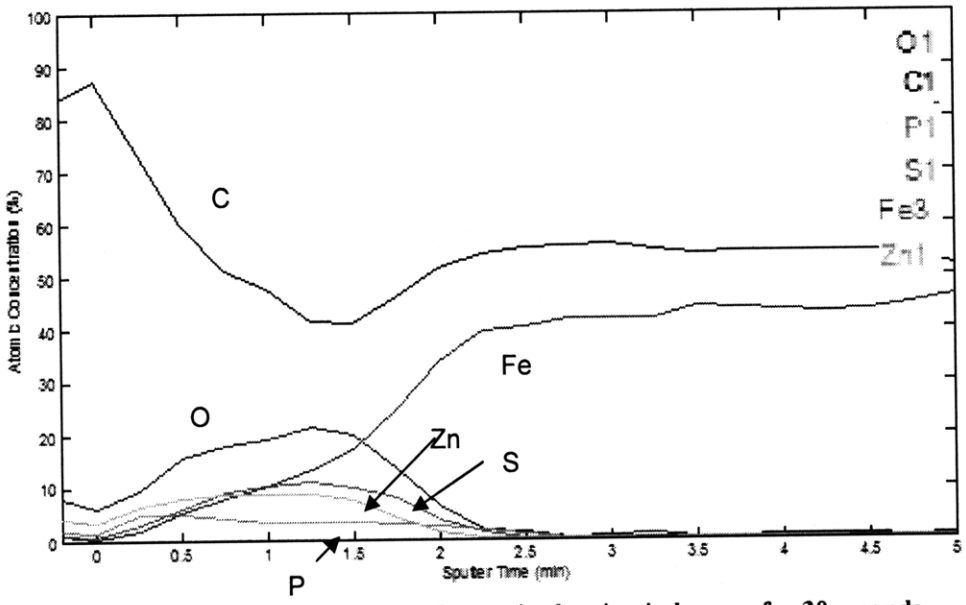

Figure 4-3 Depth profiling after ultrasonic cleaning in hexane for 30 seconds
A large amount of contamination remains, lingering on past the depth of the film, although the ZDDP film elements are clearly visible. Besides the carbon contamination, the minimal film disturbance achieved with this method is exceptional. Elemental profiling after sputtering for 5 minutes should have shown over 95% iron.

Analysis with AES was performed using a Physical Instruments PHI 700 Auger Spectrometer. Analyses consisted primarily of elemental depth profiling, using an Argon-ion gun operating at 2kV, 1μA and sputtering over a raster area of 2mm x 2mm. The etch rate was calibrated using a 50nm silicon oxide wafer. Settings that resulted in

an etch rate of 8nm/min were used, as it permitted economical analysis time and comparability with past studies [39, 40]. The sputter profile for the calibration wafer is shown in figure 4-4. The sudden change in atomic concentration signals the passage through the oxide layer.

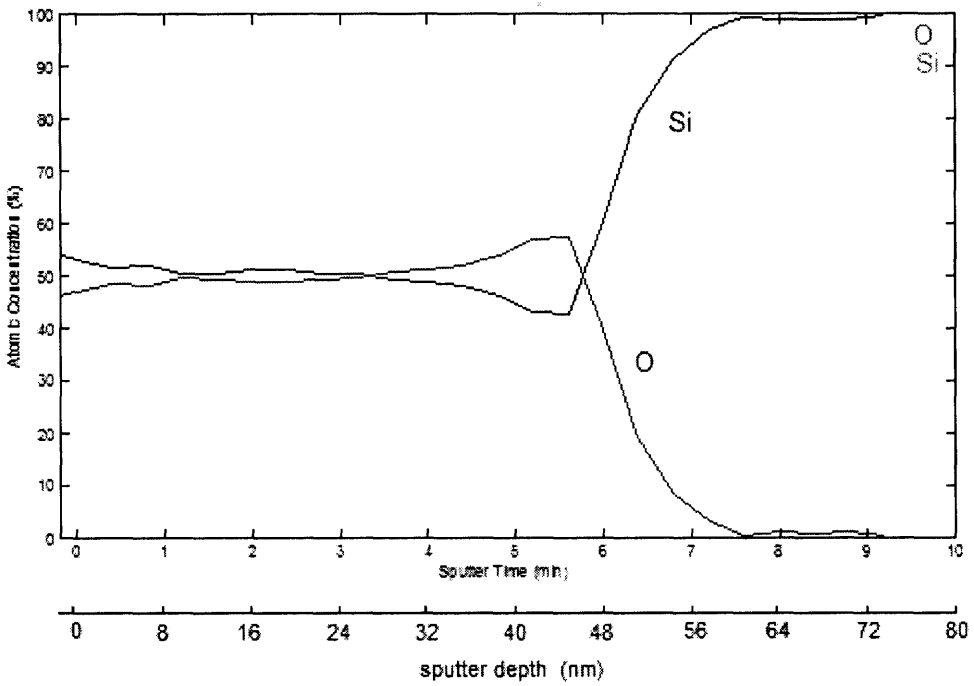

Figure 4-4 Sputter calibration using a 50nm silicon oxide wafer

Table 4-5 Operation settings for AES

Electron gun voltage	10kV
Electron gun current	10nA
Ion gun voltage	2kV
Ion gun current	1μA
Raster size	2 x 2mm
Sample position	30° tilt toward ion gun
Sputter rate	8nm/min SiO_2

As typical samples for AES are smaller than ~2cm x 2cm and weigh less than ~10 grams, effort was put into making analysis with AES physically possible for the 1" (2.54cm) x 1.4" (3.56cm), 18 gram steel sample. The standard AES sample mount was modified for weight reduction and an aluminum adaptor plate was fabricated to facilitate the mounting of the steel sample. Because the steel test plate was able to be directly placed in the AES

machine without destructive sample preparation, the plates were able to be reused for later tests.

5. Experimental Results and Analysis

5.1. Thermal Decomposition of ZDDP (Test A)

The P_{31}NMR spectra in the following plots show the presence of two peaks, a large peak at 92~93 ppm and a smaller peak at 99~100 ppm. These two peaks are attributed to the basic and neutral forms of ZDDP in equilibrium [16]. It is interesting to note that a number of changes occur as the ZDDP is introduced into the base oil. The peak corresponding to basic ZDDP decreases and shifts from 99 ppm to 99.8 ppm, suggesting an equilibrium shift from basic to neutral ZDDP and a mild interaction with the base oil, respectively. These results agree well with literature [16, 41]. Also, the neutral ZDDP peak location (chemical shift) is at 92.2 ppm for the oil samples containing 100% and 2.4% (0.2% phos.) ZDDP, but gradually shifts as detergent is added. At 3% OBCaSu, the chemical shift moves to 92.4 ppm, and 92.5 ppm at 6% OBCaSu. No further shifts are observed for the sample at 15% OBCaSu. Previous studies regarding ZDDP interactions with dispersants showed similar trends, with much larger shifts attributed to complexations [42]. Infrared spectroscopy studies by Ramakumar et al. have shown that small shifts in the P=S peak in the FTIR spectrum occur with the introduction of OBCaSu, and that these shifts are not due to complexations or the formation of chemical bonds but instead due to physical cohesion [20]. This is seen here as a small shift in the NMR peak.

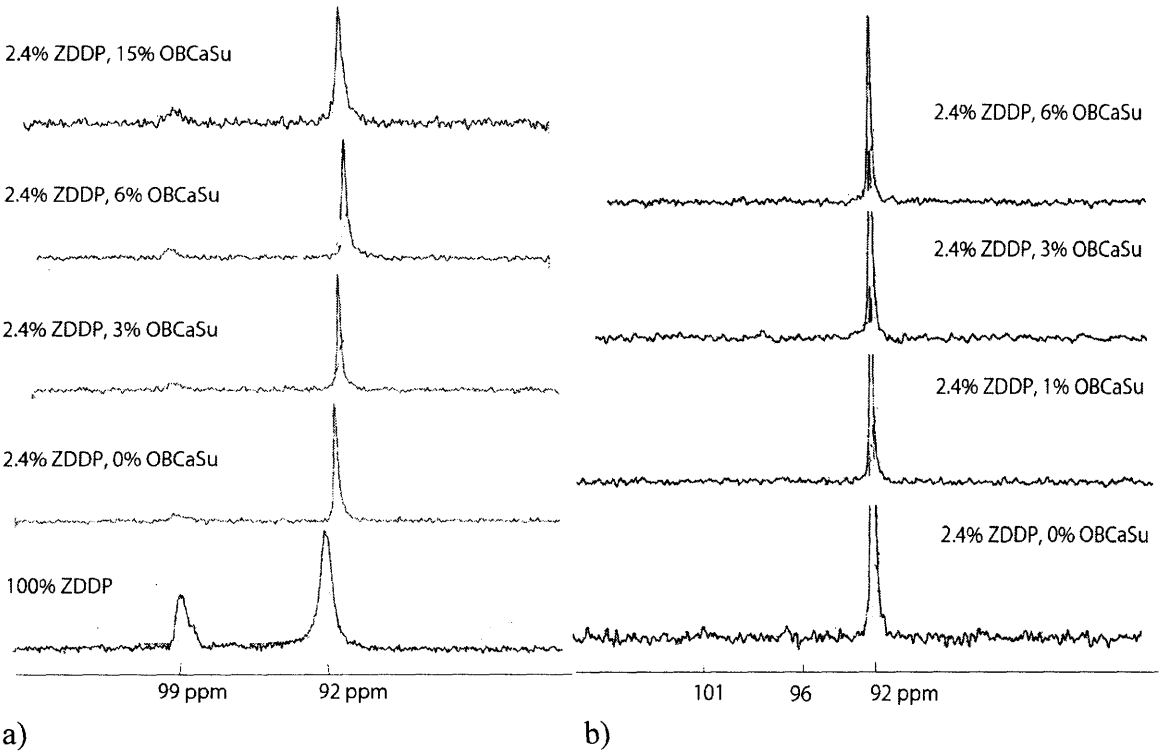

Figure 5-1 P31 NMR spectra for a) 2 hour and b) 15 hour heating tests at 120°C.
Note: The spectra are not precisely aligned with each other, so this display may not be used as a reference for peak shift. For larger size figures of the 2 hour heating teat, refer to Appendix D.

After 2 hours of heating at 120°C, a noticeable level of reduction can be seen for the basic form of ZDDP, while the neutral peak shows no signs of decrease. The decrease in the basic peak represents the reduction in the amount of basic ZDDP, which signifies a drastic change in chemical state or the reversion to its neutral form. Previous studies have shown that at elevated temperatures, the equilibrium is shifted towards the neutral ZDDP [2, 41, 13]. It is probable that a very small amount of decomposition is taking place for neutral ZDDP but is compensated by its replenishment from the reversion of basic ZDDP.

Figure 5-2 displays the effects of OBCaSu in the oil mixture through integration of the NMR spectra. As the concentration of OBCaSu is increased, the amount of basic ZDDP in the mixture is generally found to increase, though all cases show less basic ZDDP than before the heating. Similar trends have been observed in the past, in which OBCaSu was found to shift the ZDDP equilibrium towards the basic form [6].

Continued heating to 5 and 15 hours show a general disappearance of the basic peak, with the exception of 3% OBCaSu, even after 15 hours. With 15 hours of heating, the 0% OBCaSu spectrum develops a minor peak at 101 ppm from the intermediate products formed in the chemical transition from basic to neutral ZDDP [16]. However, at 120°C, even 15 hours of heating has little effect on neutral ZDDP decomposition. When the blends were heated to 150°C for 11 hours, complete decomposition was found as the NMR peaks had disappeared. Further testing at 150°C, heated for approximately 6 to 7 hours, may reveal a more clear effect of OBCaSu on ZDDP decomposition, as suggested in literature [8, 6, 43].

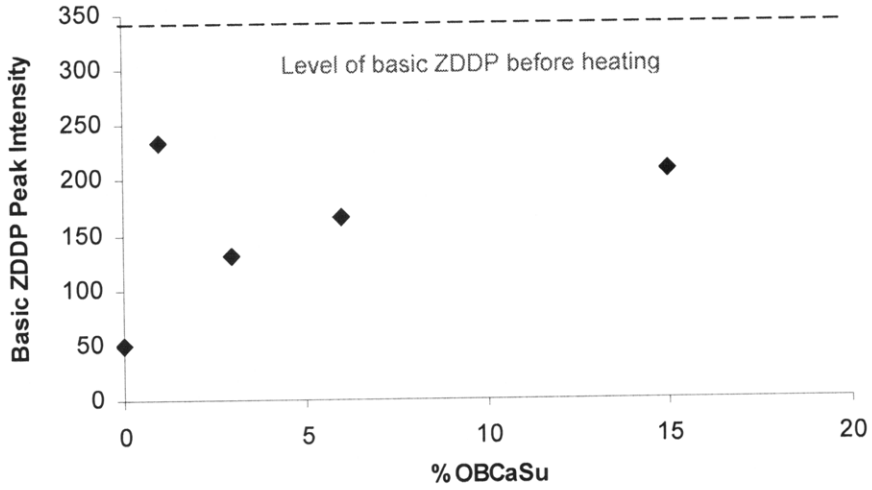

Figure 5-2 Effect of OBCaSu on the level of basic ZDDP in oil solution.
The values are integrated results of P_{31} NMR spectra. Data taken after 2 hours of heating.

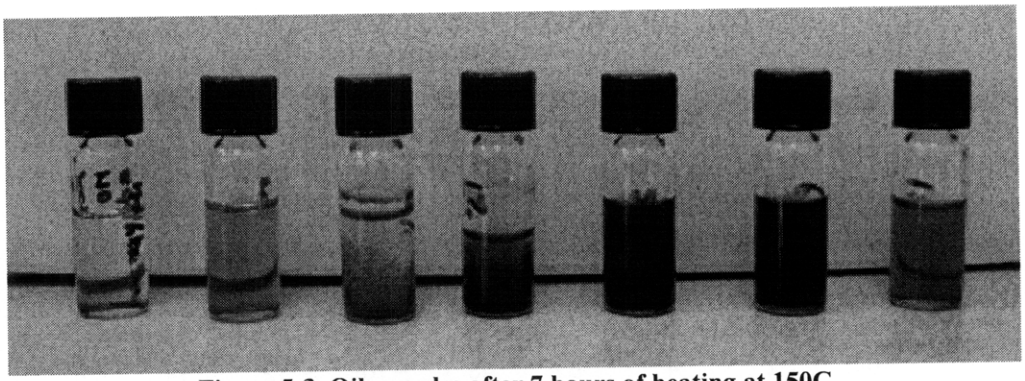

Figure 5-3 Oil samples after 7 hours of heating at 150C
From the left: base oil, no heating for visual reference // base oil // 2.4%ZDDP // 2.4%ZDDP+1%OBCaSu // 2.4%ZDDP+3%OBCaSu // 2.4%ZDDP+6%OBCaSu //2.4%ZDDP+15%OBCaSu

A visible change was observed after 7 hours of heating at 150°C (figure 5-2). Oxidation occurs in the base oil, causing a color change from clear to orange. The ZDDP decomposition takes a visible form, as solid crystalline precipitates form in the solution. This matches well with documented observations, which found the precipitates to be high in zinc and oxygen content [43]. For high ZDDP--OBCaSu ratios, the precipitates are visible and separated from the base oil. However for low ZDDP--OBCaSu ratios (towards the right on figure 5-3), the detergent either solubilizes the precipitates or strongly suppresses decomposition and crystallization. The blend with 15% OBCaSu closely resembles the heated base oil in color.

5.2. Thermal Film Formation

Oils containing 2.4% ZDDP (0.2% Phos.) and 0%, 1%, 3%, 6% and 15% OBCaSu were heated with metal coupons for 2 hours at 120°C. These tests were performed using fresh ZDDP and aged ZDDP, which was pre-heated at 150°C for 11 hours.

5.2.1. Film Formation from Fresh ZDDP (Test B)

The thicknesses of thermal films formed on metal coupons were measured using AES and are summarized in figure 5-4. The addition of even 1% OBCaSu significantly affects the thickness of film deposited, with increasing levels of detergent having marginal effect.

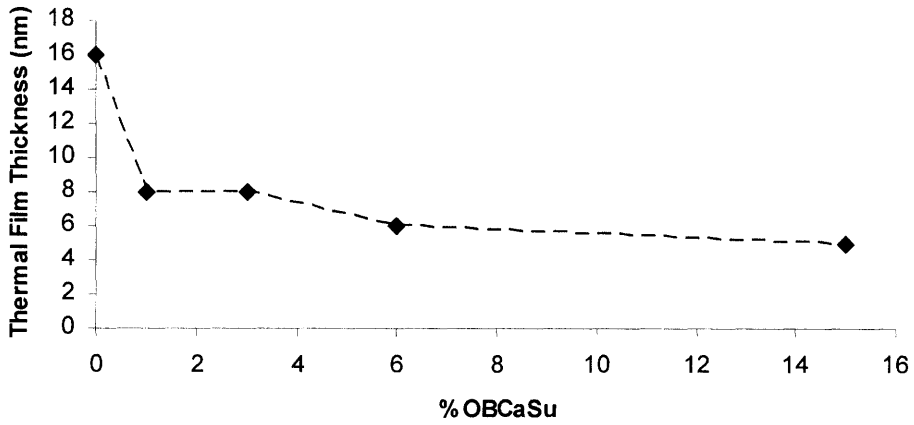

Figure 5-4 Thermal film thickness for 2 hour heating tests with fresh ZDDP in the presence of various levels of OBCaSu

These samples were analyzed with AES before the most appropriate cleaning process was determined, and hence relatively large amounts of carbon remain as residue. It is also possible that calcium deposits / films were removed during cleaning, as the samples were water-rinsed. Thus, although quantitative percentages of the elements cannot be accurately deduced from the data, measurement of the ZDDP-based films is not affected. Film thickness can be measured from the presence of zinc, sulfur and phosphorous. Reading the AES plot, the decrease in zinc, sulfur and phosphorous signifies the gradual transition from the film to the iron substrate (and therefore an increase in iron). For the purposes of this study, the anti-wear film will be represented by the depth penetration of zinc, phosphorous and sulfur. A schematic representation is shown in figures 5-5 ad 5-6. A noticeable trend with increasing OBCaSu is the increase in the relative concentration of sulfur in respect to zinc, suggesting sulfonate as another source of sulfur.

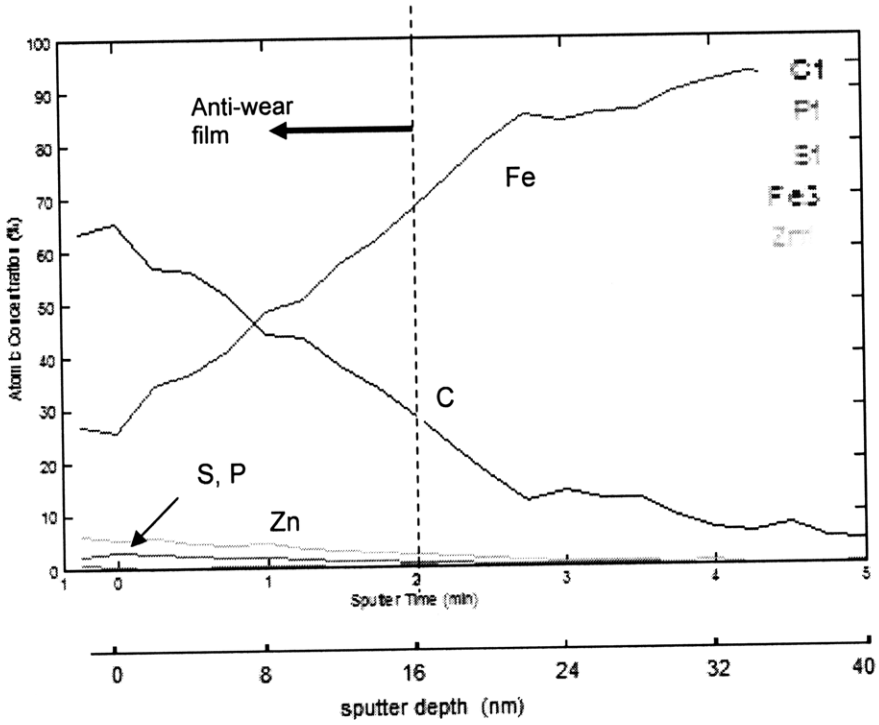

Figure 5-5 AES elemental depth profiling of thermal film with 2.4% ZDDP (0.2% Phos.) and 0% OBCaSu

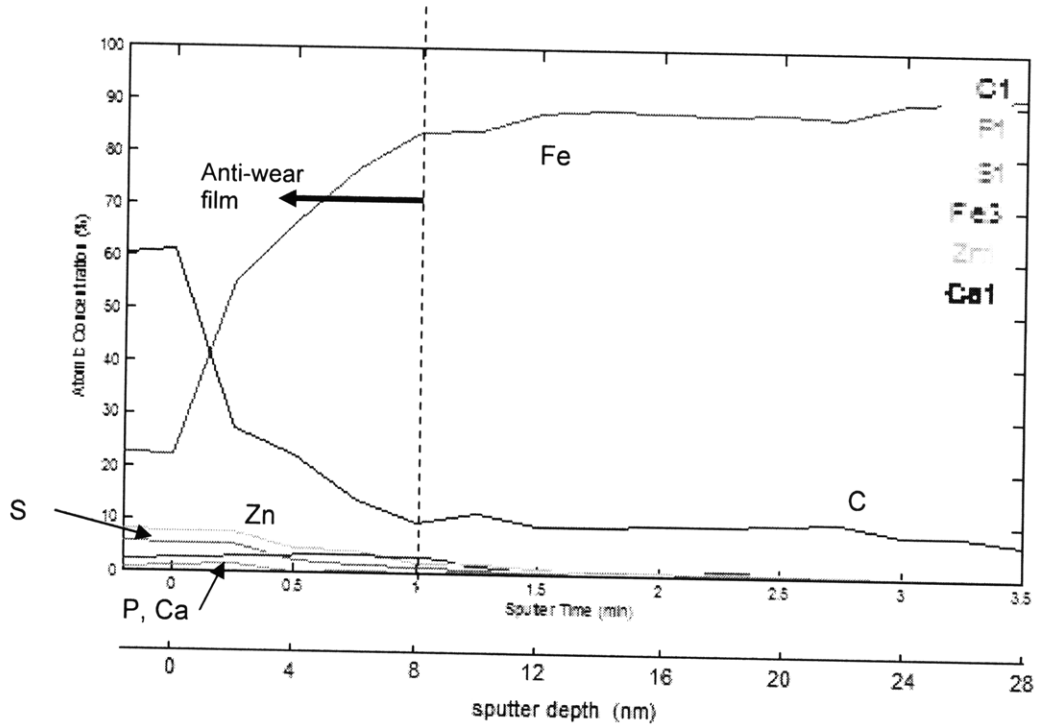

Figure 5-6 AES elemental depth profiling of thermal film with 2.4% ZDDP (0.2% Phos.) and 1% OBCaSu

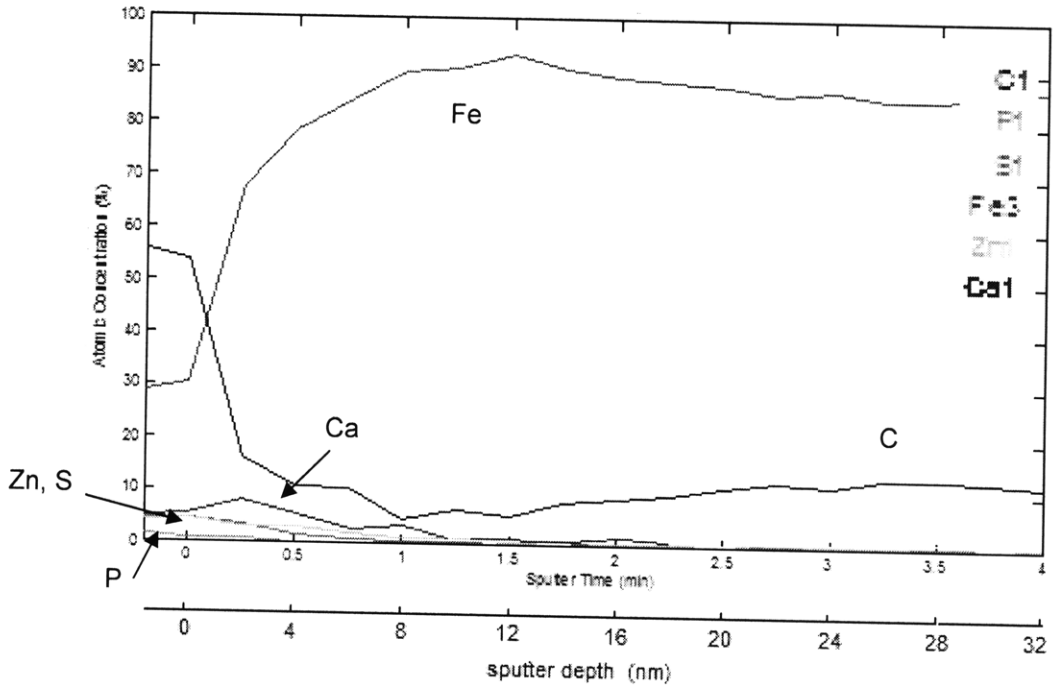

Figure 5-7 AES elemental depth profiling of thermal film with 2.4% ZDDP (0.2% Phos.) and 15% OBCaSu

5.2.2. *Film Formation from Aged ZDDP (Test C)*

Though the effect of OBCaSu is similar to the previous test with fresh ZDDP, the films are noticeably thinner. As there are more ZDDP decomposition products with aged oil, this could suggest higher OBCaSu activity in solubilizing these products or disturbing their interactions with metal surface. Another possibility is that the significant decomposition of ZDDP in the absence of metal resulted in the formation of crystalline precipitates, which may be useless for film formation.

The addition of OBCaSu halves the thermal film thickness (figure 5-8). Again, the addition of 1% OBCaSu drastically changes the thickness and composition of the film, with additional OBCaSu having observable, but less effect. Unlike the case with fresh oil, high concentrations of OBCaSu are found on the surface. It is not definitive, however, whether any film is formed at all with the addition of OBCaSu, as the films are so thin they may simply be adsorbed ZDDP molecules.

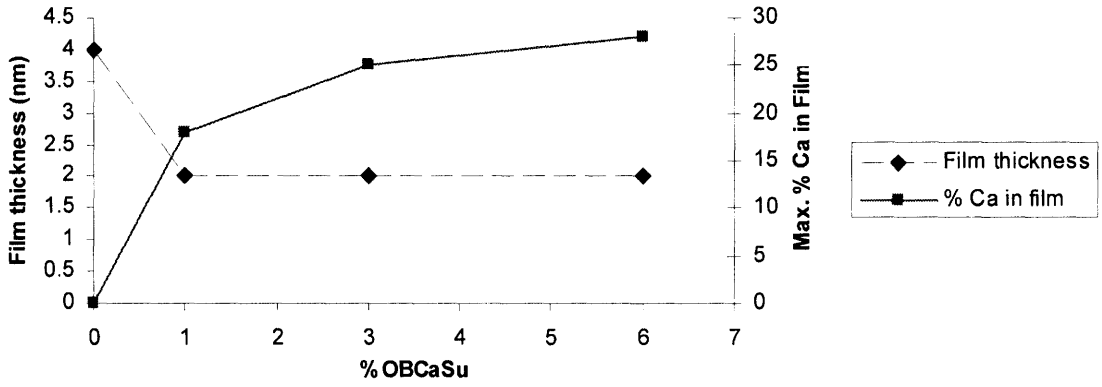

Figure 5-8 Thermal film thickness and level of calcium inclusion for 2 hour heating tests with aged ZDDP and OBCaSu. Measurements taken with AES.

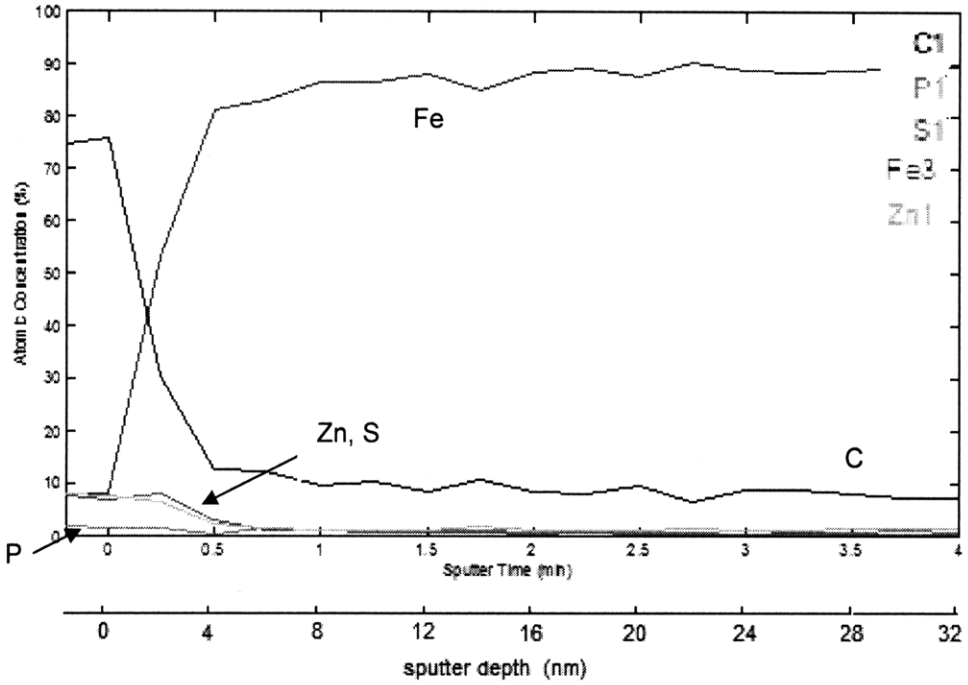

Figure 5-9 AES elemental depth profiling of thermal film with 2.4% ZDDP (0.2% Phos.) and 0% OBCaSu

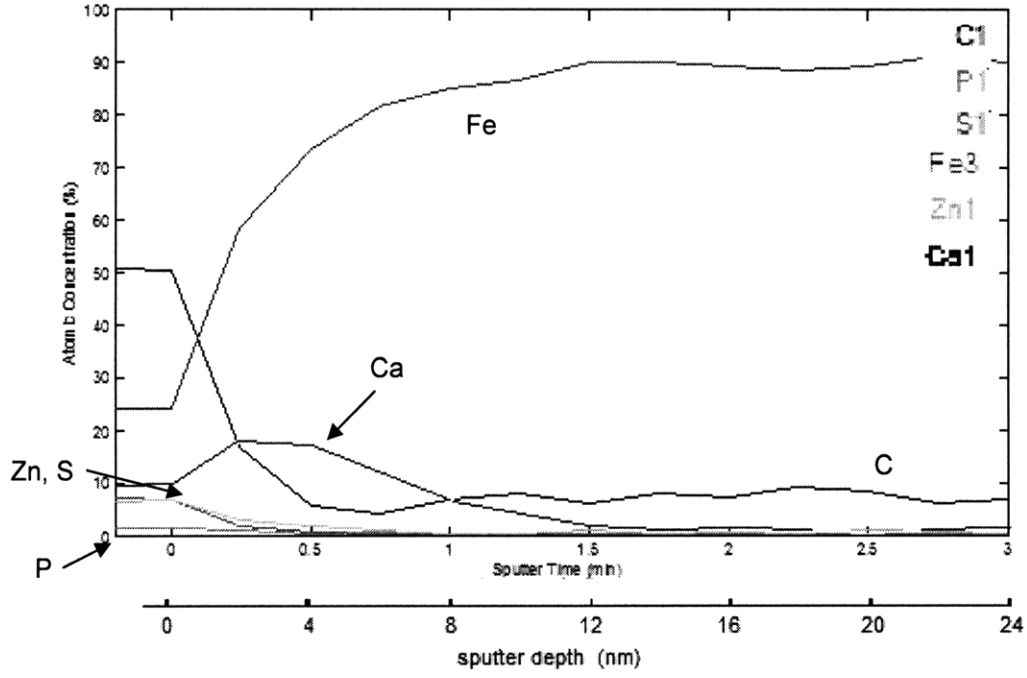

Figure 5-10 AES elemental depth profiling of thermal film with 2.4% ZDDP (0.2% Phos.) and 1% OBCaSu

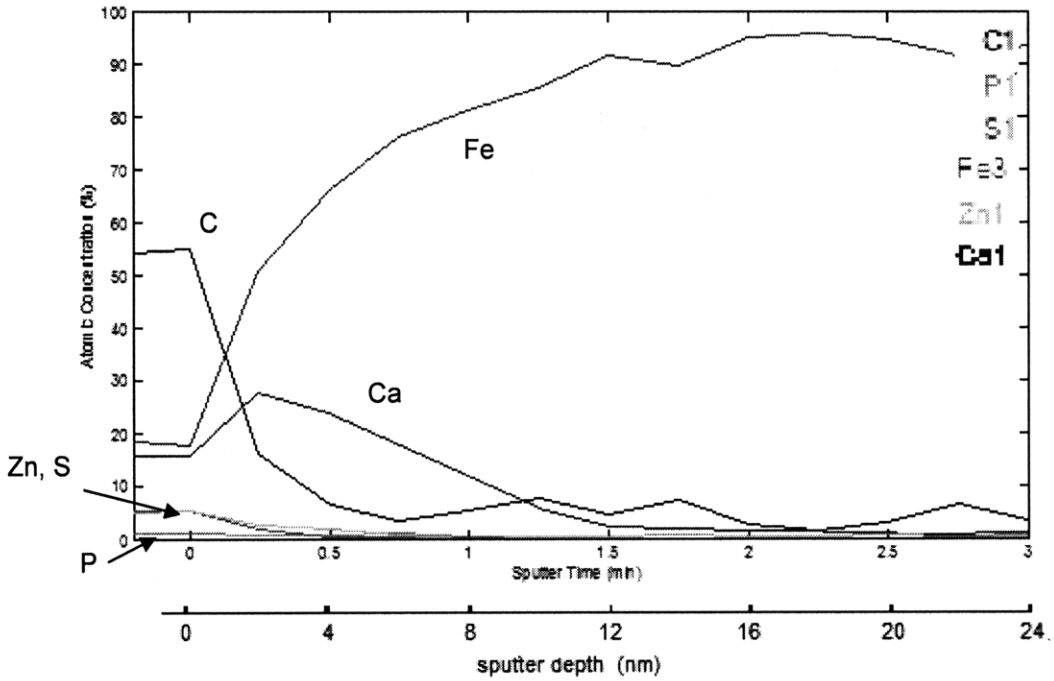

Figure 5-11 AES elemental depth profiling of thermal film with 2.4% ZDDP (0.2% Phos.) and 6% OBCaSu

5.3. Tribometer Tests

Rubbing tests were performed in light boundary lubrication for the oil blends containing 2.4% ZDDP and 0, 0.5, 1 and 3% OBCaSu. A separate blend, consisting of no ZDDP and 3% OBCaSu was also tested, to check if any film will be made from OBCaSu alone. The cylinder was rotated at 50 RPM (23 cm/s) with a load of 16 kg. The loading for this geometry was equal to a maximum Hertzian pressure of 60 MPa. The oil and the plate test piece were maintained at 105° C.

5.3.1. ECR and Friction Measurements

The development of the tribofilm was seen through the ECR measurements as a drop in voltage due to an increase in interface resistance. The addition of low levels of OBCaSu was not found to significantly affect the induction time of the film. It did, however, affect the rate of film development, seen in the rate of increase in contact resistance.

From 0% to 1% OBCaSu, the film formation drastically slowed. The decrease in measured film formation may have been due to either an overall slower film growth or the growth of a less robust film. Since the entire line contact between the metal surfaces is used in measuring interfacial contact resistance, the robustness of the film affects greatly the ECR measurement. A weaker film could lead to local metal-metal contact, thus decreasing the observed resistance.

0.5% and 1% OBCaSu runs produced nearly identical ECR traces and were only different in friction. The test with 3% OBCaSu resulted in an ECR trace different from the others with OBCaSu; the induction of the anti-wear film was noticeably faster (figure 5-16). The blend with only OBCaSu was found to produce an anti-wear film on its own, which suggests that the early induction of the film seen in the 2.4% ZDDP +3% OBCaSu test may have been due to OBCaSu instead of ZDDP. While a maximum contact resistance of 0.9 Mohm was reached with ZDDP, OBCaSu blends resulted in only a fraction of such resistance. The film formed only from OBCaSu produced a moderately resistive film, though prolonged rubbing gradually caused its removal.

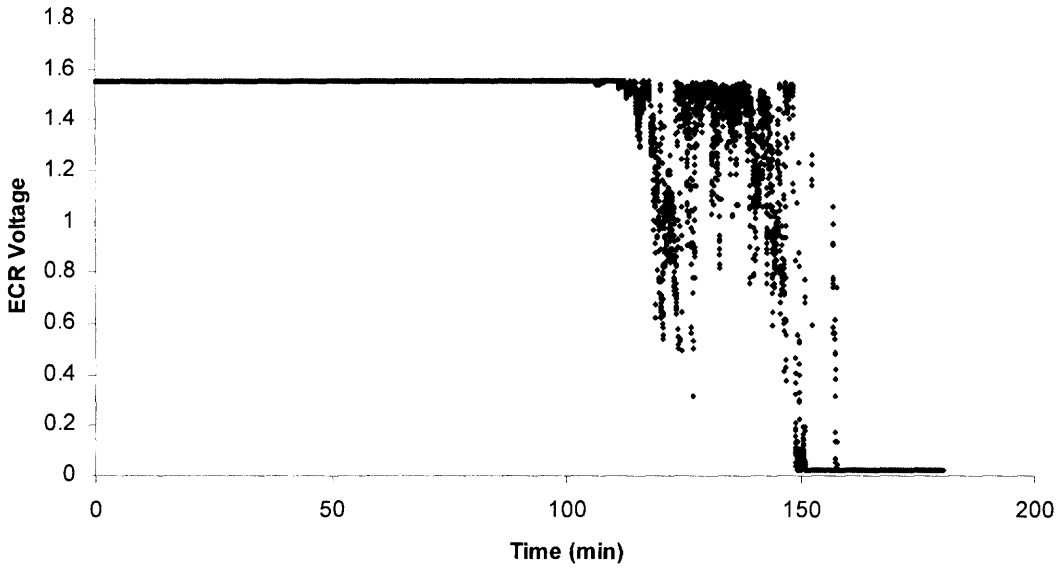

Figure 5-12 ECR trace for 2.4% ZDDP, 0% OBCaSu

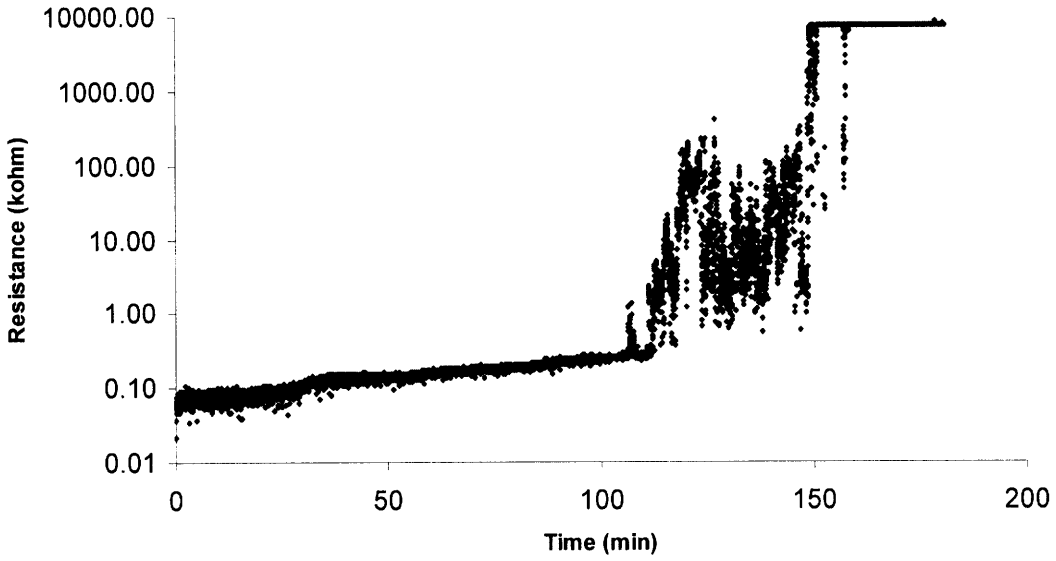

Figure 5-13 Resistance trace for 2.4% ZDDP, 0% OBCaSu
Y axis is logarithmic.

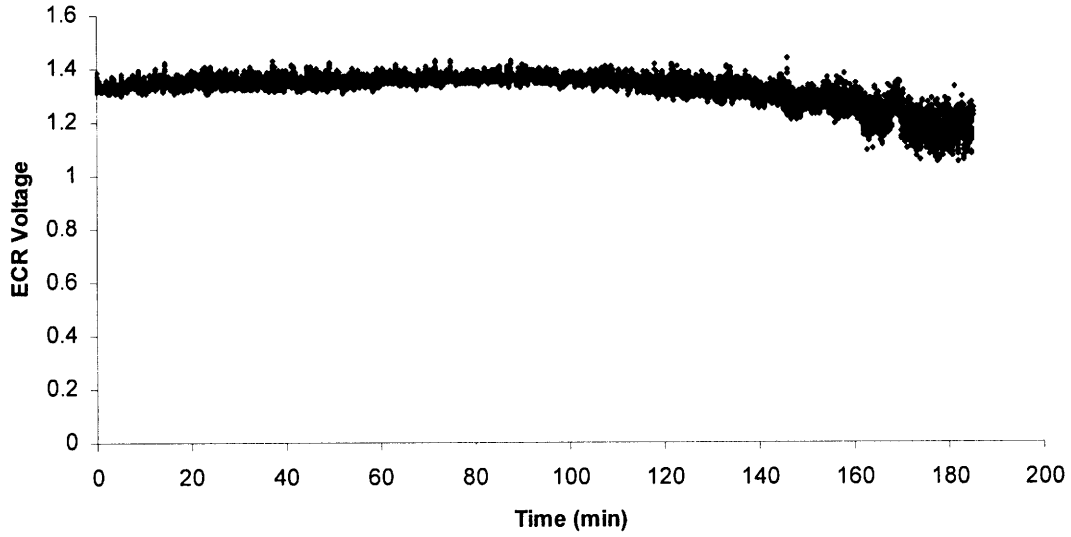

Figure 5-14 ECR trace for 2.4% ZDDP, 1% OBCaSu

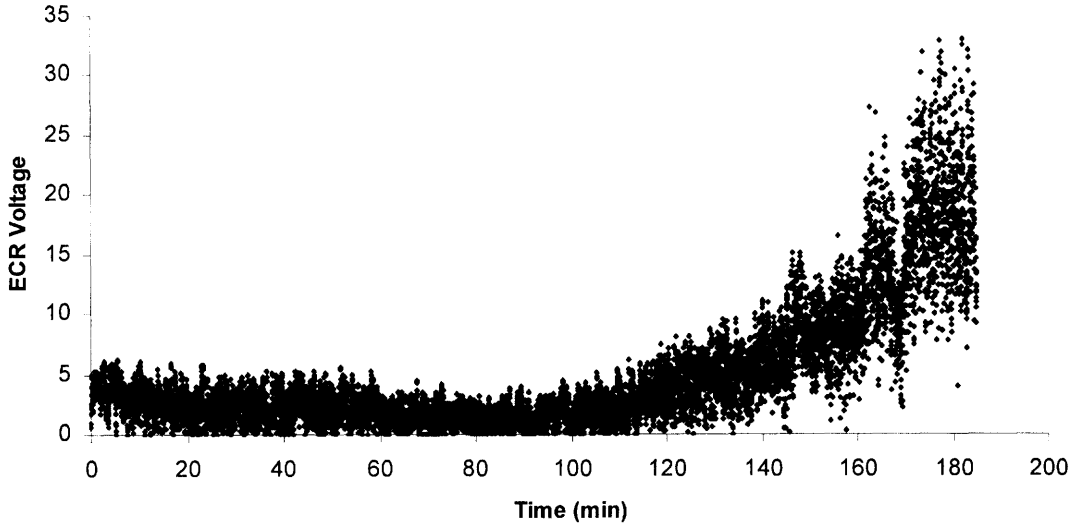

Figure 5-15 Resistance plot for 2.4% ZDDP, 1% OBCaSu

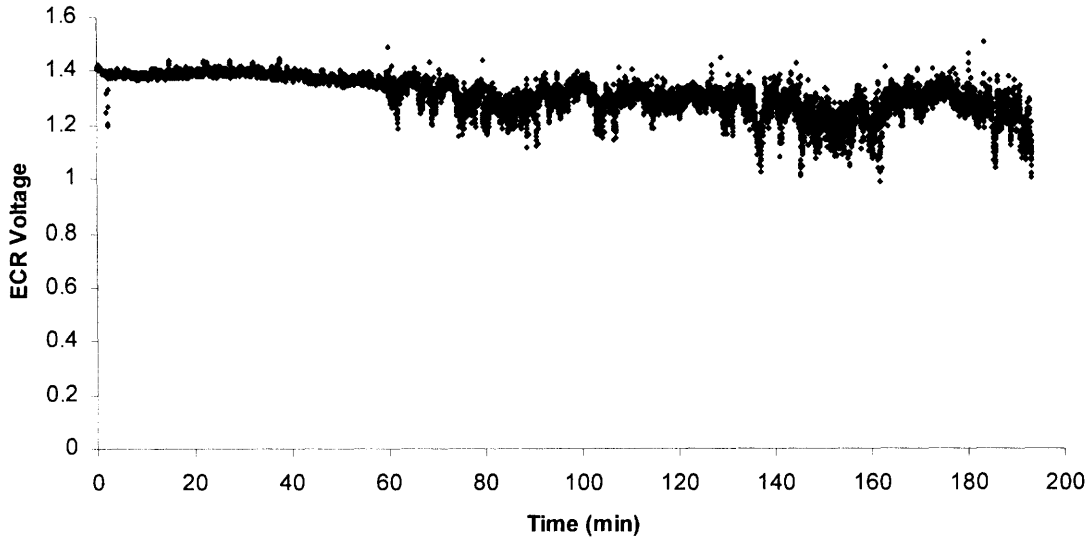

Figure 5-16 ECR trace for 2.4% ZDDP, 3% OBCaSu

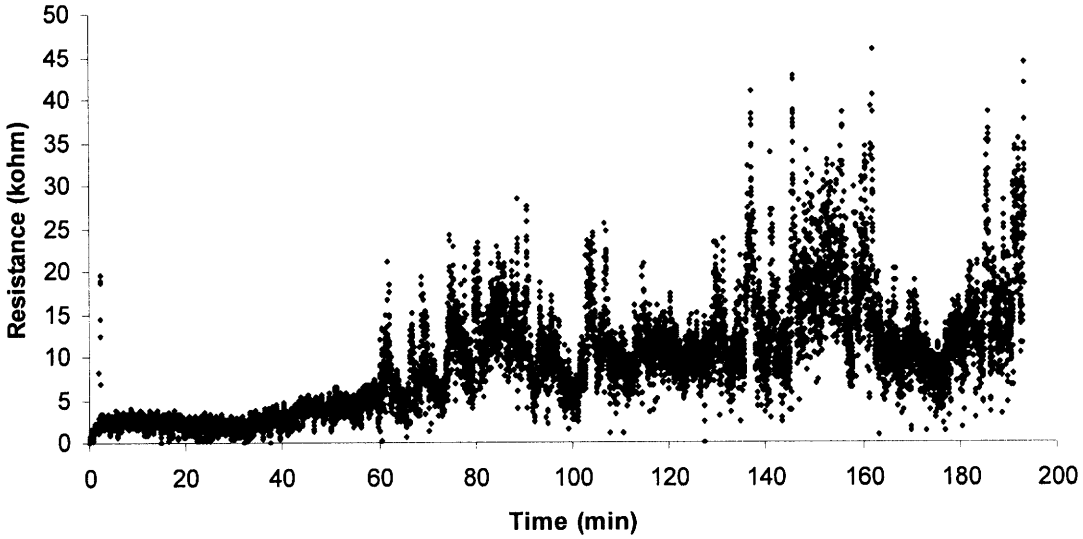

Figure 5-17 Resistance trace for 2.4% ZDDP, 3% OBCaSu

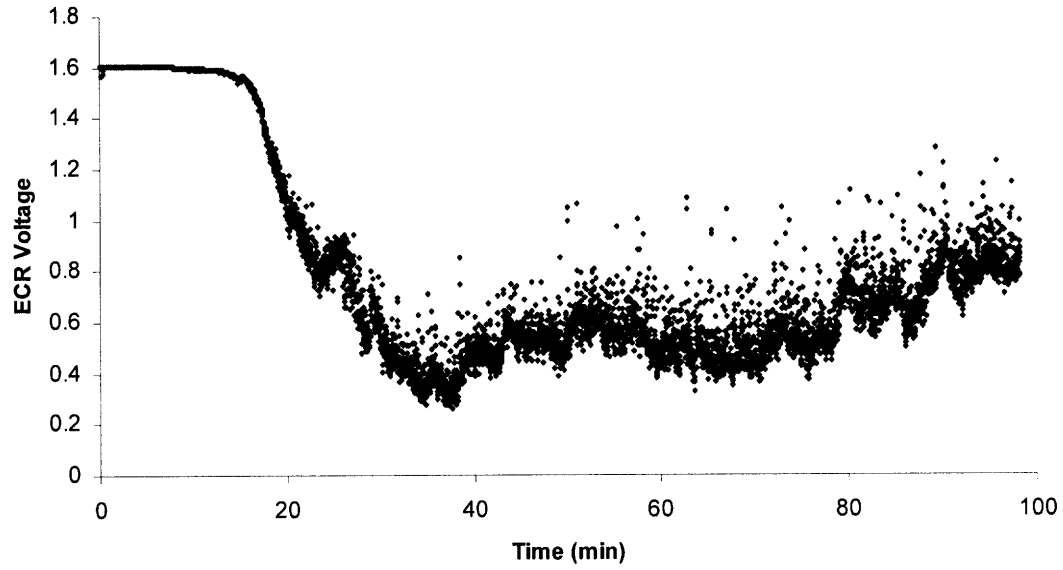

Figure 5-18 ECR trace of 0% ZDDP, 3% OBCaSu

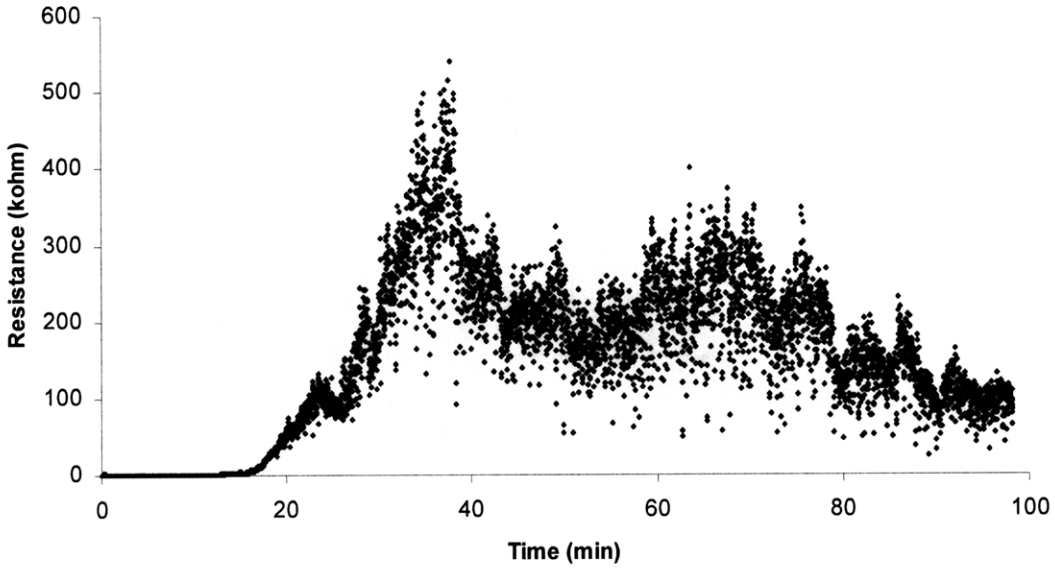

Figure 5-19 Resistance trace for 0% ZDDP, 3% OBCaSu

Friction traces are shown in figure 5-20 below. The presence of a hump (or the lack thereof) in the first few minutes of testing is due to the running in of the metal pieces. Although mixed in the extent, friction generally increased with the presence of OBCaSu. The greatest friction was observed with 1% OBCaSu, although all runs with OBCaSu exhibited similar final values.

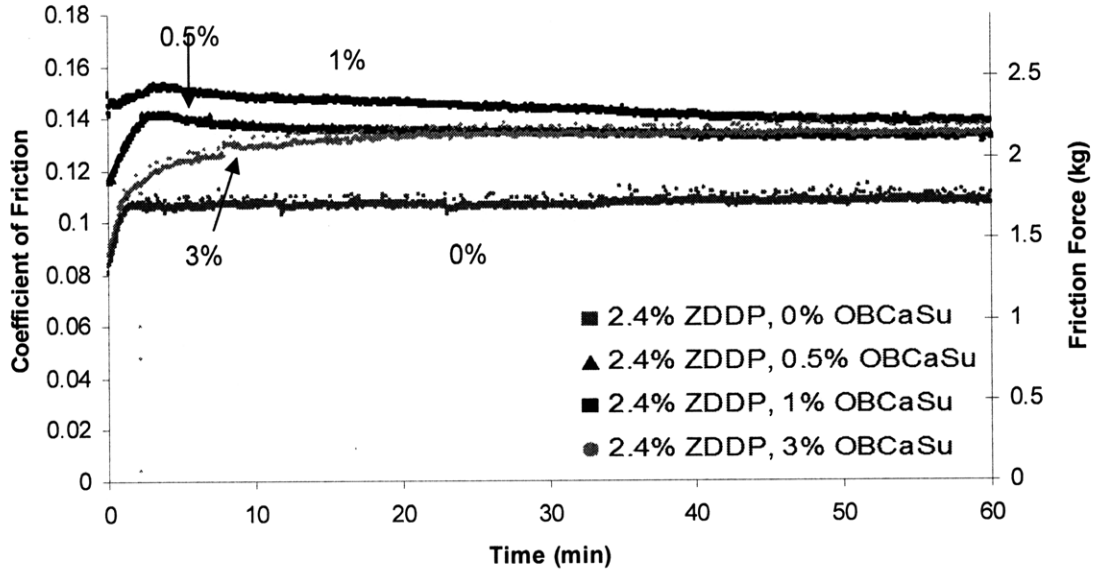

Figure 5-20 Coefficient of friction trace for the various oil blends.
Graph shows up to 60 minutes, as little change was observed after then.

5.3.2. Depth Profiling with AES

Selected AES profiles of the tribofilms developed with the different oil blends are shown in the graphs below. An AES trace of ZDDP tribofilms measured by Yamaguchi et al. is also reproduced in figure 5-25. Besides the inclusion of calcium and carbon from hydrocarbon contamination, the AES traces from this study resemble the representative AES trace of figure 5-25.

The addition of OBCaSu resulted in a substantial suppression of the ZDDP-based tribofilm. Profiles from 1% and 3% OBCaSu were nearly identical in composition and film thickness. In both, zinc and phosphorous are low in concentration and disappear after ~20 nm, while an overwhelming concentration of calcium persists. If the calcium is considered to be representative of an OBCaSu-based film, the total tribofilm continues onto ~40 nm for both 1% and 3% OBCaSu. Similar trends were found for the test with 0.5% OBCaSu but with a slightly thinner total tribofilm (~30nm). In the absence of OBCaSu, the tribofilm thickness is about 20 nm. The difference in thickness under the same lubricating conditions suggests not only an interaction between the additives but a different film forming mechanism.

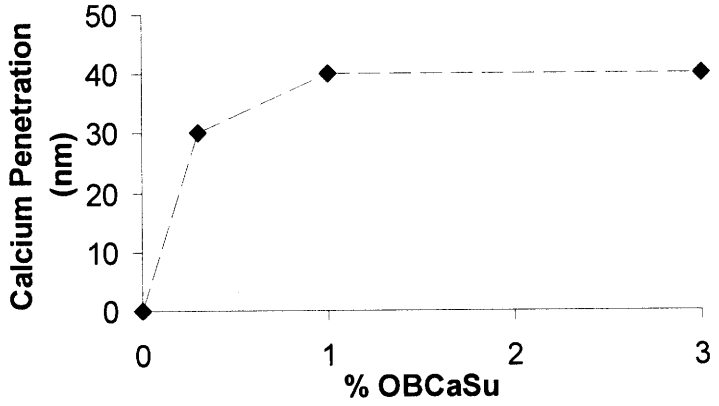

Figure 5-21 Depth of calcium inclusion in tribofilm. Measured with AES.

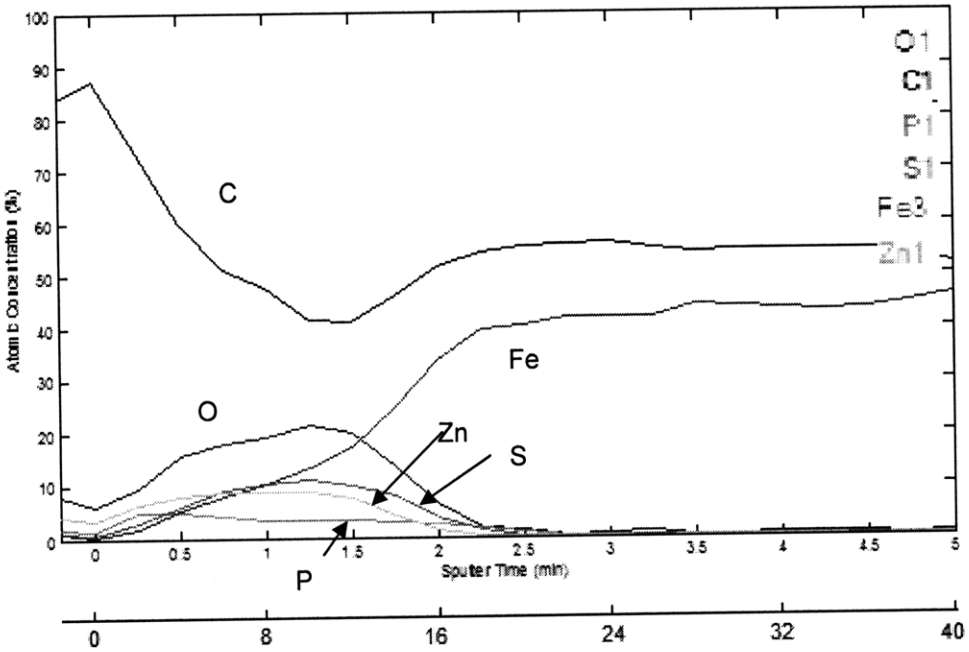

Figure 5-22 AES elemental depth profiling of tribofilm with 2.4% ZDDP (0.2% Phos.)
Significant carbon contamination exists due to incomplete cleaning, but ZDDP film elements are left untouched.

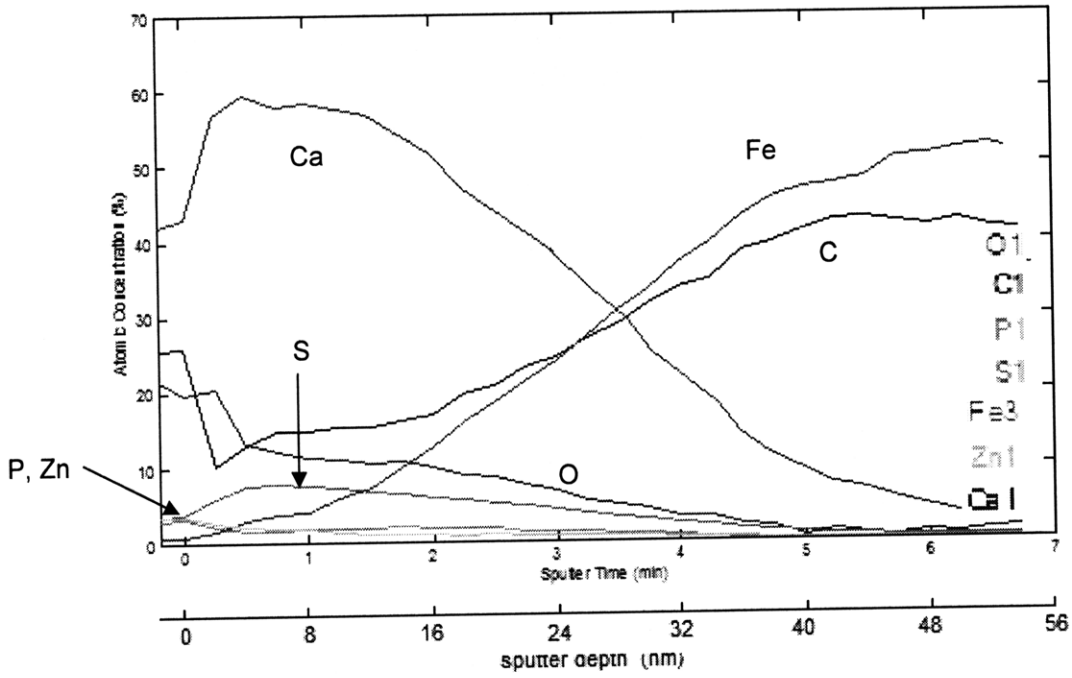

Figure 5-23 AES elemental depth profiling of tribofilm with 2.4% ZDDP (0.2% Phos.) and 1% OBCaSu.
A misrepresentative large carbon signal is present throughout the plot. Refer to Appendix-E for a detailed explanation.

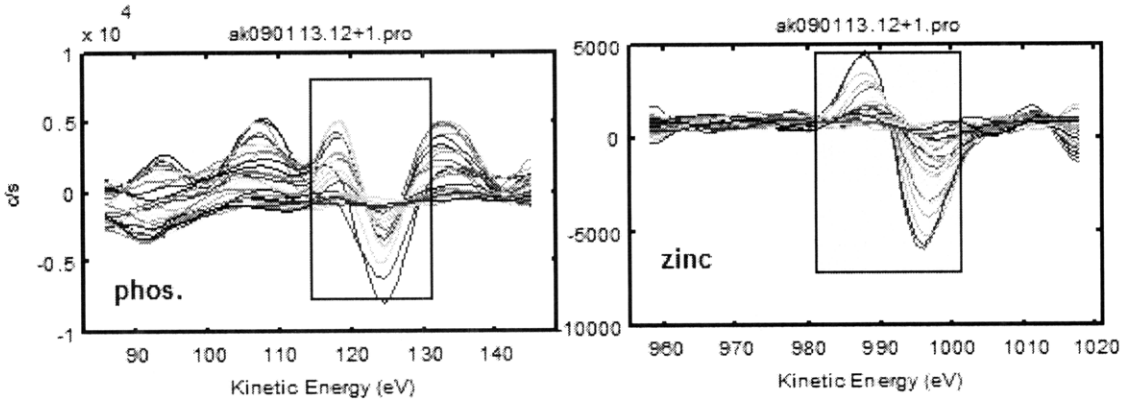

Figure 5-24 AES spectrum of tribofilm with 2.4% ZDDP (0.2% Phos.) and 1% OBCaSu. Multiple plots represent measurements made after each round of sputtering. Although figure 5-21 shows phosphorous and zinc to be in minute concentrations, their presence can be confirmed by the peaks shown.

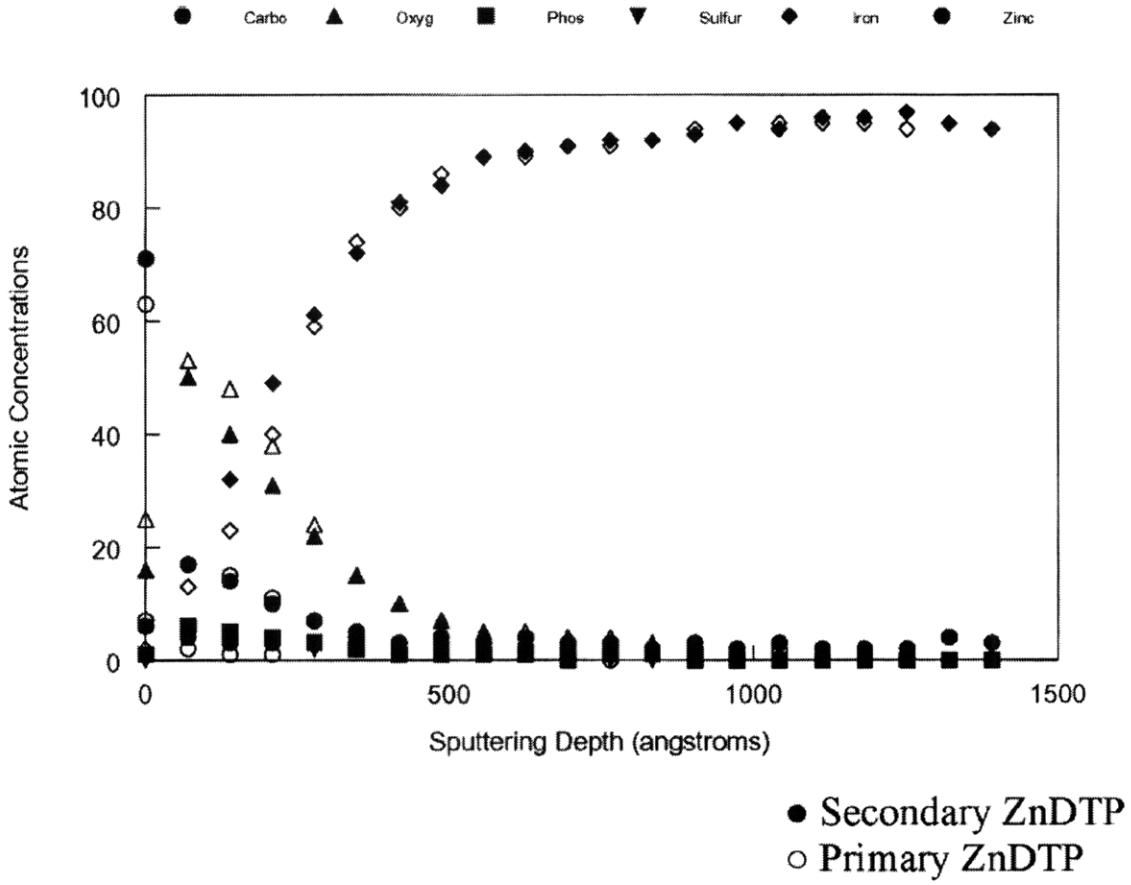

Figure 5-25 Representative AES trace for ZDDP tribofilms taken from a past study by Yamaguchi et al. [39]

5.3.3. Wear Scar Analysis

5.3.3.1. Wear Scar Size

For the conditions tested, the addition of OBCaSu had mixed results. The average wear scar of the plate test piece scoring with higher concentration of OBCaSu, a significant amount of scoring on the cylinder was also observed. Though the cylinder score marks were large enough to feel by hand (figure 5-27), every mark was found to be scratch into the cylinder, without any asperity protrusions. Due to the size and weight of the cylinder, profilometric and microscopic analysis was not possible and thus a quantifiable definition of scoring was difficult to establish. However, for sake of reference, scoring for each test is shown in figure 5-28. The wide wear scar in the 1% OBCaSu run is likely to have caused the higher friction (Section 5.3.1). In addition to the scoring, the each test with ZDDP and OBCaSu resulted in a mild, yet noticeable level of non-scoring wear, which can also be seen in figure 5-28. Interestingly, OBCaSu alone provided a level of wear protection quite comparable to ZDDP.

Table 5-1 Wear Scar widths.
(See Figure 5-28 for scoring.)

% ZDDP	% OBCaSu	Wear Scar Width	Cylinder Wear
2.4	0	0.27	negligible
2.4	0.5	0.65	scoring
2.4	1	0.76	scoring
2.4	3	0.5	deep scoring
0	3	0.4	negligible

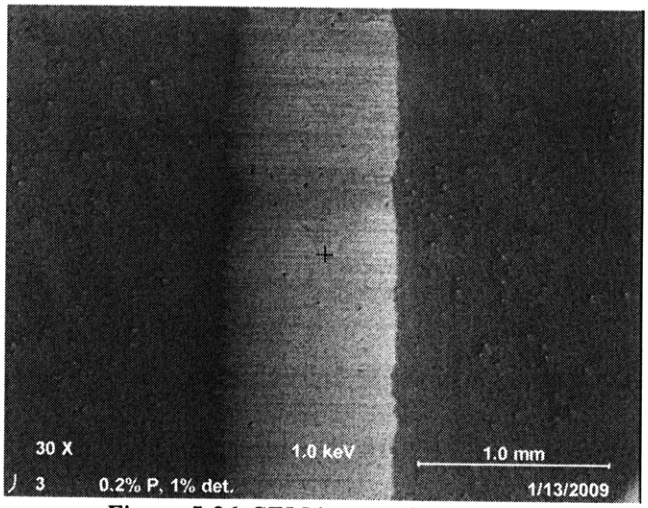

Figure 5-26 SEM image of wear scar.

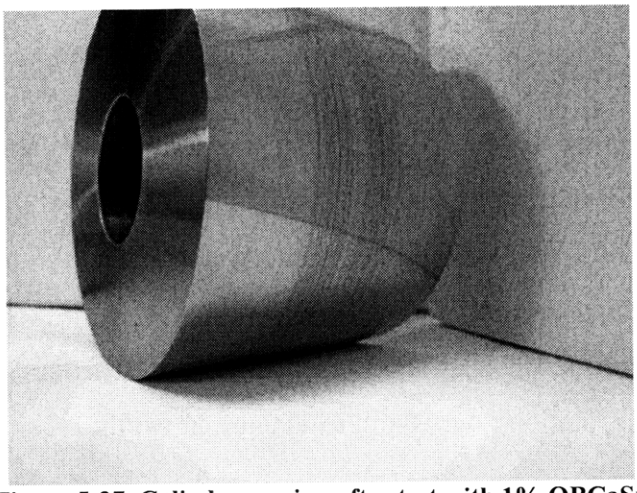

Figure 5-27 Cylinder scoring after test with 1% OBCaSu

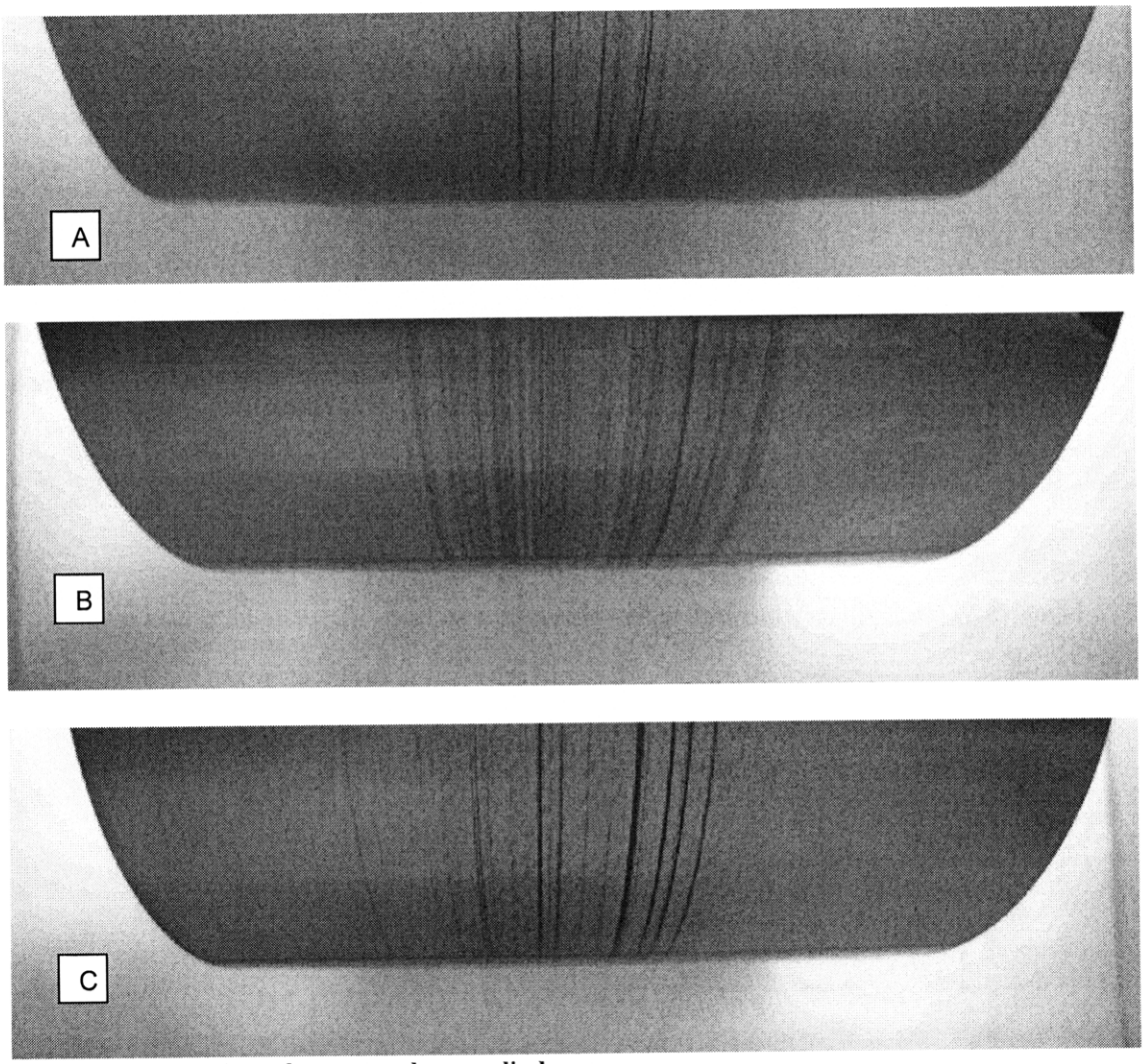

Figure 5-28 Top view of score marks on cylinder.
A) 2.4% ZDDP, 0.5% OBCaSu. B) 2.4% ZDDP, 1% OBCaSu. C) 2.4% ZDDP, 3% OBCaSu

5.3.3.2. Microstructure Analysis of Wear Scar

The most observable effect of OBCaSu on the ZDDP-lubricated wear scar was the formation of what seemed to be solid agglomerates. Evaluating these agglomerates with elemental analysis showed that the particles contained calcium and phosphorous but no iron (figure 5-27). These particles were found to be embedded in locations matching the deep grooves cut into the cylinder. A significant amount of these particles were found even in tests with only 0.5% OBCaSu. Their sizes ranged from 10 μm to 600 μm in length (along cylinder rotation) and 10 μm to 150 μm in width.

As shown in figure 5-26, the agglomerate particles were found to be clustered close to the locations that were scored on the plate; the particles are likely to have caused these marks. These score marks matched the locations of the scoring found on the cylinder.

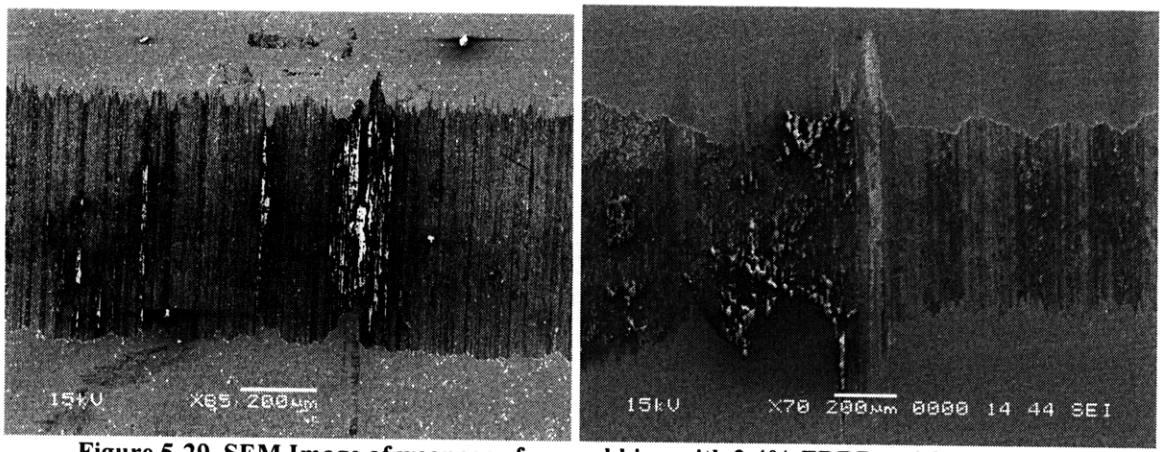

Figure 5-29 SEM Image of wear scar from rubbing with 2.4% ZDDP and 3% OBCaSu.

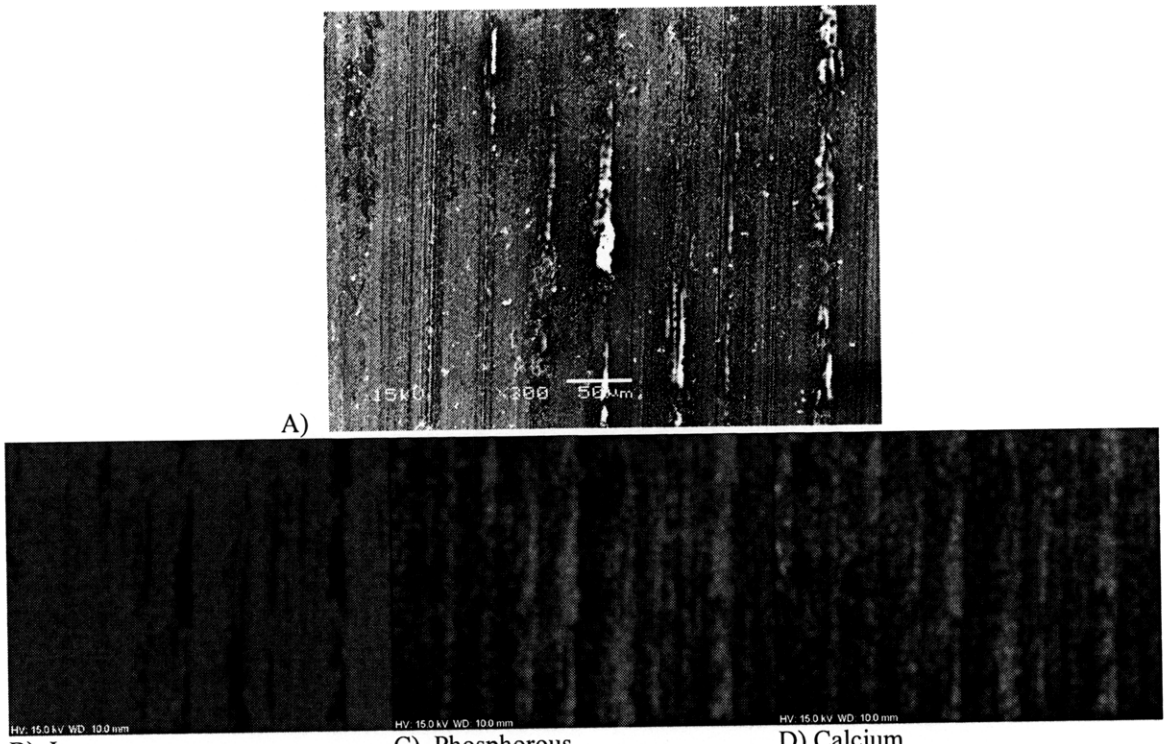

A)

B) Iron C) Phosphorous D) Calcium

Figure 5-30 SEM elemental images of wear scar from rubbing with 2.4% ZDDP and 3% OBCaSu. Elemental images B), C), and D) were taken at the location shown in A)

In locations on the wear scar that were not marked by significant scoring, a difference was still observed. Whereas the scar from the 0% OBCaSu test was "smooth," all tests with OBCaSu and ZDDP were marked with "rough" patches. Close microscopy views of the wear scars revealed a generally cellular structure, with the rough patches being cavitations of the structure.

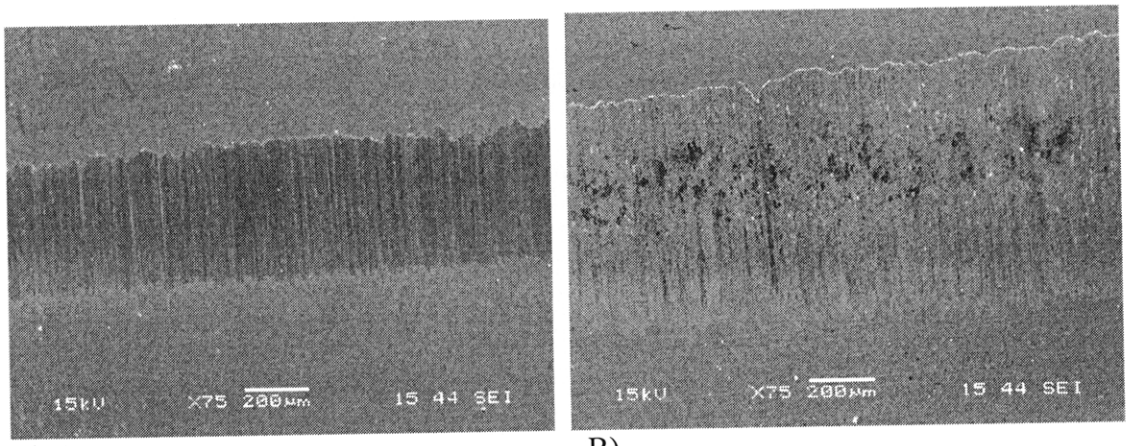

A) B)

Figure 5-31 Rough spots on wear scar with OBCaSu
A) shows the "smooth" wear scar from 2.4% ZDDP, 0% OBCaSu. B) shows the scar from 2.4% ZDDP, 3% OBCaSu. The images are of equal magnification.

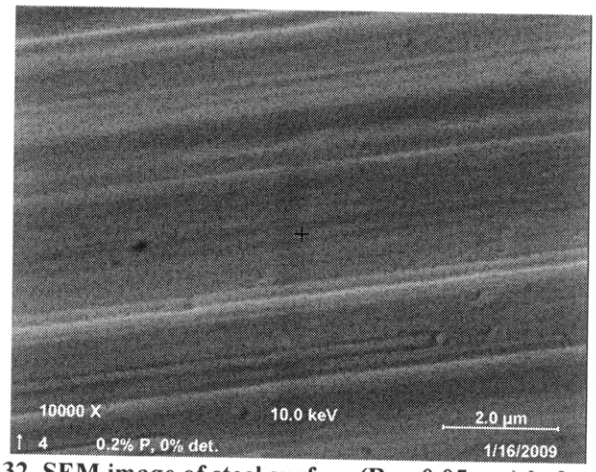

Figure 5-32 SEM image of steel surface (Ra ~0.05 µm) before rubbing

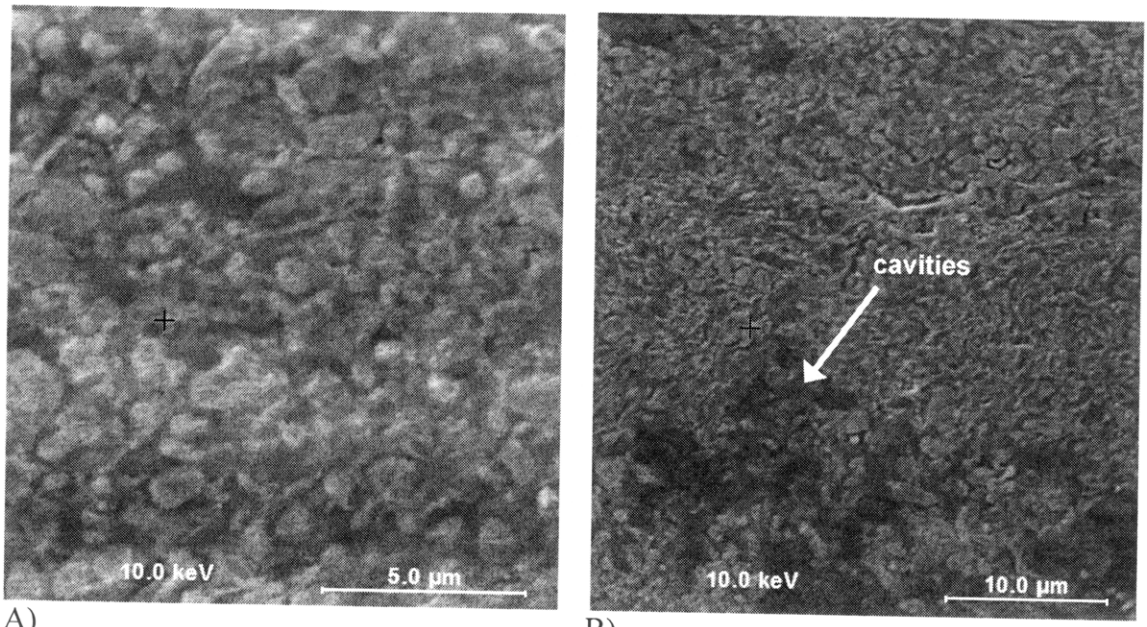

A) B)

Figure 5-33 SEM image of steel surface after rubbing with OBCaSu.
A) 2.4% ZDDP and 0% OBCaSu2 B) 2.4% ZDDP and 1% OBCaSu

6. Discussion

Several tests were performed to understand the effect of OBCaSu on ZDDP activity. Analysis was separated into three categories of focus: effect on ZDDP in solution, effect on ZDDP-metal surface interactions (effect on thermal film formation), and overall lubrication performance.

6.1. Effect on ZDDP in Solution

The presence of OBCaSu resulted in a shift towards the basic, or the compound, form of ZDDP. This was seen though the P_{31}NMR analysis in the retention of the ~100 ppm peak during heating; this effect of OBCaSu has been documented in the past [6, 16]. As heating shifts the equilibrium ZDDP state towards the neutral form, the retention of the basic peak indicates a counteracting driving force for the basic form. However, the effect of temperature on ZDDP state is ultimately stronger than the influence of OBCaSu, as extended heating eventually eliminates the peak. Nevertheless, this suggests that the addition of OBCaSu in low temperature lubrication will result in a slower rate of ZDDP tribofilm formation due to the relatively larger fraction of basic ZDDP.

6.2. Effect on Thermal Film Formation

OBCaSu suppressed the formation of thermal films, in both fresh ZDDP and aged ZDDP tests. Although significant film thickness reduction resulted from the introduction of just 1% OBCaSu, further addition had only a marginal effect. This suppression can be thought to be due to the solubilization of ZDDP by the calcium sulfonate, and this effect is seen in the NMR peak spectra. A minor shift in the neutral ZDDP peak was observed, from 92.2 ppm at 0% OBCaSu to 92.5 ppm at 6% OBCaSu. Mansuy, et al. found that chemical interactions and complexations between dispersants and ZDDP resulted in a peak shift of a few ppm [42]. Ramakumar et al. used FTIR to show that OBCaSu has a light influence on the P=S bond in ZDDP, and that this was not due to chemical but

physical interactions between the molecules [20]. Thus, the peak shift that occurs with the addition of OBCaSu is due to the solubilization of ZDDP, which in turn retards decomposition [6]. Solubilization also prevents ZDDP and its decomposition products from coming into direct contact with the metal surface, further preventing the thermal film formation.

When solutions with ZDDP were thermally aged for 11 hours at 150°C, solid crystalline precipitates were formed. Blends with aged ZDDP generally produced thinner thermal films than those with fresh ZDDP, and the addition of OBCaSu effectively stopped film development. There is a strong possibility that the production of the precipitates drastically diminished the ability of the aged ZDDP to produce anti-wear films. It was visually observed, however, that higher dosages of OBCaSu suppressed precipitate formation, with 15% OBCaSu resulting in no noticeable precipitates in the oil. This suggests that for oils in severe temperature conditions, the addition of OBCaSu, or a detergent in general, may help retain the capacity to form anti-wear film though the control of ZDDP precipitate formation. This, however, requires further experimental validation.

6.3. Effect on Rubbing Lubrication

Comparison of wear scar and friction data reveals a strong relation between the two. Tests with higher maximum friction result in wider wear scars on the plate. It should be noted, however, that the wear scars measured for the plates was an average along the length of the rubbing contact, and that the locations on the plate corresponding to the scoring on the cylinder were marked with larger local wear. Although score depth size increased with OBCaSu dosage, there was a similar level of mild, non-scoring wear on all of the tests with OBCaSu (figure 5-25).

Since the friction eventually approached close values for all of these tests, the non-scoring wear on the cylinder was likely the main source of friction. Restated, the wear scar size on the plate did not affect the "steady-state" friction values. As the wear scar

size is related to the local interfacial pressure, this suggests that ZDDP+OBCaSu blends are rather unaffected by changes in load. The scoring was not seen in the friction trace, which leads to the conclusion that the scoring is a highly localized phenomenon.

With proper sample cleaning, the AES profiles for ZDDP films closely matched those found in literature [39]. With this confirmation, AES analysis was extended to tribofilms produced in the presence of OBCaSu. A thick (~ 40nm) layer containing calcium was detected for higher OBCaSu dosages, indicating the presence of a calcium-based film. The AES profile plot illustrating this very closely matched that from a past study, of films produced only from OBCaSu (profile reproduced below in figure 6-1) [24]. Past studies have found that the calcium carbonate in OBCaSu form films as crystalline calcite or undergoes a chemical change to calcium oxide [23, 25, 26]. AES can be used on a fundamental level by comparing the decreases in the film elements during sputtering. The concomitant decrease of calcium, carbon and oxygen will suggest a calcium carbonate film, while that of only calcium and oxygen will be representative of a calcium oxide film. In the present study, however, the AES carbon signal was strongly affected by calcium, preventing possible deductions of the film material.

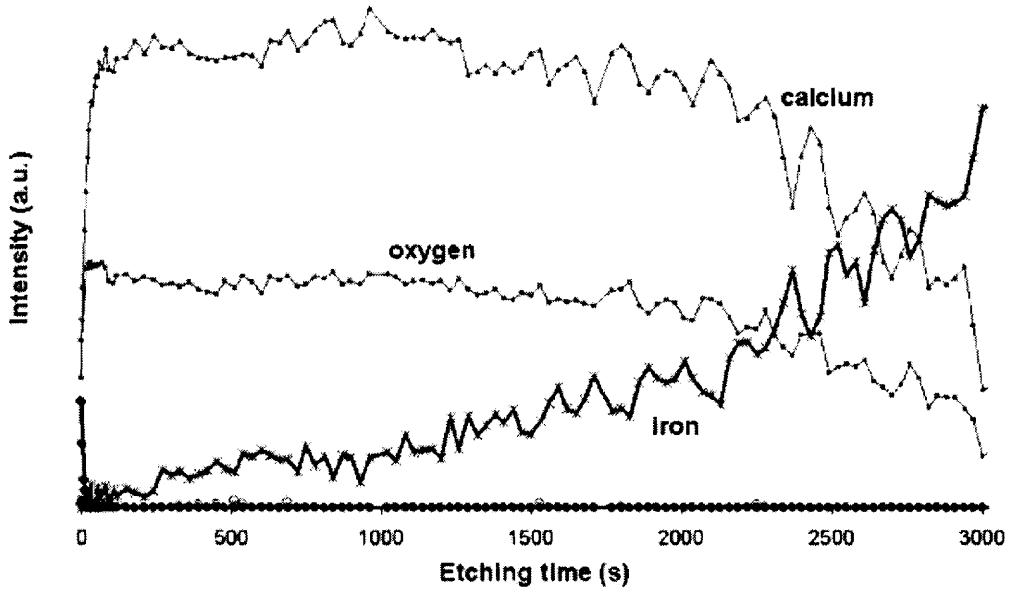

Figure 6-1 AES profile taken by Cizaire et al. of a tribofilm formed by OBCaSu [24].

ECR traces showed a slower rate of resistance development with OBCaSu, which was expected from the results from the thermal film tests. At 3%, however, a relatively early development of resistance indicates a possible synergism between the two additives. Looking at the elemental profiles, however, it is evident that the formation of ZDDP-based tribofilm was strongly suppressed, seen in the low concentrations of zinc and phosphorous. Compared to the coverage of the calcium-based film, there was little of the typical zinc oxide / zinc phosphate film. However, despite the low concentrations of the elements, measurement of the depth of their inclusion on the metal surface revealed that the film thickness was little different from case without OBCaSu. The currently accepted theory regarding the topographic structure of ZDDP tribofilms is that the films are first made on the micro-scale asperity peaks. In essence, patches of tribofilm are formed on the peaks [2, 6, 9]. Considering this, the low concentration of tribofilm elements detected with AES can be reasoned in that ZDDP tribofilm patches are still being formed with the same thickness, but less in number. This can be due to competition with OBCaSu for adsorption onto the metal surface or to the fact that ZDDP decomposition is significantly slowed by OBCaSu, delaying the film formation process. Though these effects are undoubtedly real, the large amount of calcium indicated an active formation of the calcium-based film, which posed competition with ZDDP tribofilms. Since calcium was not found on the thermal films to this concentration, it is evident that the tribofilm formation from OBCaSu is a physical or physiochemical phenomenon, affected little by temperature. This observation agrees well with literature [24] Even if flash temperatures from rubbing are considered in facilitating OBCaSu film formation, such momentary temperature increases will only amount to ~30°C for the conditions tested here [44].

OBCaSu film formation explains the early incidence of resistance measured by ECR as well. Unlike ZDDP film formation, the tribofilm development from OBCaSu does not require a chemical induction time for an intricate array of reactions. This is seen in the noticeably faster film formed with the oil blend with no ZDDP and 3% OBCaSu, through the ECR trace in figure 5-18. Given set of physical lubrication parameters, a greater concentration of OBCaSu will lead to a faster film development. For the conditions tested, ZDDP + 3% OBCaSu resulted in a film induction time that was shorter than that

for only ZDDP, as seen in the initial resistance development at 60 minutes. However, although OBCaSu gave a faster film formation, the strength of the film was inferior to that of ZDDP. This is seen in the eventual contact resistance decrease, as the film is removed prior to significant thickening.

The following model is proposed for the ZDDP–OBCaSu tribofilm structure (figure 6.2). The asperity peaks have patches of ZDDP tribofilms from rubbing contact, and the carbonate-derived film fill the valleys. As the films from carbonate are weaker than those from ZDDP, the peaks primarily only have a layer of ZDDP film. This agrees well with the AES profiles observed for the 1% and 3% OBCaSu tests, as initial sputtering removes the tribofilm from the peaks and reveals more from the valleys. The result is a decline in the zinc and phosphorous concentrations with initial sputtering and an increase in calcium.

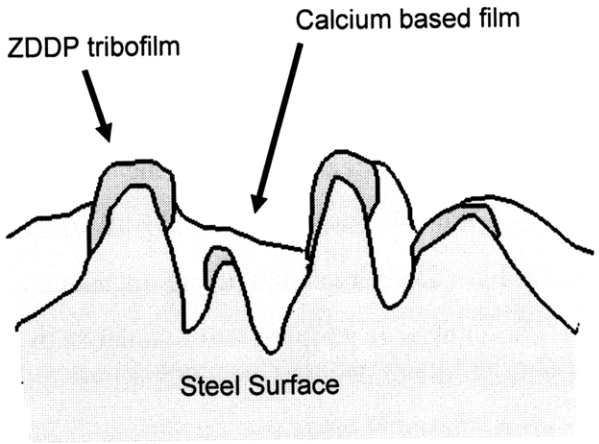

Figure 6-2 Model of proposed ZDDP – OBCaSu tribofilm structure

Despite promoting film formation, OBCaSu ultimately led to more pronounced wear. The cylinder had grooves cut into it and the plate had severe scratching in matching locations. Solid non-ferrous particles containing calcium and phosphorous were found embedded in each of these locations on the plate. The particles are likely not calcium phosphates, as calcium phosphates have been found in previous studies to be included in tribofilms without forming agglomerates [4]. Instead, it is probable that the films derived from calcium carbonate occasionally flake off of the metal surface, becoming an abrasive that entrains more carbonate-based films and also scrapes off the ZDDP tribofilms. The

particle grows in size until it eventually becomes embedded in the plate. As the cylinder rotates against it, more calcium-based sediment is deposited on the particle, further accelerating its growth as well as the wear on the cylinder itself.

Han et al. have documented a similar phenomenon of solid-like particles embedded in the wear scar, but an order of magnitude smaller [3]. The large agglomerates formed in this present test were possible due to the continuous motion of the cylinder (in contrast to reciprocating motion) and the rubbing contact geometry. The cylinder was rotated against the plate in a manner such that a small puddle of oil was formed above the line of contact, allowing the retention of the agglomerates and preventing them from being washed away.

In sum, the experiments showed the various effects of OBCaSu on ZDDP anti-wear film production. Many of the results matched those found in literature, and others were helped in explanation by past studies. Shifts in the NMR peak followed the trends seen in past investigations, as minor shifts occurred when the ZDDP was introduced to the base oil and OBCaSu to the ZDDP-oil mixture [6, 8, 16]. With sufficient cleaning, AES profiles of films produced by ZDDP matched those measured by Yamaguchi et al. Furthermore, the AES profile closely resembled that evaluated by Cizaire et al. with the inclusion of OBCaSu.

New information was found: AES was used to observe the gradated effect of OBCaSu on the thickness and elemental composition of the anti-wear film. An ECR trace was taken of an oil blend consisting solely of base oil and OBCaSu and an electrically insulating film was found to be produced, at a rate markedly faster than that of ZDDP. This was then related to the films developed with oil blends with low ZDDP – OBCaSu ratios, through the dominance of the calcium-based films. Through observation after tribo-testing, solid agglomerates were found to be produced on the plate wear scar with high repreatability when ZDDP was mixed with OBCaSu, indicating an antagonistic effect on wear when these two are combined in comparable concentrations.

7. Conclusions

The effect of the detergent, overbased calcium sulfonate (OBCaSu), on the wear-preventative performance of oils containing the anti-wear additive, zinc dialkyldithiophosphate (ZDDP), was investigated with emphasis on anti-wear film formation. Heating and rubbing tests were performed on oil blends containing ZDDP and OBCaSu. The effects of OBCaSu on ZDDP decomposition and thermal film formation were studied through the heating tests. A custom tribometer was developed to run rubbing tests on the oil blends. Tests were run in light boundary lubrication and various diagnostic techniques were applied to examine the development and structure of the tribofilm. The measurements included Auger electron spectroscopy (AES), 31-phosphorous nuclear magnetic resonance (P_{31}NMR), and electrical contact resistance (ECR). It was found that although OBCaSu independently forms calcium-based tribofilms, its addition to ZDDP decreased overall anti-wear performance. The key findings that lead to this conclusion are the following.

1. *OBCaSu solubilizes ZDDP and retards its decomposition.*

   P_{31}NMR was used to analyze the chemical changes undergone by ZDDP in the presence of various levels of OBCaSu. The addition of OBCaSu resulted in a shift in the NMR peak corresponding to neutral ZDDP, and this shift was greater for higher levels of OBCaSu. When the oils were heated for extended periods of time at elevated temperatures, different levels of ZDDP decomposition were observed. Blends with less OBCaSu showed more signs of decomposition.

2. *OBCaSu shifts ZDDP equilibrium towards the basic form, which is less active in anti-wear film production*

   Although heating shifts the ZDDP equilibrium towards the neutral form, P_{31}NMR analysis showed otherwise [2, 8, 16]. After 2 hours of heating at 120°C, the NMR peak corresponding to basic ZDDP diminished rapidly in the absence of OBCaSu, but decreased less for the blends containing OBCaSu.

3. *OBCaSu slows the rate of ZDDP film formation*

   Tests were run on the tribometer and tribofilm development was monitored with ECR. Although large differences in film induction time were not seen, the rate of tribofilm development was found to be slowed in the presence of OBCaSu. Heating tests in conjunction with P_{31}NMR analysis revealed the solubilization of ZDDP by OBCaSu, preventing contact of ZDDP with the metal. As a result, for a given heating time, thinner films were made in the presence of OBCaSu.

4. *OBCaSu forms a film by a physical / physiochemical mechanism, and thick films are produced for concentrations higher than 1%,*

   ZDDP is known to form films in both tribo-stressed and non-stressed conditions. Heating ZDDP in the presence of metal will result in a thermal film deposited on the metal, as ZDDP film formation is a thermally activated chemical process. Films formed by OBCaSu, on the other hand, were found to form only in tribo-stressed conditions. Much thicker films were formed with OBCaSu than ZDDP for OBCaSu concentrations greater than 1%, indicating the relative ease with which the OBCaSu film is produced.

5. *The OBCaSu film itself can lead to abrasive wear.*

   Significant scoring of the cylinder was observed with the addition of even 0.5% OBCaSu. In contrast, cylinders from tribo-tests with oil blends containing only ZDDP saw minimal wear or change in surface roughness. Close examination of the plate test piece revealed that hard agglomerates were embedded in the locations where the scoring occurred. As a high concentration of calcium was found on the particles, it is very likely that the agglomeration of OBCaSu film removed during rubbing led to their formation.

References

1. Barnes, A. M., Bartle, K. D., Thibon, V. R. A., "A Review of ZDDPs: Characterisation and Role in the Lubricating Oil," Tribology International, Vol. 34, pp. 389-395.
2. Spikes, H., 2004, "The History and Mechanisms of ZDDP," Tribology Letters, Vol. 17, pp. 469-489.
3. Han, N., Liu, W., Xue, Q., Shui, L., Zhang, C., "Study of Lubrication Behaviors of the Overbased Ca Sulfonate with ZDDP," SAE paper 2004-01-3052, 2004.
4. Kasrai, M., Fuller, M. S., Bancroft, G. M., Yamaguchi, E. S., Ryason, P. R., 2003, "X-Ray Absorption Study of the Effect of Calcium Sulfonate on Antiwear Film Formation Generated From Neutral and Basic ZDDPs: Part 1 – Phosphorous Species," Tribology Transactions, Vol. 46, pp. 534-542.
5. Semthuramiah, A., *Lubricated Wear Science and Technology*, Elsevier, Amsterdam, 2003.
6. Pawlak, Z., *Tribochemistry of Lubricating Oils*, Elsevier, Amsterdam, 2003.
7. Fujita, H., Spikes, H. A., 2004, "The Formation of Zinc Dithiophophate Antiwear Films," Journ. Engi. Tribology, Vol. 218, pp.265-277.
8. Nicholls, M. A., et al., 2005, "Review of the Lubrication of Metallic Surfaces by Zinc Dialkyl-Dithiophosphates," Tribology International, Vol 38, pp. 15-39.
9. Thomas, B., 2007, "Wear Modeling with Sensitivity to Lubricant Chemistry," S.M. Thesis, Massachusetts Institute of Technology.
10. Ji, H., Nicholls, M. A., Norton, P. R., Kasrai, M., Capehart, T. W., Perry, T. A., Cheng, Y., 2005, "Zinc-Dialkyl-Dithiophosphate Antiwear Films: Dependence on Contact Pressure and Sliding Speed," Wear, Vol. 258, pp. 789-799.
11. Fujita, H., Glovnea, R. P., Spikes, H., A., 2005, "Study of Zinc Dialkyldithiophosphate ANtiwear Film Formation and Removal Processes, Part 1: Experimental," Tribology Transactions, Vol. 48, pp. 558-566.
12. Hsu, S. M., Lin, R. S., "Interactions of Additives and Lubricating Base Oils," SAE paper 831683, 1983.
13. Yamaguchi, E. S., Ryason, P. R., Yeh, S. W., Hansen, T. P., 1998, "Boundary Film Formation by ZnDTPs and Detergents using ECR," Tribology Transactions, Vol. 41, pp. 262-272.
14. Komvopoulos, K., Pennecot, G., Yamaguchi, E. S., Yeh, S. W., 2009, "Antiwear Properties of Blends Containing Mixtures of Zinc Dialkyl Dithiophosphates and Different Detergents," Tribology Transactions, Vol., 52, pp. 73-85.

15. Yamaguchi, E. S., Ryason, P. R., Hansen, T. P., 1997, "Electrical Contact Resistance Studies on Zinc Dithiophosphates," Tribology Letters, Vol. 40, pp. 27-33.
16. Harrison, P. G., Kikabhai, T., 1987, "Proton and Phosphorous-31 Nuclear Magnetic Resonance Study of Zinc(II) O,O'-Dialkyl Dithiophosphates in Solution," J. Chem. Soc. Dalton Transactions, pp. 807-814.
17. Heuberger, R., Rossi, A., Spencer, N. D., 2007, "Pressure Dependence of ZnDTP Tribochemical Film Formation: A Combinatorial Approach," Tribology Letters, Vol. 28, pp209-222.
18. Yin, Z., Kasrai, M., Fuller, M., Bancroft, G. M., Fyfe, K., Tan, K. H., 1997, "Application of Soft X-Ray Absorption Spectroscopy in Chemical Characterization of Antiwear Films Generated by ZDDP Part I: the Effects of Physical Parameters," Wear, Vol. 202, 172-191.
19. Diesel Engine Lubrication, http://:WWWdeiselnet.com/tech/fuel_lube.html, 2005.
20. Ramakumar, S. S. V., Madhusudhana Rao, A., Srivastava, S. P., 1992, "Studies on Additive-Additive Interactions: Formulation of Crankcase Oil Towards Rationalization," Wear, Vol. 156, pp. 101-120.
21. Chinas-Castillo, F., Spikes, H. A., 2000, "Film formation by Colloidal Overbased Detergents in Lubricated Contacts," Tribology Transactions, Vol. 43, pp. 357-366.
22. Giasson, S., Espinat, D., Palermo, T., 1993, "Study of Microstructural Transformation of Overbased Calcium Sulphonates During Friction," Lubrication Engineering, Vol. 5, pp. 91-111.
23. Kubo, T., Fujiwara, S., Nanao, H., Minami, I., Mori, S, 2006, "TOF-SIMS Analysis of Boundary Films Derived from Calcium Sulfonates," Tribology Letters, vol. 23, pp. 171-176.
24. Cizaire, L., Martin, J. M., Gresser, E., Truong Dinh, N., Heau, C., 2004, "Tribochemistry of Overbased Calcium Detergents Studied by ToF-SIMS and Other Surface Analysis," Tribology Letters, Vol. 17, pp715-721.
25. Topolovec-Miklozic, K., Reg Forbus, T., Spikes, H., 2008, "Film Forming and Friction Properties of Overbased Calcium Sulphonate Detergents," Tribology Letters, Vol. 29, pp. 33-44.
26. Aoki, S., Masuko, M., Suzuki, A., 2007, "Application of Ellipsometry to the Characterization of Reaction Films formed by ZnDTPs on Sliding Steel Surfaces," Tribology International, Vol. 40, pp. 1454-1465.
27. Walls, J. M., *Methods of Surface Analysis*, Cambridge university Press, New York, 1989.
28. Watts, J. F., *An Introduction to Surface Analysis by XPS and AES*, Wiley, New York, 2003.

29. Briggs, D., Seah, M. P., *Practical Surface Analysis: By Auger and X-Ray Photoelectron Spectroscopyi,* Wiley, New York, 1983.
30. Wikipedia: Auger Electron Spectroscopy, http://en.wikipedia.org/wiki/Auger_electron_spectroscopy, 2009.
31. Wikipedia: NMR Spectroscopy, http://en.wikipedia.org/wiki/NMR_spectroscopy, 2009.
32. MIT Department of Chemistry Instrumentation Facility Handout, "Introduction to NMR," 2008.
33. Shaw, B. T. Hoult, D. P., Wong, V. W., "Development of Engine Lubricant Film Thickness Diagnostics Using Fiber Optics and Laser Fluorescence," SAE paper, 920651, 1992.
34. Folund, K., Schramm, J., Noordzij, B., Tian, T., Wong, V, "An Investigation of the Cylinder Wall Oil Film Development During Warm-Up of an SI-Engine Using Laser Induced Fluorescence," SAE paper 971699, 1997.
35. Hoult, D. P., Lux, J. P., Wong, V. W., Billian S. A., "Calibration of Laser Fluorescence Measurements of Lubricant Film Thickness in Engines," SAE paper 881587, 1988.
36. Furey, M. J., 1961, "Metallic Contact and Friction between Sliding Surfaces," ASLE Trans., Vol. 4, pp. 1-11.
37. Heuberger, R., Rossi, A., Spencer, N. D., 2006, "XPS Study of the Influence of Temperature on ZnDTP Tribofilm Composition," Tribology Letters, Vol. 25, pp. 185-196.
38. Eglin, M., Rossi, R., Spencer, N. D., 2003, "X-Ray Photoelectron Spectroscopy Analysis of Tribostressed Samples in the Presence of ZnDTP: A Combinatorial Approach," Tribology Letters, Vol. 15, pp. 199-209.
39. Yamaguchi, E. S., Roby, S. H., Yeh, S. W., 2005, "Time Dependent Film Formation from ZnDTPs and Nonphosphorous Antiwear Agents," Tribology Transactions, Vol. 48, pp. 57-68.
40. Costello, M. T., Urrego, R. A., 2007, "Study of Surface Films of the ZDDP and the MoDTC with Crystalline and Amorphous Overbased Calcium Sulfonates by XPS," Tribology Transactions, Vol. 50, pp.217-226.
41. Li, Y., Pereira, G., Lachenwitzer, A., Kasrai, M., Norton, P. R., 2008, "Studies on ZDDP Thermal Film Formation by XANES Spectroscopy, Atomic Force Microscopy, FIB/SEM and 31P NMR," Tribology Letters, Vol. 29, PP. 11-22.
42. Mansuy, H., Gautier, S., Palermo, T., 199, "31P NMR and IR Spectroscopy Study of Interactions Between Anti-wear and Dispersant Additives," J. Chim. Phys., Vol. 89, pp. 525-532.

43. Huq, M., Z., Chen, X., Aswath, P. B., Elsenbaumer, R. L., 2005, "Thermal Degredation Behavior of Zinc Dialkyldithiophosphate in Presence of Catalyst and Detergents in Neutral Oil," Tribology Letters, Vol. 19, pp. 127-134.
44. Discussion with Kai Liao, Graduate Student Researcher at MIT Sloan Automotive Laboratory, September, 2008.

.

Appendix A. LIF Diagnostics

A.1. System Layout

LIF is an oil film measurement technique used since the 1980's at MIT. A typical setup includes a laser, light sensor, optic fiber and optical lenses and filters. The laser is used to irradiate the sample and impart energy the species measured. The species, called fluorophores, are momentarily excited to a higher energy level and later revert to their original, base, state. During the reversion, the excess energy is given off as fluorescence. This reversion occurs in 10^{-11} ~10^{-7} seconds from excitation, allowing for high temporal resolution [1]. The fluorescence is captured by a light detector, which can be a photomultiplier tube, diode array or spectrometer. Lasers typically used for LIF are argon (488 nm), helium-cadmium (442nm) or Nd-Yag (523 nm) lasers [2, 3, 4]. Laser dyes have been used as fluorophores for lasers in the visible light region, but engine oil has been found to have a nascent fluorescence when irradiated with ultraviolet light (423, 488nm) [2, 3]. Common dyes are of the Coumarin and Rhodamine family. For the case of oil film thickness measurement, the most common setup is as shown in figure XXX.

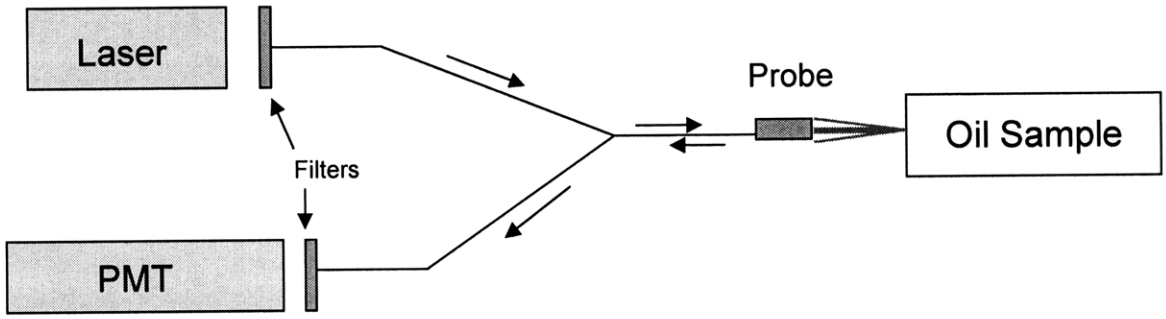

Figure A- 1 Typical LIF layout.
LIF layout as used in most in-engine applications for oil film measurement, and as used in this project as well. The laser light is channeled to the oil sample and PMT through a Y-shaped optic fiber

For this application, a Nd:YVO_4 diode-pumped solid state laser at second harmonic (532nm) was chosen due to its affordability and minimal maintenance. For directing the laser light, a bifurcated (Y-shaped) fiber optic cable was used. The cable allows the passage of two independent signals at the common end, which is separated into the

individual legs. The bifurcation is made possible by bundling the strands of fibers in a 6 to1 orientation, in which the 6 fibers directing one signal is bundled around the singular fiber that transmits the other signal. The LIF hardware is listed below.

The laser is directed through a 532 nm laser filter into the leg of the optic cable. The light is then sent out form the common end of the optic cable and through a focusing probe, which irradiates the oil as well as transmits the fluorescence back into to the cable. The fluorescent light is then directed back through the other leg of the bifurcated cable, through a 570nm bandpass filter, and into a photomultiplier tube used to detect the light intensity.

Table A- 1 Compents of LIF system

Hardware	Model	Specifications
Laser	Crystalaser GCL-025L	35 mW, continuous mode laser, Nd:YVO_4
Optic Fiber	CeramOptec Bundled fiber	Bifurcated 6-1coaxial silica fiber, SMA connection
Optical filters	Newport 10LF10-532	532±2nm Center, 10±2nm FWHM
	Newport 10BPF10-570	570±2nm Center, 10±2nm FWHM
Photomultiplier tube	Hamamatsu R4220	1250V Max. Supply Voltage, ~71% of max. cathode radiant sensitivity at 532nm

A.2. Theory

The intensity of fluorescence is strongly dependent on the intensity of the incident excitation light on the fluorophore-solvent mixture. Likewise, it can be imagined that if the solvent, or even the fluorophore species itself, has a high absorptivity, less light will see the deeper regions. However, whether the fluorophore fluoresces must also be dependent on its absorptivity; the species must absorb enough photonic energy to be excited. Thus, fluorescence is directly proportional to the intensity of the incident excitation light and absorbance of the dye but inversely proportional to the total absorbance of the solvent and dye. Taking these factors into account, a relation has been developed to describe the fluorescent signal incident on the detector [4]:

$$I_{fluoro\,detected} = S\frac{I_o C_{dye}\varepsilon_{dye}}{C_{dye}\varepsilon_{dye}+2\sigma_{oil}}\left[1-\exp\left(-\left(C_{dye}\varepsilon_{dye}+2\sigma_{oil}\right)\cdot h\right)\right]\cdot\int_{\nu_1}^{\nu_2} f(\lambda)\varphi(\lambda)d\lambda \qquad (3.1)$$

Where

$I_{fluoro\,detected}$: intensity of the detected fluorescence

I_o: intensity of excitation laser light

S: shape factor, relating the position of the detector to the fraction of fluorescent photons detected

C_{dye}: concentration of dye

ε_{dye}: dye absorptivity coefficient

σ_{oil}: oil absorptivity

h: oil film thickness

$\varphi(\lambda)$: quantum yield efficiency at wavelength λ

$f(\lambda)$: filter transmittance at wavelength λ

ν_1: minimum wavelength transmitted by bandpass filter

ν_2: maximum wavelength transmitted by bandpass filter

The equation is based on the Lambert law and is an integrated result taking into account the absorption of incident laser light as successive differential layers of oil are penetrated. The light seen by an oil sample at a certain depth in the oil film will only be a fraction of the excitation light intensity. The tendency for the dye to fluoresce at the specific

wavelength is represented by the quantum yield efficiency; fluorescence is equal to the light absorbed by the fluorophore multiplied by the quantum yield efficiency. Factors involving the transport of fluorescent light to the detector are included as well. The relative ease with which the fluorescence can travel to the sensing location of the detector is included in the shape factor, which is system-specific. The level of fluorescence seen by the detector is also limited by the bandpass filter (in this case from 560 to 580nm) and is calculated by an integration multiplying filter transmittance to the quantum yield efficiency. It is noted that the intensity of the detected fluorescence is an exponential function of the film thickness and the combined absorbance of the oil and dye.

Given the hardware, dye, and the physical design of the LIF system, the equation reduces to:

$$I_{fluoro\,detected} = S \cdot I_o \cdot \varphi_{effective} \frac{C_{dye}\varepsilon_{dye}}{C_{dye}\varepsilon_{dye} + 2\sigma_{oil}} \left[1 - \exp\left(-\left(C_{dye}\varepsilon_{dye} + 2\sigma_{oil}\right) \cdot h\right)\right] \qquad (3.3)$$

Where

$\varphi_{effective} = \int_{\lambda_1}^{\lambda_2} f(\lambda)\varphi(\lambda)d\lambda$, representing quantum yield through filter transmission.

Equation 3.3 can also be rewritten as:

$$I_{fluoro\,detected} = S \cdot I_o \cdot \varphi_{effective} \frac{C_{dye}\varepsilon_{dye}}{\sigma_{total}} \left[1 - \exp\left(-\sigma_{total} \cdot h\right)\right] \qquad (3.4)$$

Where

$\sigma_{total} = C_{dye}\varepsilon_{dye} + 2\sigma_{oil}$, the combined absorbance of the oil and dye

For the case in which the combined absorbance and/or the film thickness is small, $\sigma_{total} \cdot h << 1$, equation 3.4 can be approximated to be linear by,

$$I_{fluoro\,detected} = S \cdot I_o \cdot \varphi_{effective} \frac{C_{dye}\varepsilon_{dye}}{\sigma_{total}} \left[\sigma_{total} \cdot h\right] \qquad (3.5)$$

Thus, the LIF signal can be increased by increasing the excitation light intensity or by selecting a dye with a high absorptivity and quantum efficiency. Caution must be

exercised, however, in increasing the light intensity as photobleaching may occur, where the fluorophore is excited beyond its capacity and undergoes a chemical change.

It must be noted here that establishing a linear relationship between film thickness and fluorescence is crucial to LIF. If the detected fluorescence cannot be approximated as linearly dependent on the film thickness, calibration of the signal will require complete mapping of the exponential curve. If the relationship is linear, the detected signal can be compared to a line calibration curve, which is formulated much more easily.

A.3. Selection of Dye

The appropriate dye was chosen to optimize the LIF signal. This translated to a dye with a high inherent quantum yield efficiency and strong thermal stability. High quantum yield efficiency results in greater fluorescence for the same excitation light, and thermal stability allows for a wider range of operating temperatures. Care was taken to find a dye with a high melting point to avoid any possibility of thermal bleaching.

Literature review on the quantum efficiency and thermal properties of dyes excited at 532nm narrowed the options to three selections tabulated below [4, 6, 10]. Rhodamine 590 was found to have the best properties, and was thus chosen for this setup.

Table A- 2 Specifications of Rhodamine dyes excited at 532nm

Dye	Max fluo. wavelength (nm)	Quantum eff. nomal to Rh610	Melting point (deg C)
Rh590	570	1	255-315
Rh610	59	0.95	112-210
Rh640	620	0.92	~210

A.3. Effects of Dye Concentration

To further optimize the fluorescence for LIF, various tests outlining the effects of dye concentration and temperature were performed. Focus was directed at optimizing the dye concentration, as it was the only parameter that was easily adjusted to improve the LIF signal. Temperature effects on the signal throughput were studied to determine the operating limits of the system, as the quantum yield efficiency and therefore fluorescence rapidly diminishes as temperature increases [1, 4].

In order to achieve linearity for a wide range of oil film thicknesses, it is necessary to reduce the combined absorbance. For a given combination of oil and dye, σ_{oil} and ε_{dye} cannot be adjusted, leaving only dye concentration for linearity optimization. Therefore, if a significantly thick film is to be measured, the dye concentration must be minimized. However, this also has the effect of reducing the fluorescence, resulting in a weaker signal-to-noise ratio. A tradeoff exists between the maximization of the linearly approximated regime and signal size. In optimizing the LIF signal, the dye concentration must be increased within limits as to not disturb the desired range for linear approximation.

To ensure a wide operating range of the tribometer, the maximum film thickness measurement was set to be 100μm. Referencing past applications of Rhodamine 590 for fluorescence, three levels were chosen for analysis: 10^{-4}, $5*10^{-4}$ and 10^{-3} mol/L [6]. A custom bench-tester was made for the tests. Two plates were bolted together, and a screw-type adjuster on the top plate was used to vary the local separation. Opposite the adjuster, a flush-mounted window was fitted in the bottom plate to allow optical access for the laser. A cartridge heater and thermocouple was installed into the top plate, allowing for temperature control. LIF measurements were taken while adjusting the screw. Testing was done at 90° C with a PMT excitation voltage of 1kV.

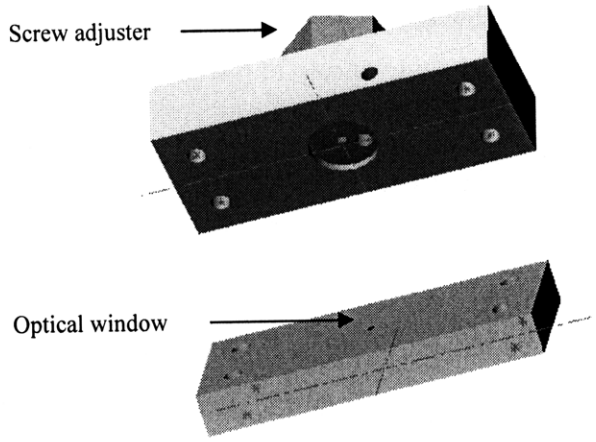

Figure A- 2 Dye concentration calibration rig

The screw on the top plate provides local separation (height) adjustment between the two plates. The small window on the bottom plate allows laser access. The small hole on the top plate allows the insertion of a 1/8" diameter cartridge heater for temperature control.

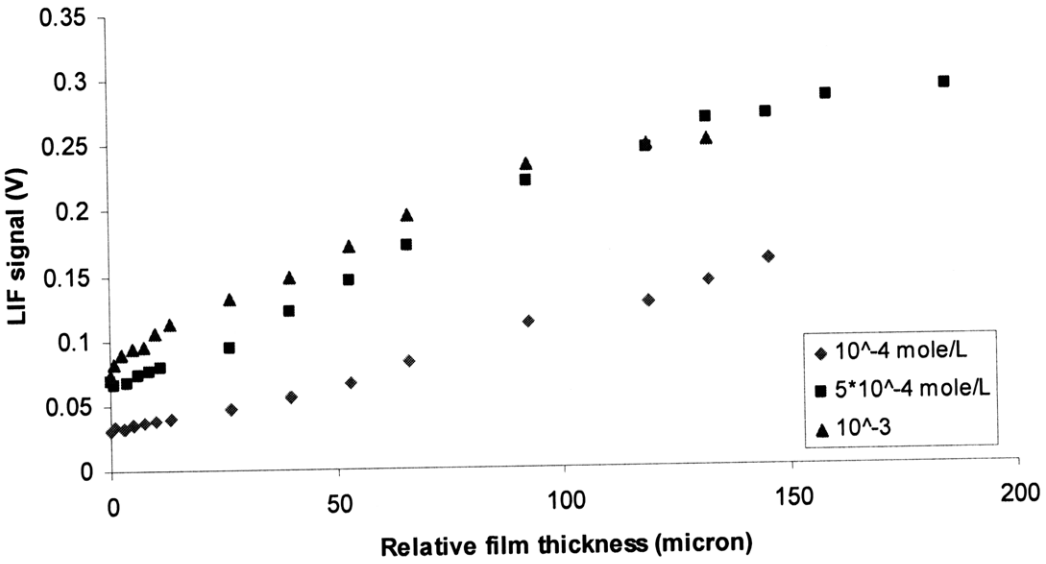

Figure A- 3 LIF signal vs. oil film thickness, showing the effects of dye concentration on signal size.

Figure A-3 shows the results of the test; it can be seen that the increase in signal from 10^{-4} to $5*10^{-4}$ mol/L is almost two-fold but the increase from $5*10^{-4}$ and 10^{-3} mol/L is not as significant. Figure A-4 displays the same data, but normalized to the "zero" thickness signal. It is noted that imperfect mating of the screw to the LIF window is causing a remnant fluorescence even at "zero" film. Due to the fabrication limitations of the test setup, "zero" film thickness exhibits some fluorescence from the combined effects of

surface roughness and imperfect flatness. However, this merely results in a shift in the curves and does not undermine the actual validity of the test.

With a dye concentration of 10^{-3} mol/L, linearity continues to ~80μm, followed by an immediate plateau. Linearity continues for the entire range tested with 10^{-4} mol/L, whereas the signal from $5*10^{-4}$ mol/L enters a gradual decrease in slope from about 100μm. Given that the signal is almost doubled from 10^{-4} to $5*10^{-4}$ mol/L and little is gained from $5*10^{-4}$ to10^{-3} mol/L, $5*10^{-4}$ mol/L was chosen as the optimal dye concentration.

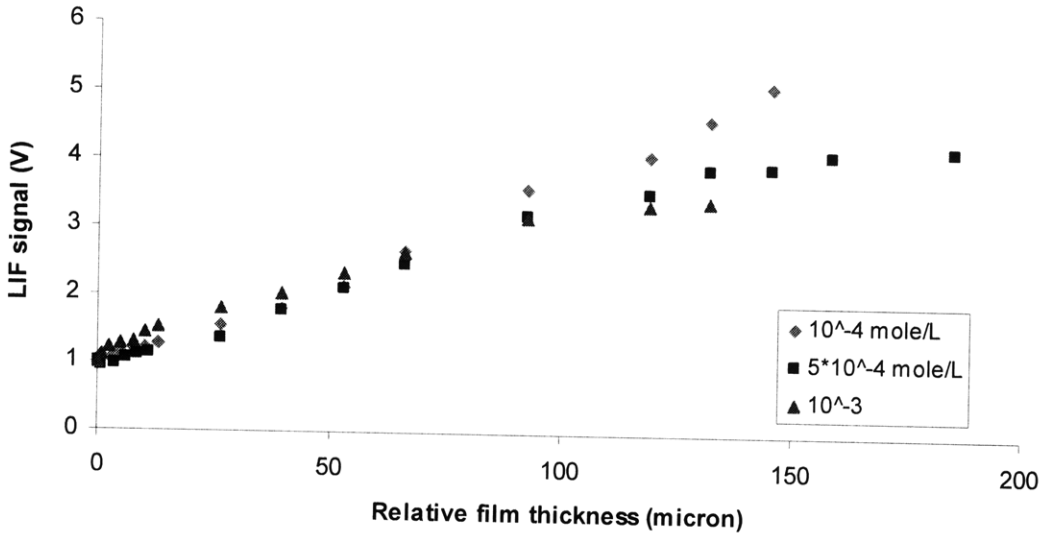

Figure A- 4 Normalized LIF signal vs. oil film thickness, showing the effects of dye concentration on linearity.
The LIF signal (volts) of each concentration is normalized to that taken at zero film thickness.

A.5. Effects of Temperature

The same test rig was used to measure the effects of temperature on fluorescence. With the screw set to a separation of 100μm and a dye concentration of $5*10^{-4}$ mol/L, the temperature was adjusted from 20° to 140° C. Figure XX shows a rapid decrease in fluorescent intensity, dropping by a factor of ten from 20° to 100° C. However, previous tests adjusting dye concentration show that even if the LIF signal is 0.1V at 100 μm (case of 10^{-4} mol/L), the PMT still has sufficient sensitivity to detect a linear change. Thus it was judged that the LIF at the current settings could be used safely up to 110° C.

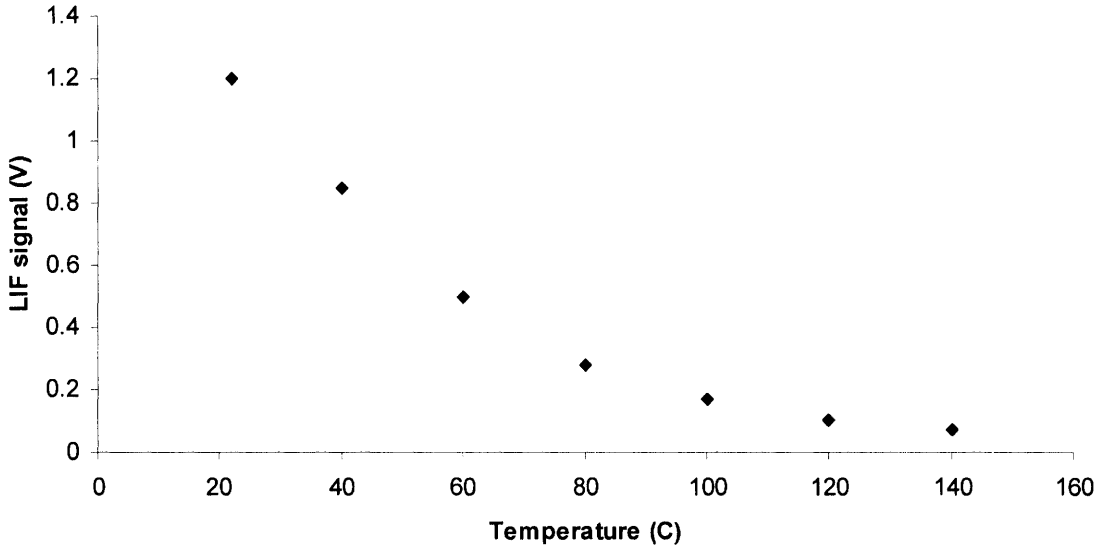

Figure A- 5 The effect of temperature on fluorescent intensity. Measurements were taken at 100μm.

A.6. Calibration of LIF

Calibration of oil film measurements with LIF in the past have been divided into two trains of thought. One favors bench-top calibration before application into the actual system, and the other favors in-situ calibration. Arguments for bench-top calibration cite better control reached over parameters that affect LIF signal such as temperature. Examples of bench-top calibration include sandwiching oil between two microscope slides and micrometer-like rigs that adjust oil thickness with a screw motion [7].

Others have used in-situ calibration of LIF and argue that calibration must take place in the geometries and conditions representative of where the actual measurements will take place, in the conditions of measurement. This method of calibration has often been implemented by engraving etch marks with known depths on the rubbing surface. A calibration curve was made using the measurements at these depths and subsequent measurements were then processed using the calibration. For film measurements in the piston ring pack, etch marks were made on the piston skirt, allowing for dynamic calibration with each cycle. This method has benefits and drawbacks different from bench-top calibration. It may be considered better than bench calibration in that the calibration is dynamic, in which changes in oil condition are continuously accounted. However, as often the case for oil film measurement in the piston ring pack, rapid temperature changes may thwart in-situ calibration to such an extent that it is difficult to decipher. This has been amended in the past using dual-dye fluorescence to compensate for temperature effects [4]. Another issue documented in past applications is the failure for the oil to completely fill the etched engravings.

In-situ calibration was chosen for this system due to the ease of application and the benefits of calibration in actual experimental conditions. 15μm and 30μm etchings were made on the surface of the cylinder using laser-EDM. The etch marks were made in 1mm x 0.7mm rectangles, larger than those documented in the past to facilitate the entry of oil. Also, steady state cylinder temperatures and slow rotation during calibration allowed more favorable conditions for calibration than in engine applications.

A.6. Application of LIF to the Tribometer

The necessity for optical access to the rubbing interface required that each test plate be custom fabricated with a transparent window. Engine applications of LIF for oil film measurements have often employed a stepped cylindrical window in the cylinder liner but a conical window was used for this application [3, 7]. This was possible due to the absence of high pressures seen in engine combustion chambers. The conical window was made of impact-resistant fused silica, with the transmitting surfaces polished to an optical-grade 80-50 scratch-dig. Fused silica was used due to its scratch resistance, low machining costs, and exceptional transmission of visible light. A high temperature ceramic epoxy with a low volumetric expansion coefficient was used to fix the window to the flat and the combined surface was ground flush to the desired smoothness. Care was taken to prevent voids from forming in the epoxied interface, since contamination of these voids with the fluorescent species will result in erroneously high LIF signals. The conical design provided for optical access while keeping the surface area of the window at the rubbing interface to a minimum. Of the entire rubbing interface length of 2.5", only 0.05" was that of the window, so the effect of the glass on the metal-to-metal lubrication was considered to be negligible.

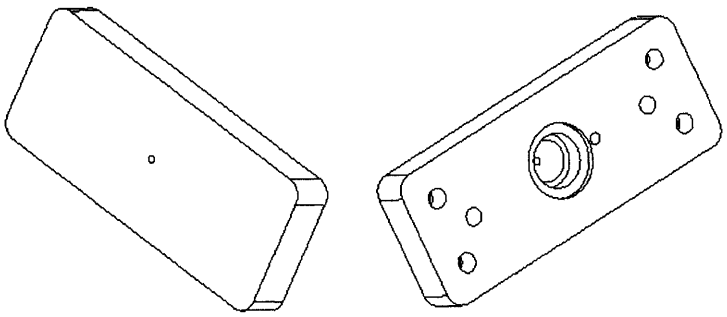

Figure A- 6 Test plate for use with LIF.

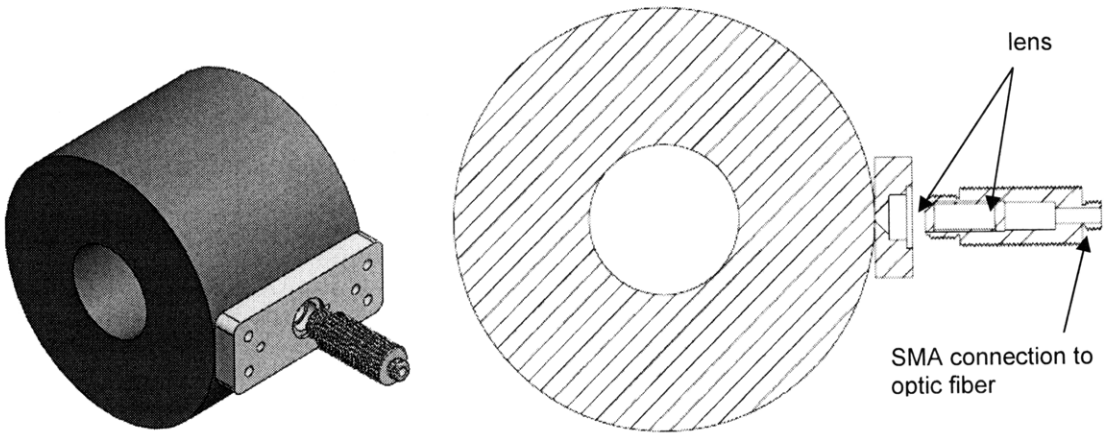

Figure A- 7 Orientation and design of laser probe for LIF

In addition to the optical access window in the test plate, a laser probe was made to focus the excitation light. The probe was connected to the common end of the bifurcated optic fiber, and had a dual role of sending forth a focused beam of light from the laser to excite the oil sample and transmitting the fluorescent light from the oil back into the fiber. The probe consists of a stainless steel housing, two convex 6.2mm diameter lenses and a 12.5mm brass spacer. Though the probe housing is a unique design to this project, the lens geometry was taken from the probe designs of previous applications of LIF at MIT [8, 9].

A.7. References

1. Schafer, F. P., "Topics in Applied Physics Volume 1, "Dye Lasers"," Springer-Verlag, New York, 1973.
2. Brown, M. A., McCann, H., Thompson, D. M., "Characterization of the Oil Film Behavior Between the Liner and Piston of a Heavy Duty Diesel Engine," SAE paper 932784, 1993.
3. Przesmitzki, S., Vokac, A., Tian, T., "An Experimental Study of Oil Transport Between the Piston Ring Pack and Cylinder Liner," SAE paper 2005-01-3823, 2005.
4. Thirouard, B., 2001, "Characterization and Modeling of the Fundamental Aspects of Oil Transport in the Piston Ring Pack of Internal Combustion Engines," PhD thesis, Massachusetts Institute of Technology.
5. Guilbault, G. G., "Practical Fluorescence," Sevond Edition, Marcel Dekker Inc., New York, 1990.
6. Exciton Wavelength Chart, http://www.exciton.com/wavelength_chart.html, 2007.
7. Shaw, B. T. Hoult, D. P., Wong, V. W., "Development of Engine Lubricant Film Thickness Diagnostics Using Fiber Optics and Laser Fluorescence," SAE paper, 920651, 1992.
8. Tamai, G., 1995, "Experimental study of engine oil film thickness dependence on liner location, oil properties and operating conditions," MS thesis, Massachusetts Institute of Technology.
9. Lopez, O., "Experimental study of lube oil characteristics in the PCV system and effects on engine oil consumption," MS thesis, Massachusetts Institute of Technology.
10. Duarte, F. J., "Selected Papers on Dye Lasers," SPIE Optical Engineering Press, Bellingham, WA, 1992.

Appendix B. Tribometer Operation Check

With the completion of design, fabrication and assembly, the tribometer was checked for proper operation. Tests were done at various loads (1kg to 16kg weights) and cylinder speeds (0.4 to 5 m/s) to characterize the system in terms of lubrication regime. Friction force and film thickness measurements were taken during these tests, and are as plotted below. Chevron Delo 15W-40 CJ-4 diesel oil, with kinematic viscosity of 125 and 15.7 cst at 40° and 100° C respectively, was used in the tests at 25° C.

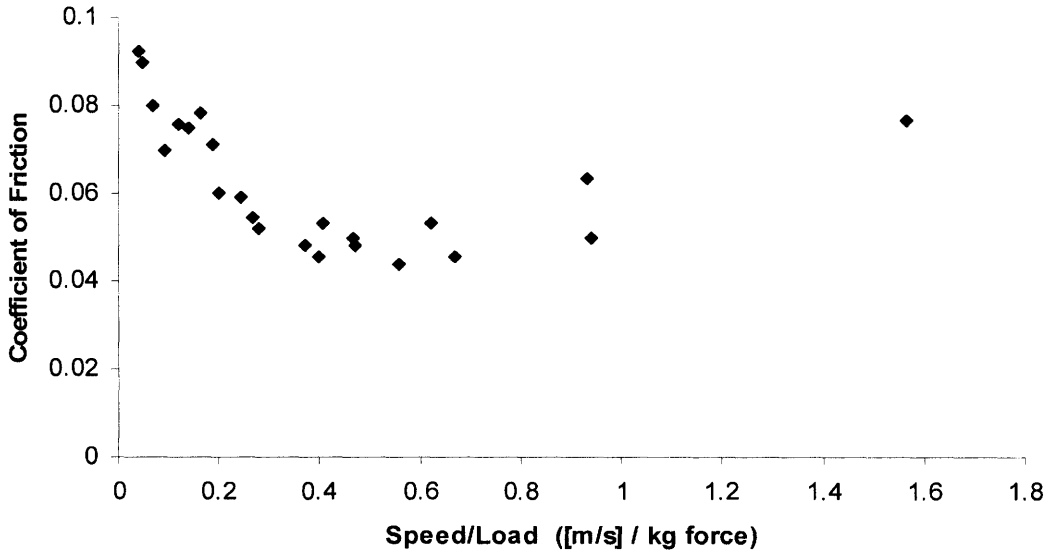

Figure B- 1 Stribeck curve for tribometer operation check

A Stribeck curve was made with the data from the tests, and is shown in Figure B-1. The Sommerfield number was estimated to be the ratio of cylinder speed and normal load, neglecting the effects of viscosity as temperature changes were considered to be minimal during the tests. For the 15W-40 oil, the transition from mixed to hydrodynamic lubrication was found to occur at about a speed/load ratio of 0.4. This finding provided validation for the tribometer to successfully operate in the two regimes.

Figure B-2 displays the effect of speed on friction. The steady decrease in friction observed for the higher loads is representative of the decrease in the friction coefficient characteristic of mixed lubrication. The slight increase in friction as speed in increased at

lower loads suggests a transition into hydrodynamic lubrication. This change in slope is more evident in Figure B-3.

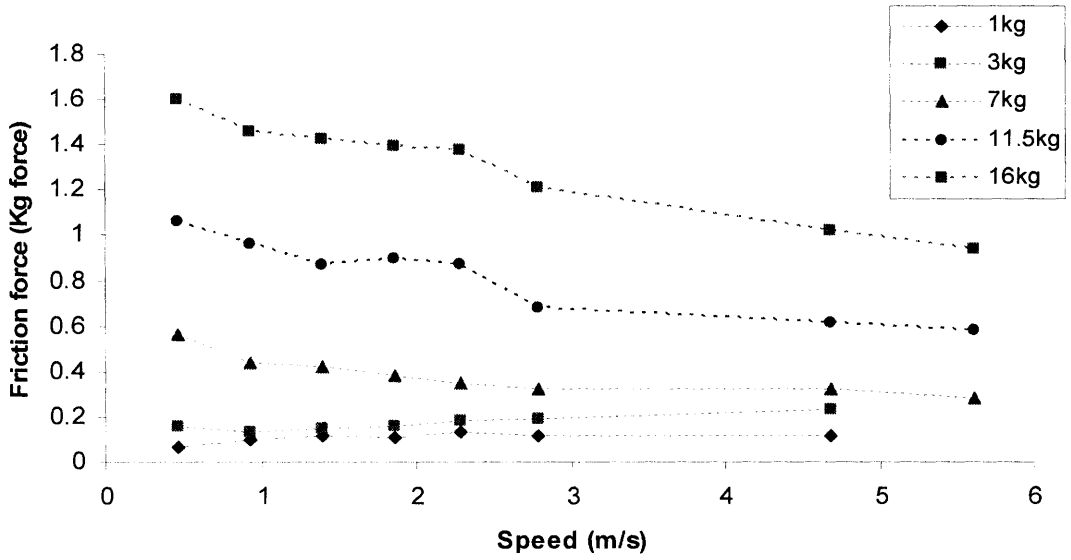

Figure B- 2 Effect of speed on friction force

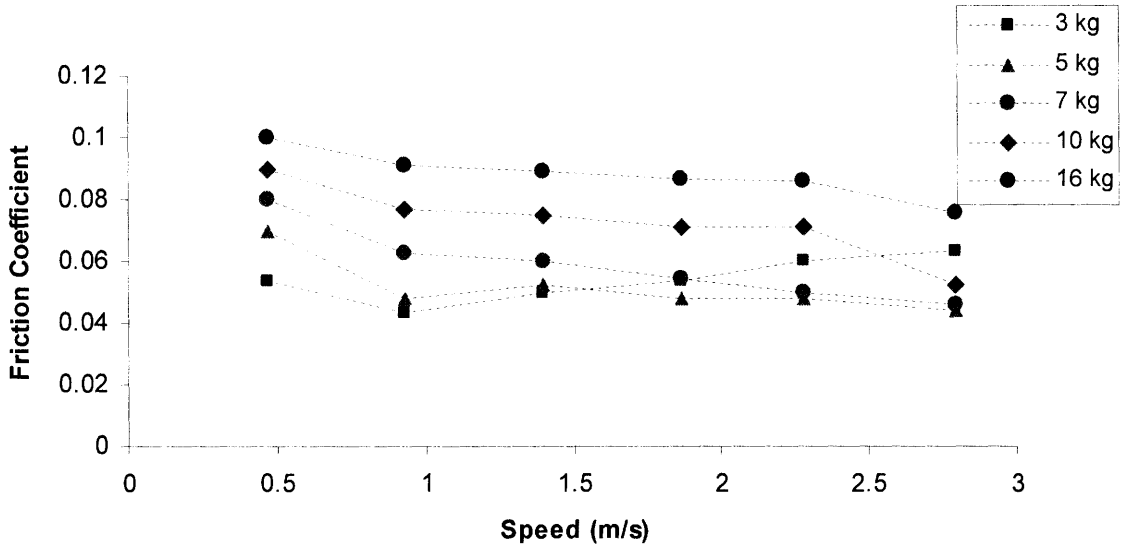

Figure B- 3 Effect of speed on friction coefficient

The effects of load on friction force were consistent. Increasing load directly resulted in a responsive increase in friction force. For higher loads, more friction was observed at lower loads, as expected in mixed lubrication. This trend was reversed at low loadings, as higher speeds resulted in relatively higher friction due to greater viscous shear.

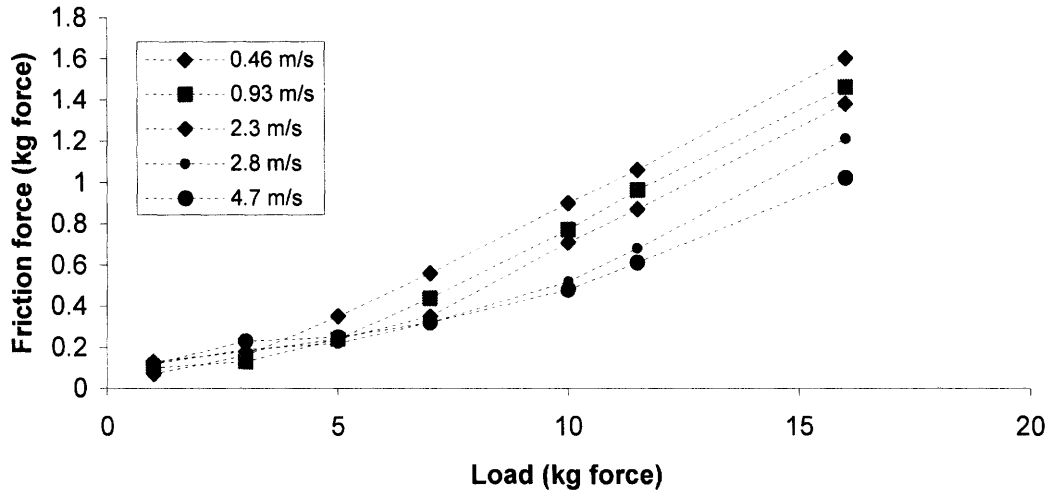

Figure B- 4 Effect of loaf on friction force

Film thickness decreased with load, with the slopes for decrease generally larger at lower speeds. Although this substantiated an expected result, higher speeds were measured to have thinner films. This was contrary to expectation, as greater levels of hydrodynamic force would be expected to form between the lubricated contacts, leading to thicker films. Later analyses revealed that this was due viscous heating of the oil which decreased fluorescence.

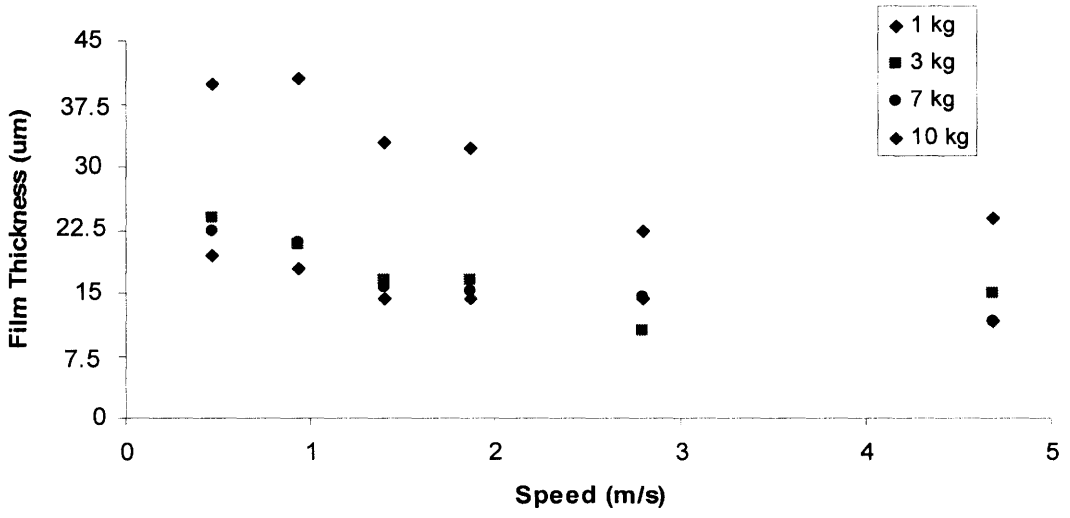

Figure B- 5 Effect of speed on film thickness

Appendix C. Selected P_{31}NMR Spectra

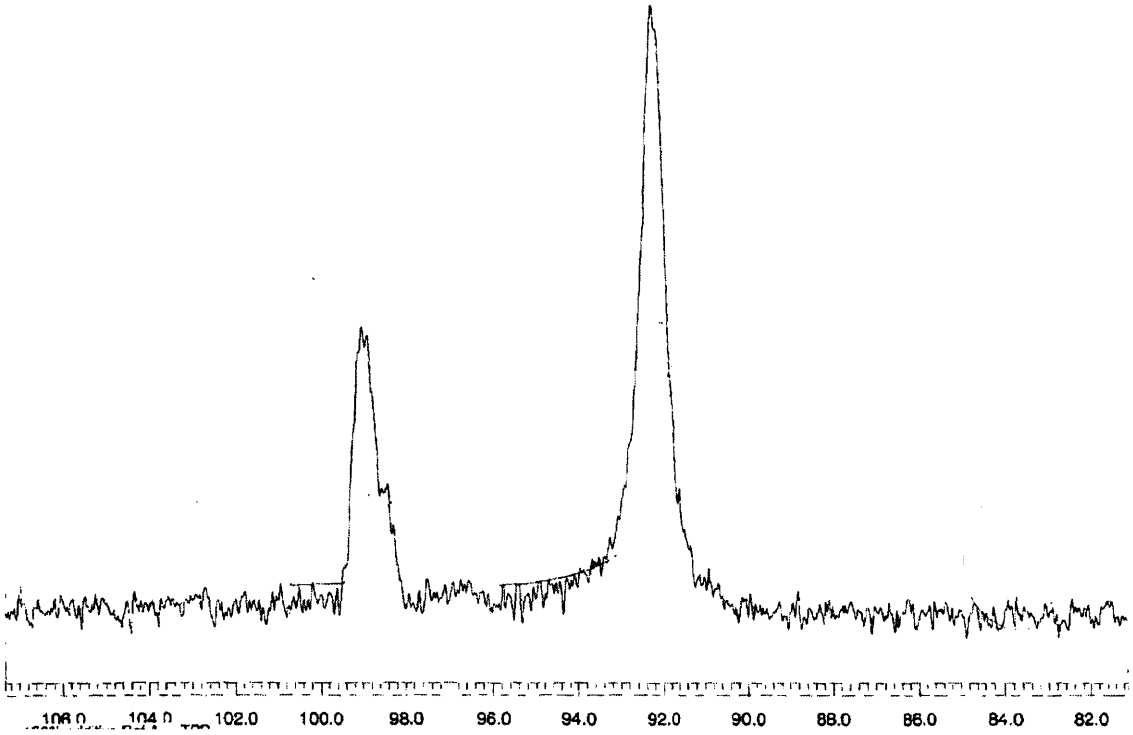

Figure C- 1 P_{31}NMR spectrum for 100% ZDDP. Units are in ppm.

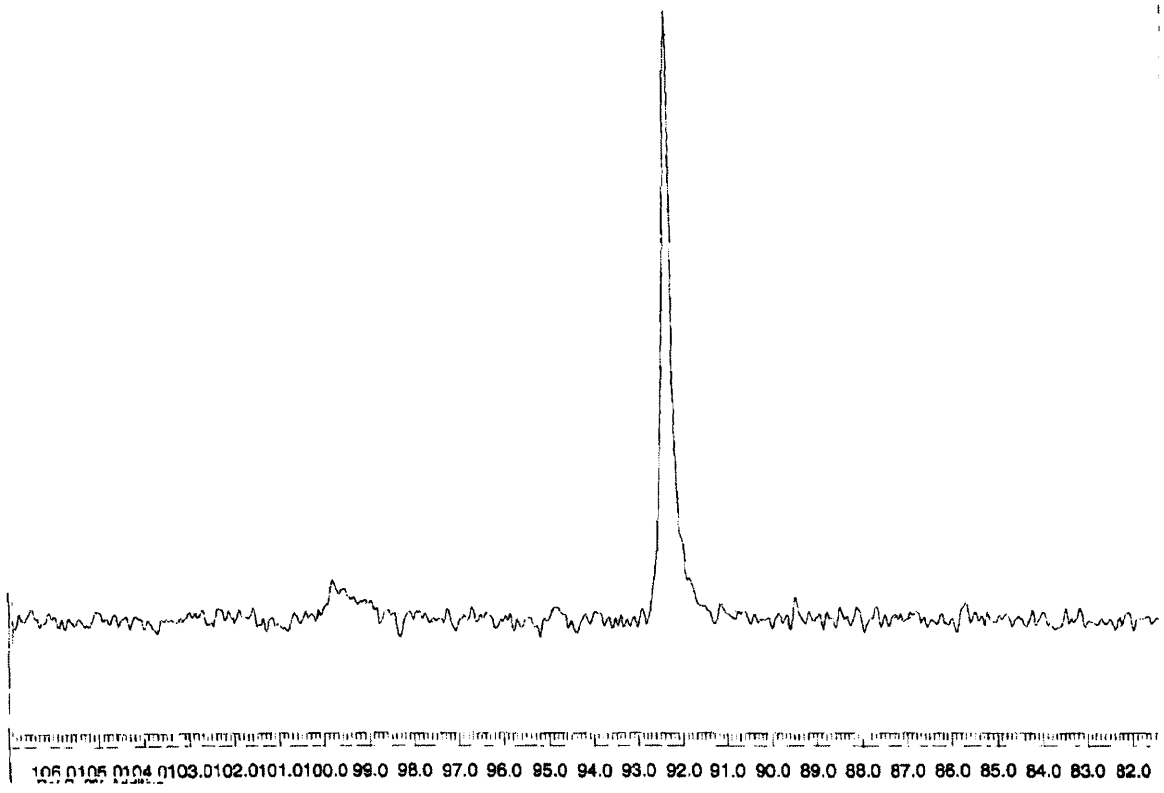

Figure C- 2 P_{31}NMR spectrum for 2.4% ZDDP, 0% OBCaSu, 2 hours heating at 120° C. Units are in ppm.

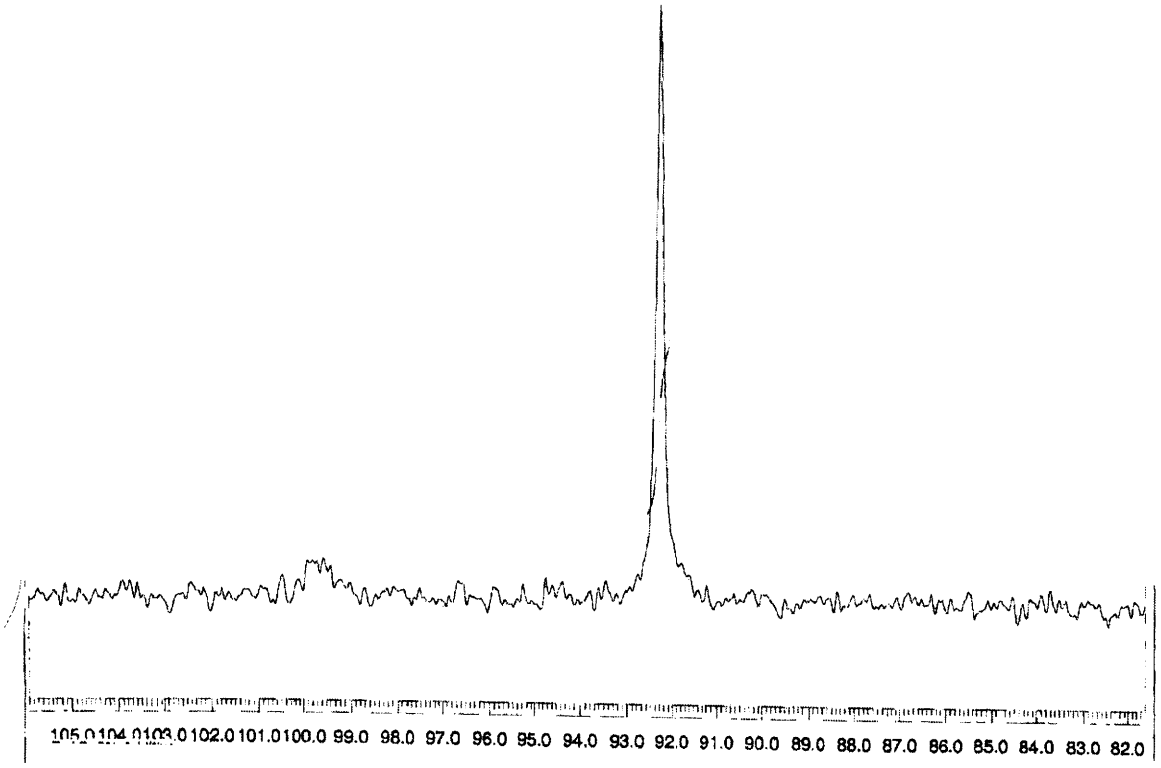

Figure C- 3 P_{31}NMR spectrum for 2.4% ZDDP, 3% OBCaSu, 2 hours heating at 120°C. Units are in ppm.

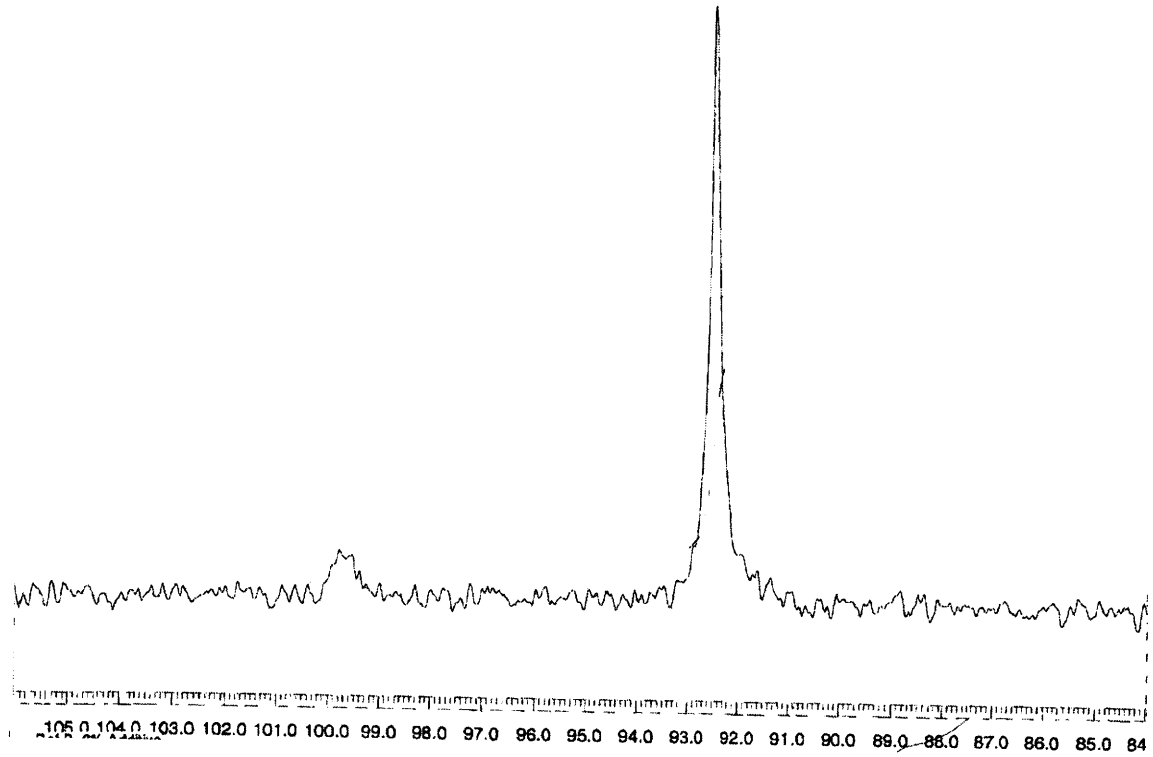

Figure C- 4 P_{31}NMR spectrum for 2.4% ZDDP, 6% OBCaSu, 2 hours heating at 120°C. Units are in ppm

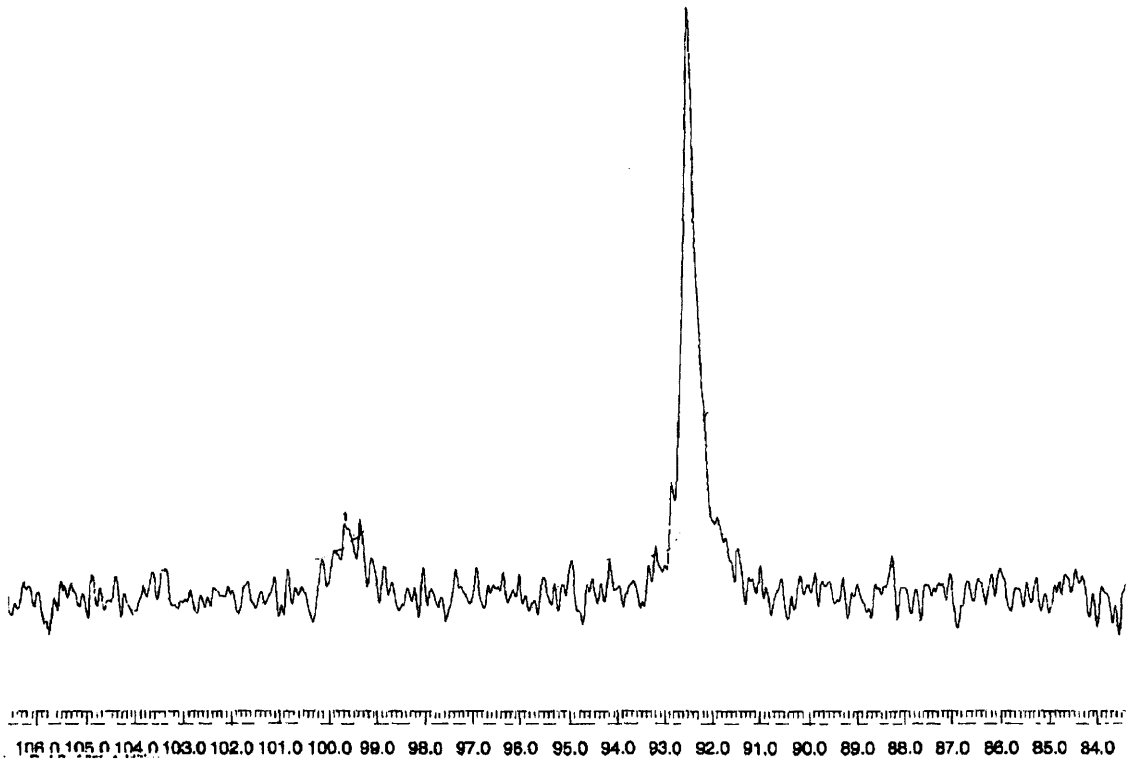

Figure C- 5 P_{31}NMR spectrum for 2.4% ZDDP, 15% OBCaSu, 2 hours heating at 120°C. Units are in ppm.

Appendix D. Considerations with AES Data Processing

AES was used to measure the presence of 7 elements in the anti-wear film (table D-1). The AES machine was programmed to take two rounds of elemental data before sputtering, and this is seen in the profile plots as measurements at a "negative time." Multipak, a MATLAB-based program, was used to analyze the acquired data.

Table D- 1 Elements analyzed with AES

Element	Auger Peak	Acquisition Range (eV)	AES Sensitivity
Oxygen	O1	499 - 520	High
Carbon	C1	231 - 291	High
Phosphorous	P1	86 - 146	Low
Sulfur	S1	115 - 175	Moderate
Iron	Fe3	668 - 728	High
Zinc	Zn1	958 - 1018	Low
Calcium	Ca1	254 - 314	High

In analysis of the AES data (differentiated raw data) for carbon and calcium, the closeness of the respective peaks presented difficulty in distinguishing between the two. Shown in figure D-1 a), there is an overlap in the range of acquired data for the two. However, looking at the differentiated spectrum for carbon in the absence of calcium, a dip is observed from 270 to 290 eV without a subsequent peak at 290 ev. The peak at 290 eV can therefore be said to belong to calcium. With this in consideration, the data for carbon was taken using the peak-dip from 265 to 285 eV and that for calcium was taken from 285 to 300 eV, as shown figure A-4 a).

For certain cases, however, this estimation was not sufficient. As different sensitivity factors for carbon and calcium are used to calculate the atomic concentrations, mistaking one for the other can result in an severe overestimation of one element and an underestimation of the other (seen in figure 5-21 in section 5.3.2)

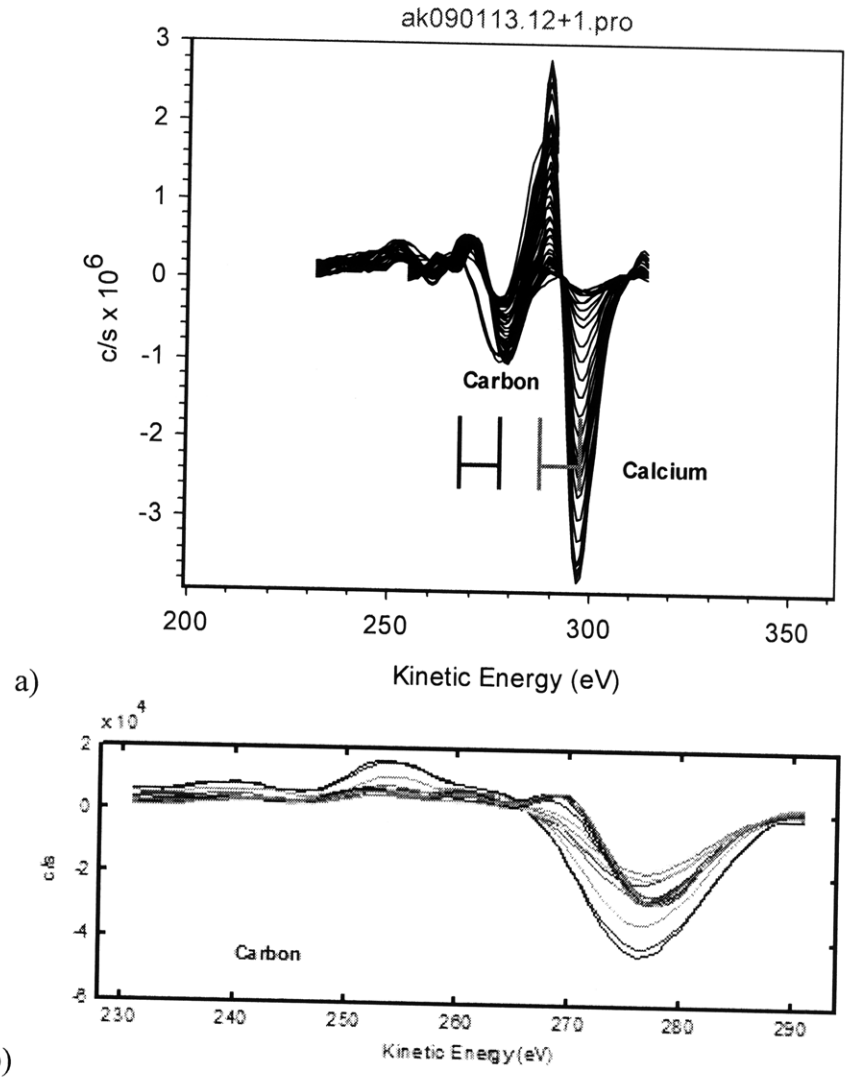

Figure D- 1 Differentiated plot of raw AES spectrum showing overlap between carbon and calcium signals
a) Case for lubrication with OBCaSu. The carbon peaks/dip and calcium peaks/dip are almost overlapping.
b) Carbon peak in the absence of calcium.